EXPERIMENTAL STUDIES BEARING ON THE NATURE OF SILICATE MELTS AND THEIR ROLE IN TRACE ELEMENT GEOCHEMISTRY

by

EDWARD BRUCE WATSON

B.A. UNIVERSITY OF NEW HAMPSHIRE (1972)

SUBMITTED IN PARTIAL

FULFILLMENT OF THE REQUIREMENTS

FOR THE

DEGREE OF DOCTOR OF PHILOSOPHY

at the

MASSACHUSETTS INSTITUTE OF TECHNOLOGY

September, 1976

Signature of Author.....
Department of Earth and Planetary Sciences, August, 1976

Certified by.....
Thesis Supervisor

Accepted by.....
Chairman, Departmental Committee on Graduate Students

Lindgren
WITHDRAWN FROM MIT LIBRARIES
DEC 21 1976

ABSTRACT

EXPERIMENTAL STUDIES BEARING ON THE NATURE OF SILICATE MELTS AND THEIR ROLE IN TRACE ELEMENT GEOCHEMISTRY

by

EDWARD BRUCE WATSON

Submitted to the Department of Earth and Planetary Sciences on August 9, 1976 in partial fulfillment of the requirements for the degree of Doctor of Philosophy.

Part I: Two-liquid Partition Coefficients: Experimental Data and Geochemical Implications

Partition coefficients for Cs, Ba, Sr, Ca, Mg, La, Sm, Lu, Mn, Ti, Cr, Ta, Zr, and P between immiscible basic and acidic liquids in the system K_2O-Al_2O_3-FeO-SiO_2 were experimentally determined at 1180°C and 1 atm. Phosphorus is most strongly enriched in the basic melt (by a factor of 10), followed by rare earth elements, Ta, Ca, Cr, Ti, Mn, Zr, Mg, Sr, and Ba (enriched by a factor of 1.5). Of the elements studied, only Cs is enriched in the acidic melt. The two-liquid partition coefficients of Zr, Ta, Sm, and Mn are constant for concentrations ranging from less than 0.1% to as high as 1 wt%, suggesting that Henry's law is applicable in silicate melts (at least for these elements) to concentrations well above typical trace element levels in rocks. The strong relative preference of many elements for the basic melt implies that the structural characteristics of basic melts more readily permit stable coordination of cations by oxygen. Partitioning of elements between crystal and liquid in a magma must therefore be influenced by the composition (and consequent structure) of the liquid. Crystal-liquid partition coefficients of elements showing strong fractionation between immiscible melts (e.g. P, Ta, REE) will vary extensively with liquid composition.

Application of the two-liquid partition coefficients to possible occurrences of liquid immiscibility in magmas reveals that typical basalt-rhyolite associations are probably not

generated by two-liquid phase separation. However, liquid immiscibility cannot be discounted as a possible origin for lamprophyric rocks containing felsic segregations.

Part II: Partitioning of Mn between Forsterite and Liquid: the Effect of Liquid Composition

One atmosphere partition coefficients for Mn between pure forsterite and liquid in the system MgO-CaO-Na_2O-Al_2O_3-SiO_2 (+ about 0.2% Mn) were measured by electron microprobe for a variety of melt compositions over the temperature range 1250-1450°C. The forsterite-liquid partition coefficient of Mn (mole ratio, D_{Mn}) depends on liquid composition as well as temperature: at 1350°C, D_{Mn} ranges from 0.60 (basic melt, SiO_2= 47 wt%) to 1.24 (acidic melt, SiO_2=65 wt%). At lower temperatures, the partition coefficient is more strongly melt composition dependent.

The effects of melt composition and temperature on D_{Mn} can be separately evaluated by use of the Si/O atomic ratio of the melts. A plot of D_{Mn} measured at various temperatures vs. melt Si/O for numerous liquid compositions reveals discrete, constant-temperature curves that are not well defined by plotting D_{Mn} against other melt composition parameters such as MgO content or melt basicity. For constant Si/O in the melt, $\ln D_{Mn}$ vs. reciprocal absolute temperature is linear; however, the slope of the plot becomes steeper for higher values of Si/O, which indicates a higher energy state for Mn^{2+} ions in acidic than in basic melts.

Comparison of the Mn partitioning data for the iron-free system used in this study with data of other workers on iron-bearing compositions suggests that the effect of iron on Mn partitioning between olivine and melt is small over the range of reasonable basalt liquidus temperatures.

Thesis Supervisor: Dr. J.S. Dickey

Title: Associate Professor of Earth and Planetary Sciences

ACKNOWLEDGMENTS

The completion of this thesis was made possible largely through the efforts of John Dickey and Fred Frey, who, even in these hard times, were always willing and able to obtain the funds required for experimental and analytical work. I also wish to thank them for the confidence they maintained in me and my work, and for their patience with my sometimes too independent approach to graduate study.

My sojourn at M.I.T. was kept at four years with the help of an M.I.T. Sloan Fellowship and a Predoctoral Fellowship at the Geophysical Laboratory. I am grateful to the individuals who helped me to obtain these fellowships, and to Dr. Yoder of the Geophysical Lab for giving me the opportunity to work there.

My education at M.I.T. has benefited in many ways from contact with faculty and fellow students who cannot all be individually acknowledged, but whose influence on my work and life is important and lasting.

Finally, I wish to thank my family and friends, at M.I.T. and elsewhere, for their encouragement and confidence in me both as a scientist and as a person--it was they, in the long run, who helped get me over many of the obstacles of graduate school.

TABLE OF CONTENTS

	page
Abstract	2
Acknowledgments	4
List of Figures and Tables	9
General Introduction	12
Previous Work on Silicate Melts and Glasses	15
1. Theoretical Models	15
The Temkin "ideal ionic" solution and its application to silicate melts	16
The Bernal "random close-packing model	23
Phase diagram analysis	24
2. X-ray and Spectroscopic Studies	26
X-ray diffraction and the structure of simple melts	27
Mössbauer spectroscopy and the coordination of Fe ions in glass	31
Optical absorption studies of simple glasses	32
3. Experimental Studies of Glass and Melt Structure	36
Aqueous dissolution	36
Ion exchange techniques	36
Systematic studies of physical properties	37
Systematic liquidus shifts	41
Solubility of volatile components	42
4. Concluding and Cautionary Remarks	42

TABLE OF CONTENTS
(cont'd)

	page
Part I. Two-liquid Partition Coefficients: Experimental Data and Geochemical Implications	45
1. Introduction	45
2. Experimental Philosophy and Objectives	46
3. Experimental and Analytical Methods	50
Starting materials	50
Leucite synthesis	51
Fayalite synthesis	51
Experimental apparatus and run conditions	52
Preliminary experiments	55
Partitioning Experiments	56
Analysis of Charges	58
Criteria for equilibrium and reversal of Ti experiments	59
4. Results and Interpretations	61
Partition coefficients	61
Alkali and alkaline earth elements	61
Rare earth elements	64
Transition elements	66
Highly-charged incompatible elements	68
Effect of minor components on coexisting liquid compositions	68

TABLE OF CONTENTS
(cont'd)

	page
5. Discussion	72
Systematics of two-liquid partitioning	72
Geochemical implications of two-liquid partitioning data	77
Henry's law	77
Implications to solid-liquid partitioning	79
6. Concluding Remarks	83
Part II. Partitioning of Manganese Between Forsterite and Silicate Liquid: The Effect of Liquid Composition	85
1. Introduction	85
2. Experimental and Analytical Methods	86
Selection of compositions	86
Specific techniques	89
Starting materials	89
Apparatus and run conditions	89
Preliminary Experiments	90
Criteria for equilibrium	90
The effect of oxygen fugacity	90
Concentration dependence of partition coefficients	92
Scope of partitioning experiments	94
Analysis of Charges	95
3. Results	101

TABLE OF CONTENTS
(cont'd)

	page
4. Discussion	111
Implications for melt structure	111
Geochemical implications	122
Melt composition effects in natural systems	122
Other transition elements	122
Geothermometry	123
5. Concluding Remarks	133
Summary and Synthesis, with some Speculations	136
1. Melt Structure	136
2. Geochemistry	141
3. Future Work	143
Bibliography	147
Appendix I	158
Appendix II	167

LIST OF FIGURES AND TABLES

		page
Figure 1	Concentration of various types of oxygen ions vs. mole fraction of SiO_2 in a binary silicate melt	20
Figure 2	$N_{O^{2-}}$ vs. N_{SiO_2} curves compared with oxide activity vs. N_{SiO_2} curves	22
Figure 3	Structure of fused silica	29
Table 1	Coordination numbers of transition metal ions in glass	33
Figure 4	Effect of aluminum on the presence of nonbridging oxygens in Na_2O-SiO_2 glass	35
Figure 5	Changes in physical properties of sodium aluminosilicate melts with the Na/Al ratio	40
Figure 6	Isothermal section through the immiscibility volume (1180°C)	48
Table 2	Compositions of immiscible acidic and basic melts compared with common igneous rocks	49
Figure 7	Charge container for two-liquid experiments	54
Figure 8	Photomicrograph of two-liquid charge	57
Table 3	Summary of two-liquid partitioning data	62
Figure 9	Weight % in basic glass vs. weight % in acidic glass for Cs, Ba, Sr, Ca, and Mg doping experiments	63
Figure 10	Weight % in basic glass vs. weight % in acidic glass for rare earth elements	65
Figure 11	Weight % in basic glass vs. weight % in acidic glass for transition elements	67
Figure 12	Weight % in basic glass vs. weight % in acidic glass for Zr, Ta, and P	69

LIST OF FIGURES AND TABLES
(cont'd)

		page
Figure 13	$D_{B/A}$ vs. weight % in basic glass for alkali, alkaline earth, and transition elements	70
Figure 14	$D_{B/A}$ vs. weight % in basic glass for rare earth elements, Zr, Ta, and P	71
Figure 15	Effect of a fifth component on compositions of immiscible liquids	73
Figure 16	Cation charge/radius vs. $D_{B/A}$	76
Figure 17	Forsterite-anorthite-albite liquidus diagram	88
Figure 18	Electron microprobe traverse across forsterite crystal and glass in run #6R1	91
Figure 19	Mole % MnO in forsterite vs. mole % MnO in glass for selected experimental compositions	93
Table 4	a) Major element analyses and Si/O values of glasses in Mn partitioning experiments	96
	b) Analyses of forsterite in selected Mn partitioning experiments	100
Table 5	Summary of forsterite-liquid partitioning data for Mn	102
Figure 20	$\ln D_{Mn}^{Fo\text{-}liq}$ vs. $(T^{o}K)^{-1}$	106
Figure 21	$D_{Mn}^{Fo\text{-}liq}$ vs. $[MgO]^{-1}$	108
Figure 22	$\ln K$ vs. $(T^{o}K)^{-1}$ for Mn partitioning experiments	110
Figure 23	$D_{Mn}^{Fo\text{-}liq}$ vs. Si/O for Mn partitioning experiments	112
Figure 24	$\ln D_{Mn}^{Fo\text{-}liq}$ vs. $(T^{o}K)^{-1}$ for constant values of Si/O	119

LIST OF FIGURES AND TABLES
(cont'd)

		page
Table 6	Anionic structures in simple silicate glasses	120
Figure 25	Mn partitioning data of other workers compared with this study	126
Table 7	Summary of Mn partitioning data of other workers for iron-bearing olivine-liquid pairs	128
Table 8	Comparison of Duke, Leeman, and Watson geothermometers	132
Figure 26	Polymerization path of a simple silicate melt	138
Figure 27	Speculative diagram showing consistency between two-liquid and forsterite-liquid partitioning data for Mn	140

GENERAL INTRODUCTION

In past years, the study of igneous rocks has been restricted primarily to examination of the solid phases that crystallize from natural molten silicate. Relatively little emphasis has been placed on the liquid phase itself, in spite of its important role in both the physical and chemical processes of igneous rock genesis. Recent studies of the physical properties of silicate melts (Kushiro et.al., 1976; Bottinga and Weill, 1972; Murase and McBirney, 1973) place constraints on physical models of magmatic processes, and also indirectly provide information on melt structure. However, to the geochemist studying igneous rocks, whose major concern is the distribution of elements between coexisting crystals and liquid in a magma, the melt phase remains an obscure entity, lacking regular structure and easily-characterized atomic site types.

There are two main reasons for this lack of knowledge on the nature of complex silicate melts. First, the importance of characterizing the melt phase has long been camouflaged by the apparent success of the geochemical "rules" and principles proposed by Goldschmidt (1937), Ahrens (1953), and Ringwood (1955) to predict the incorporation of elements from a melt into minerals. Because the "rules" are based solely on knowledge of ionic parameters and crystal structure, they appear to be independent of bonding or site type in the liquid. Although their validity has been challenged by Shaw (1953), and more recently

by Burns and Fyfe (1967) and Whittaker (1967), the geochemical "rules" remain well embedded in the minds of geochemists.

The second, more fundamental, reason for ignorance on the subject of silicate melts is that direct structure analysis is difficult: even the super-cooled equivalent (glass) does not yield to many of the structural analysis methods applicable to crystalline compounds. Most of the existing knowledge of silicate melt structure is either entirely theoretical or based on qualitative inference from experimental data.

The primary intent of the work described in this thesis was to evaluate the influence of silicate melt composition (and structure) on the behavior of trace elements in magmas. Two experimental approaches to the problem were taken: 1) equilibration of immiscible acidic and basic melts with respect to numerous trace cations of variable properties; and 2) partitioning of manganese between pure forsterite and a wide range of liquid compositions. The first approach gave direct insight into the relative compatibility of fourteen elements in acidic versus basic melts, while the second set of experiments resulted in detailed knowledge of the compatibility of one element (Mn) in a variety of complex liquids. Although the conclusions of the two studies are entirely consistent and complementary, this thesis is divided into two major parts for the sake of clarity in presentation. At the end of each part, as well as in the synthesis and summary, the implications of the experimental data to silicate melt structure and trace element geochemistry are

discussed.

In this thesis, I do not presume to answer all questions regarding the role of silicate melts in igneous geochemistry; I only hope that this work has established a sound experimental basis for educated speculation and further study on the subject.

PREVIOUS WORK ON SILICATE MELTS AND GLASSES

This section is not intended as a comprehensive, state-of-the-art summary of information — the goal is more to introduce the reader to silicate liquids and to previous theoretical and experimental approaches to the problem of their structure. I have brought in numerous references from outside of the geological literature, and, as far as possible, I have attempted to put these in a geochemical perspective. Many of the articles that are briefly summarized here will be referred to in later sections of this thesis.

In general, the glassy and liquid states are not distinguished unless I feel that the distinction is important [for a discussion of structural similarity between a glass and its melt, I refer the reader to Riebling (1968).]

1. Theoretical Models

Several workers have attempted to adapt structural or thermodynamic models of relatively simple non-silicate liquids to complex silicate melts. Most of these models fall into one or a combination of the following three groups: ionic; statistical; or polymeric. Some success has been achieved with these models in deciphering the structure of binary and ternary silicate melts, but quantitative extrapolation to geologically realistic compositions is not possible.

The Temkin "ideal ionic" solution and its application to silicate melts.

Temkin (1945) proposed that mixtures of fused salts could be treated as two independent ideal solutions, one composed of anions and the other of cations. In such a solution, there is no heat of mixing, and the entropy change on mixing is given by the sum of the entropy changes associated with the permutations among cations and similar permutations among anions:

$$\Delta S_{MIX} = \Delta S^{+}_{MIX} + \Delta S^{-}_{MIX} = -R(\Sigma n^{+} \ln X^{+} + \Sigma n^{-} \ln X^{-}) \qquad (1)$$

where n^{+} and n^{-} refer to the number of moles of a given cation or anion, respectively, and the X's represent "ionic fractions" or mole fractions of ions relative to the total number of ions of the same charge. The basic assumptions of this model are that all cations are surrounded by anions and all anions by cations, and that no vibrational entropy or heat effects result from the interchange of ions of like charge. Because ΔH_{MIX} is assumed to be zero, an expression for the free energy of a salt component in a mixture eventually takes the form:

$$\bar{G}_{salt} = G^{\circ}_{salt} + RT\ln(X^{+})(X^{-}) \qquad (2)$$

where X^{+} and X^{-} are the ionic fractions of the cation and anion composing the salt, and the reference state is the pure molten salt. Thus, the activity of a salt component in a mixture of fused salts may be expressed as:

$$a_{salt} = (X^{+})(X^{-}) \qquad (3)$$

By analogy to electrolyte thermodynamics (Lewis and Randall, 1961), where the activity of a salt in dilute solution is defined as the product of the activities of its ionic constituents (i.e. $a_{salt} = a^+ \cdot a^-$), Temkin further defined the activity of an ion in a fused salt solution as equal to its ionic fraction, i.e.:

$$\left.\begin{aligned} a^+ &= X^+ \\ \text{and} \\ a^- &= X^- \end{aligned}\right\} \quad (4)$$

For example, in a CaO-FeO-CaS-FeS melt, the activity of Fe^{2+} is given by the ratio $\frac{\text{moles } Fe^{2+}}{\text{moles } Fe^{2+} + \text{moles } Ca^{2+}}$. Similarly, the activity of O^{2-} is $\frac{\text{moles } O^{2-}}{\text{moles } O^{2-} + \text{moles } S^{2-}}$. The activity of an electrically neutral molecule, say FeO, is then

$$a_{FeO} = a_{Fe^{2+}} \cdot a_{O^{2-}} \quad (5)$$

referred to pure molten FeO.

Because it allows formulation of thermodynamic parameters of components, the Temkin model has proved useful in dealing with fused salt solutions and basic slags. In particular, activities of components are required for quantitative description of solid-liquid or metal-slag equilibria by means of equilibrium constants.

Like mixtures of fused salts, silicate melts are strongly ionic in nature, as evidenced by electrical conductivities resembling those of strong electrolyte solutions (Bockris et. al., 1948). Potentially, then, the Temkin model might be a

good starting point for dealing with silicate melts and their equilibria with crystalline phases. Unfortunately, however, the problem is complicated by difficulty in identifying the ionic species that actually exist in molten silicates. As I will discuss in more detail later in this section, the presence of a glassforming cation (Si^{4+}) in a melt results in complex anionic silicate species, the most fundamental of which is the silicate tetrahedron, SiO_4^{4-}. In very basic melts, the isolated tetrahedron is probably the dominant silicate species, coexisting perhaps with some free oxygen anions and metal cations. More acidic melts are composed of combinations of tetrahedra, linked at the corners to form chains, rings, and even more complex 2- and 3-dimensional units. In short, direct application of the Temkin model to molten silicate is tenuous, because complete dissociation into simple ions cannot be assumed.

Toop and Samis (1962a,b) combined a polymer model of silicate melts with the Temkin concept of ionic solutions to estimate activity-composition relations in some simple silicate systems. They described the extent of melt polymerization in terms of an equilibrium constant for the following polymerization reaction:

$$2O^- \rightarrow O^0 + O^{2-} \qquad (6)$$

where O^{2-}, O^-, and O^0 represent free oxygen ions, oxygens bonded to a single silicon (nonbridging oxygens), and oxygens bonded to two silicons (bridging oxygens), respectively. This reaction is the generalized version of dimer formation from two

isolated silicate tetrahedra:

$$SiO_4^{4-} + SiO_4^{4-} \rightarrow Si_2O_7^{6-} + O^{2-} \qquad (7)$$

where two nonbridging oxygens are converted to a bridging oxygen and a free O^{2-} ion. The equilibrium constant for reaction (6) is

$$K = \frac{[O^0][O^{2-}]}{[O^-]^2},$$

where the bracketed symbols represent numbers of moles of the various types of oxygens. Toop and Samis proposed that K is constant at a given temperature and characteristic of a given binary or ternary silicate system. Material and charge balance considerations allow construction of a diagram such as Fig. 1, where the value of K is arbitrarily chosen as 0.06. The most important information in Fig. 1 is that acidic (high SiO_2) melts contain a large proportion of bridging oxygens, with virtually no free oxygen ions. Melts more basic than $N_{SiO_2} \approx 0.5$, however, are dominated by nonbridging oxygens, with appreciable concentrations of free O^{2-} ions. Fig. 1 does not specifically characterize the silicate anions present in the melt, but it does indicate the general extent of polymer formation.

By invoking Temkin's (1945) concept of "ionic fractions", Toop and Samis were able to estimate values of the equilibrium constant of equation (6) for several binary silicate systems. First, they observed that, for ionic solutions

$$a_{MO} = a_{M2+} \cdot a_{O2-} \qquad (8)$$

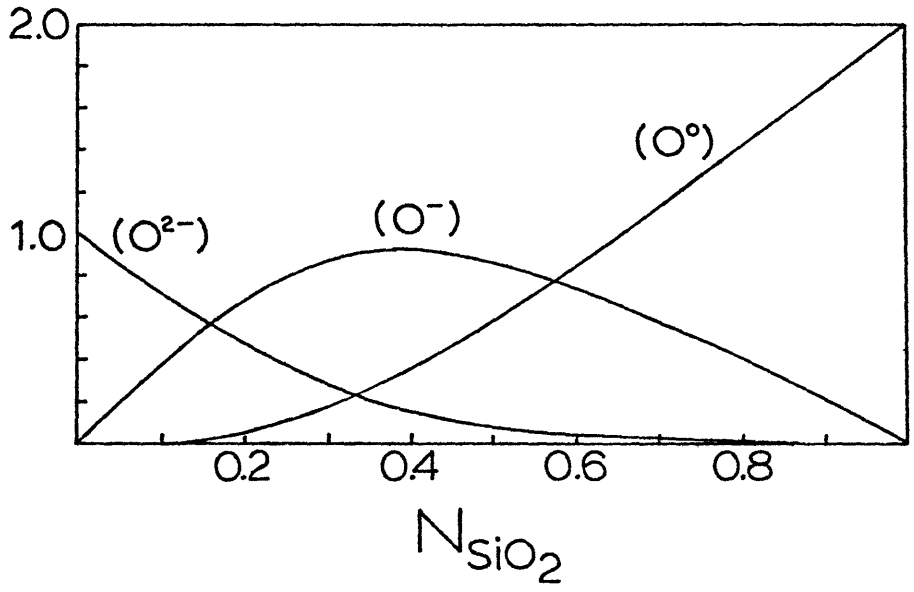


Figure 1. Equilibrium values of (O^{o}), (O^{-}), and (O^{2-}) vs. mole fraction of SiO_2 in a binary silicate melt for K = 0.06 (from Toop and Samis, 1962a; see text)

where M is a divalent metal cation. In a binary silicate melt $MO-SiO_2$, M^{2+} is the only cationic species (Si exists only in anionic complexes, not as free Si^{4+}). Therefore, according to the Temkin model, the ionic fraction of M^{2+} is unity, so $a_{M2+} = 1$. From equation (8), this implies that $a_{MO} = a_{O2-}$. Indeed, Toop and Samis then observed that experimentally determined activity-composition curves for metal oxides in binary silicate systems closely resemble plots of Temkin's ionic fraction of O^{2-} ions versus composition if an appropriate value of K is selected for calculating the ionic fraction of O^{2-} (see Fig. 2). By matching experimentally determined a_{MO} curves with calculated a_{O2-} curves, it was therefore possible to obtain values of K for several binary systems. For the systems $FeO-SiO_2$ and $CaO-SiO_2$, K = 0.17 and 0.0017, respectively. Thus, the value of 0.06 assumed for plotting Fig. 1 is realistic, and the figure may be taken seriously.

Drawing upon the contribution of Toop and Samis (1962a) and the statistical methods of established polymer theory, Hess (1970) further developed and systematized structural models of binary silicate systems. One of the most important conclusions of this work is that, for a given mole percentage of SiO_2, binary silicate melts containing cations of high ionic potential (charge/radius) are more polymerized than melts containing cations of low ionic potential. This is equivalent to stating that cations of high ionic potential result in large values of

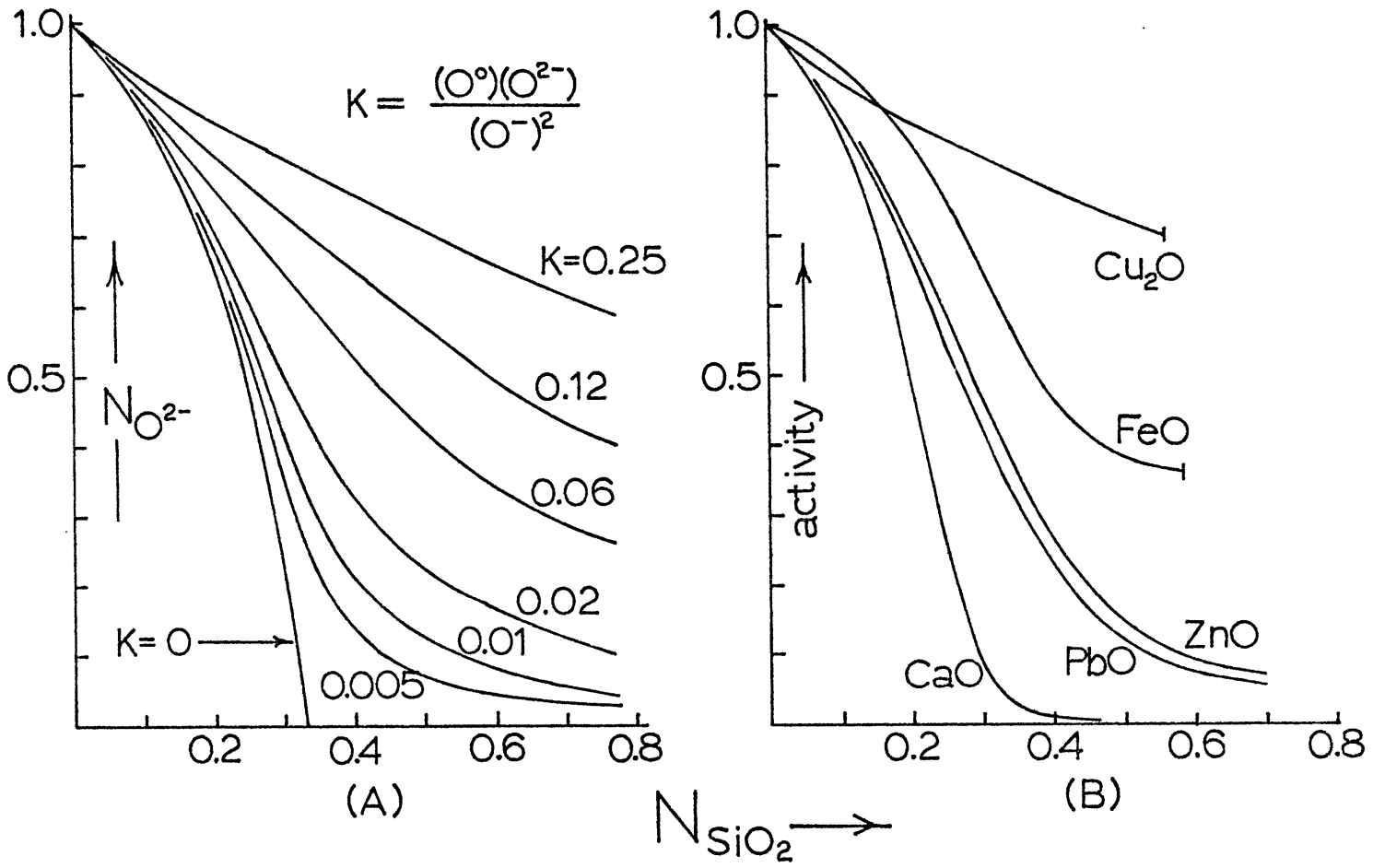


Figure 2 a). Temkin's ionic fraction of oxygen ions vs. the mole fraction of SiO_2 in a binary silicate melt for various values of K (see text)

b) Activities of various metal oxides in binary silicate melts with respect to the pure liquid oxides. Cu_2O and PbO curves are for 1100°C; CaO and FeO curves are for 1600°C; and ZnO curve is for 1300°C. Note similarity in shape of these curves to those of Fig. 2a

K for reaction (6). This conclusion might be qualitatively extrapolated to geological melt compositions.

In addition to the theoretical melt-structure models described above, the Temkin ionic solution concept has been used by geochemists in the formulation of crystal-liquid partition coefficients. Banno and Matsui (1973), for example, used a simple Temkin model to show that conventionally-expressed partition coefficients must depend on silicate melt composition. In calculating equilibrium constants for plagioclase-melt equilibria, Drake (1972) used a Temkin-like approach to define the mole fraction of an oxide in the melt phase. He assumed that a melt comprises tetrahedral and octahedral sites (rather than anions and cations, as in a strict Temkin model), between which most cations are not interchangeable. Therefore, the mole fraction or activity of a cation is given by the number of moles of that cation divided by the total number of moles of cations likely to occupy the same type of site.

The Bernal "Random Close-Packing" Model.

Bernal (1964) proposed a purely geometrical solution to the problem of liquid structure. Using the well-known fact that liquids have no long-range regularity, and assuming that the atoms of a liquid can be approximated by hard, neutral spheres, Bernal showed that the interstitial cavities in a randomly close-packed structure occupy 35 per cent of the total volume, and are of five types: tetrahedra, half-octahedra, tetragonal dodecahedra, trigonal prisms, and square antiprisms.

Whittaker (1967) suggested that the Bernal model could be applied to silicate melts, in which case the large (∿1.40Å radius) oxygen atoms could be regarded as randomly close-packed, with all cations occupying the interstices. In a Bernal-type silicate melt, the number of interstitial tetrahedral sites (73 per 24 oxygens) exceeds the number of octahedral and larger sites by the ratio 4.4:1. As noted by Burns and Fyfe (1964) and Whittaker (1967), the implication for natural melt compositions (especially basic ones) is that cations whose radii would generally favor octahedral coordination by oxygen may be forced into tetrahedral sites.

Whittaker (1967) emphasized that application of the Bernal model to liquid silicates is rather tentative at the present time. Such a geometrical model does not take account of energetic considerations that arise, for example, when two cations are inserted into face-sharing interstitial polyhedra. Also, indiscriminant application of the Bernal model to all silicate melts implies identical cationic site distribution for the complete spectrum of geological melt compositions. This conclusion is not supported by the experimental results reported in later sections of this thesis.

Phase Diagram Analysis.

Theoretical models based on binary phase diagram analysis have provided considerable insight into the structure of simple silicate melts. For feldspar-silica joins, Flood and Knapp

(1968) assumed that melts can be approximated as ideal solutions if the structural units that contribute to the entropy of mixing can be identified. Essentially by trial and error, these authors selected different types of complex anions, calculated the "ideal" liquidus curves given by the different mixing entropies, and compared these curves to experimentally determined phase diagrams. When a near match between calculated and actual liquidus curves was obtained, the hypothetical structural units were considered correct. In this manner, Flood and Knapp reached the following conclusions about binary feldspar-silica melts:

1. Silica-rich mixtures of alkali-feldspar and silica comprise a random distribution of SiO_4 and AlO_4 tetrahedra, with an alkali cation associated with each AlO_4 unit.
2. Silica-rich celsian- and anorthite-silica binary melts probably contain Al_4O_8 aluminate groups randomly mixed with SiO_4 tetrahedra.
3. Feldspar-rich albite-silica melts can be approximated by a random mixture of $NaAlO_4$ and SiO_4 units, although the existence of small amounts of more complex species is suggested.
4. Feldspar-rich anorthite-silica melts comprise a random distribution of $[4AlO_2 \cdot 3SiO_2]$ and SiO_2 groups (each of the former has two associated Ca^{2+} cations).

The most important overall conclusions of the Flood and Knapp structural models is that binary feldspar-silica melts

are not simply mixtures of endmember "molecules" such as $NaAlSi_3O_8$ or $CaAl_2Si_2O_8$ and SiO_2.

The same conclusion was reached by Haller et.al. (1974) in a phase diagram analysis of the Li_2O-, Na_2O-, and BaO-SiO_2 binary systems. In this study, metastable two-liquid solvus curves rather than liquidus curves were calculated. The authors observed that experimentally-determined solvus curves in these systems are assymetric when plotted in terms of the chemical endmembers SiO_2 and M_2O or MO. However, by re-defining the endmember components, they were able to symmetrize the miscibility gaps, thereby allowing application of a simple solution model to describe the immiscibility. Excellent agreement with experimental data was achieved if the mixing endmembers were considered to be: $[Li_2O \cdot 2SiO_2]$ and $[(SiO_2)_6]$, $[Na_2O \cdot 3SiO_2]$ and $[(SiO_2)_8]$, and $[BaO \cdot 2SiO_2]$ and $[(SiO_2)_8]$, respectively, for the systems Li_2O-SiO_2, Na_2O-SiO_2, and BaO-SiO_2. This coincidence of experimental and theoretical results is good evidence that, on the average, the re-defined endmember molecules represent the actual structural units of the glasses. Like the work of Flood and Knapp (1968), this paper convincingly demonstrates that simple silicate melts are composed of complex molecules, and are not simply random mixtures of the chemical oxide endmembers.

2. X-ray and Spectroscopic Studies

X-ray diffraction and Mössbauer and absorption spectroscopic methods have yielded direct, quantitative information on

the structure of silicate glasses. In general, the x-ray diffraction method gives insight into the average structural characteristics of the glass on the whole, while spectroscopic methods are useful for estimating oxygen coordination polyhedra of specific cations. Potentially, therefore, the combined results of the two methods could create a fairly complete picture of glass structure. Unfortunately, however, only simple glasses are susceptible to x-ray diffraction analysis, and absorption spectroscopic methods are not always applicable or definitive. An additional consideration is that measurements made on glasses at low temperature may not represent the structure actually present in high-temperature melts. The validity of extrapolating from the glassy to liquid state depends upon the quenchability of the structures examined, as will be discussed later in this section.

X-ray diffraction and the structure of simple melts.

Fused silica is structurally the simplest of all glass-forming melts, and its basic nature has been understood for some time. With remarkably little experimental evidence, Zachariasen (1932) deduced that the structure of vitreous silica is a random 3-dimensional network composed of corner-sharing silicate tetrahedra. In comparing vitreous compounds in general to their crystalline counterparts, Zachariasen stated that "the network in glass is characterized by an infinitely large unit cell containing an infinite number of atoms", and that the

"absence of periodicity and symmetry in the network distinguishes a crystal from a glass." The Zachariasen model of vitreous silica was most convincingly confirmed by the x-ray diffraction study of Mozzi and Warren (1969). These authors concluded that:

1. Each silicon is tetrahedrally coordinated by oxygen atoms, with a mean Si-O distance of 1.62Å (the same Si-O bond length as found in crystalline silicates).
2. Each oxygen atom is bonded to two silicons (i.e. all oxygens are bridging).
3. The distribution of Si-O-Si bond angles ranges from 120° to 180°, with a maximum value of 144° (almost all angles fall within ±10% of the maximum).

The observed distribution of bond angles about a mean value is sufficient to distinguish the glass from a crystalline structure. The strong maximum in the bond angle distribution indicates that the glass structure is fairly uniform on the scale of several tetrahedra, but loses regularity when considered on a larger scale (see Fig. 3). This model is compatible with the low entropy of fusion of cristobalite (Hicks, 1969).

Warren and Biscoe (1938) examined five different sodium silicate glasses by x-ray diffraction; again, their results suggested a random network structure of silicate tetrahedra, in which some oxygen ions were bridging and some were nonbridging (note that in fused silica all oxygens are bridging). Their data also indicated that discrete "endmember" molecules such as SiO_2, Na_2O, $Na_2O \cdot 2SiO_2$, and $Na_2O \cdot SiO_2$ were not present in the

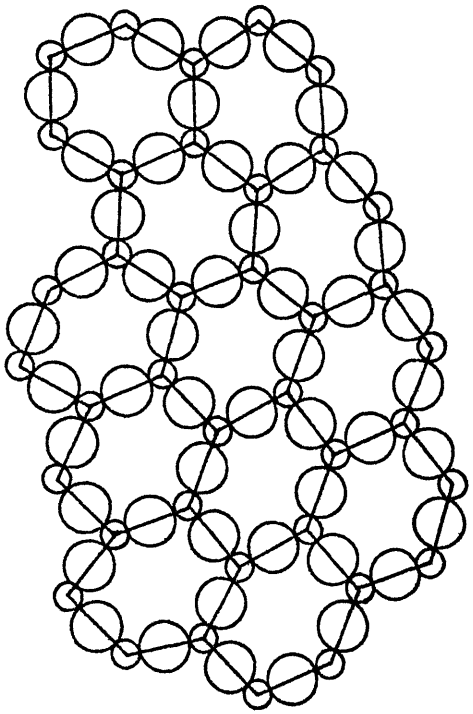


Figure 3. Schematic diagram of a two-dimensional structure of fused silica (after Doremus, 1973, p.27). The relative size of silicon atoms is increased somewhat, and (for portrayal in two dimensions) only three oxygens are attached to each silicon. The O-Si-O bond angle is varied instead of the Si-O-Si angle. Note close similarity of adjacent "rings", but loss of regularity on the scale of several SiO_4 units

glasses.

More recent x-ray diffraction studies of binary and ternary silicate glasses have shown that the distribution of cations is not uniform. Ohlberg and Parsons (1964), for example, demonstrated that the average Na-Na distance in a soda-lime-silica glass is considerably less than that resulting from a uniform distribution of Na^+ ions. Clustering of sodium ions in the glass must therefore be inferred. Milberg and Peters (1969) observed the same phenomenon in a series of thallium silicate glasses, and reached the important conclusion that "it is not necessary to postulate a direct attraction between the thallous ions to account for the clustering since, with a suitable network arrangement involving clustering of nonbridging oxygens, the cations will form clusters as a result of the attraction between themselves and the nonbridging oxygens." In a comparative x-ray diffraction study of Na_2O-SiO_2 and Na_2O-Al_2O_3-SiO_2 glasses, Urnes (1969) concluded that clustering of sodium ions occurs in both glasses, but the average Na-Na distance is greater than that proposed by Ohlberg and Parsons (1964).

In general, the information obtained by x-ray analysis of glasses seems consistent with the structural models described earlier in this section. In particular, x-ray and phase diagram analysis methods both rule out the existence of chemical end-member molecules in simple glasses. The work of Haller et.al. (1974) indirectly supports the x-ray evidence for clustering

of cations: lithium disilicate is considered by Haller et.al. to be one of the actual mixing molecules in Li_2O-SiO_2 melts, and as pointed out by Doremus (1973), definite clustering of lithium ions occurs in crystalline lithium disilicate.

Mössbauer spectroscopy and the coordination of Fe ions in glass.

As noted previously, spectroscopic methods are useful for determining the immediate environment or oxygen coordination polyhedron of a cation in glass. The general approach of these methods is to compare spectra measured on glasses with those obtained on materials in which the environment of the ion of interest is known.

The susceptibility of iron to the Mössbauer effect and its importance in both geology and glass science have resulted in several studies of the coordination of Fe^{3+} and Fe^{2+} in glasses. Kurkjian and Sigety (1968) combined Mössbauer with optical absorption measurements to conclude that ferric iron is tetrahedrally coordinated in ternary silicate glasses, and that the coordination number does not depend upon iron concentration. Also using Mössbauer spectroscopy, Boon (1971) found that ferrous iron occupies primarily two types of sites in Na_2O-FeO-SiO_2 glasses; with the aid of optical absorption data (Boon and Fyfe, 1972), he later assigned a coordination number of 6 to these sites. Boon and Fyfe (1972) extended their Mössbauer investigations to FeO-K_2O-SiO_2, FeO-CaO-SiO_2, FeO-Al_2O_3-SiO_2, and FeO-K_2O-Al_2O_3-SiO_2 glasses, all of which were found to con-

tain Fe^{2+} in basically two octahedral site types.

In a good review of theory and application, Kurkjian (1970) summarized data obtained by Mössbauer spectroscopy on glasses, including results for the less common elements Sn and Tm.

Optical absorption studies of simple glasses.

The widespread use of glass for decorative and optical purposes has stimulated many studies of absorption and transmission phenomena in simple glass systems. These studies are too numerous to summarize here, so I will single out those which contribute geochemically relevant information not obtainable by other methods. For a summary of absorption spectroscopy in glasses, see Wong and Angell (1970).

Williams (1959) and Burns and Fyfe (1964) presented evidence that crystal field stabilization is an influential factor in the uptake of transition metal ions by crystals in a magma. In order to develop this theory rigorously, it is necessary to have some knowledge of site types or coordination numbers of ions in magmatic liquids. Because of the experimental difficulties in taking optical absorption measurements on molten materials, all existing data were obtained on glasses at low temperature. Table 1 summarizes visible optical absorption data on coordination numbers for some of the first series transition elements in silicate glasses. It should be noted that the most commonly occurring coordination is octahedral, although some of the data are ambiguous.

Table 1. Coordination numbers (with oxygen) of transition metal ions in soda-lime silicate glasses, determined by visible optical absorption.

ion	no. of d electrons	coordination no. with oxygen	reference
Cr^{3+}	1	6	Bates (1962)
V^{4+}	1	6?	Kumar (1959)
V^{3+}	2	6	Kumar (1959)
Mn^{3+}	4	6	Weyl (1959)
Mn^{2+}	5	4,6?	Weyl (1959), Bingham and Park (1965), Kumar and Nath (1966)
Fe^{3+}	5	4?[a]	Kurkjian and Sigety (1968)
Fe^{2+}	6	4,6?	Bishay (1959)
Ni^{2+}	8	6,8[b]	Turner and Turner (1972)
		4,6[c]	Burns and Fyfe (1964)
Cu^{2+}	9	6	Kumar (1959)

[a] potassium silicate glass

[b] alkali and alkaline earth silicate and aluminosilicate glasses

[c] sodium aluminosilicate, diopside, diopside-albite, "granite", and "tholeiite" glasses

Absorption measurements in the infrared and ultraviolet regions have been used to examine the effects of adding other oxide components to pure silica glasses. Crozier and Douglas (1965) and Hanna and Su (1964) measured the infrared absorption spectra of sodium silicate glasses, and were able to attribute the appearance of absorption peaks to the formation of non-bridging oxygens as the Na_2O content of the glasses was increased. Simon (1960) remarked on the similarity in infrared reflection spectra of alkali silicate and alkaline earth silicate glasses, and concluded that nonbridging oxygens contribute to the spectra in both cases. Sigel (1971) systematically examined absorption in the ultraviolet region by alkali silicate and alkali aluminosilicate glasses. He found that increased absorption in some ultraviolet wavelengths was directly proportional to the alkali concentration of the glass. However, if alumina was added in a 1:1 molar ratio with the alkali oxide, absorption dropped to levels resembling pure SiO_2. Again, these results suggest that the increase in absorption with alkali content in a binary silicate glass is due to formation of nonbridging oxygen ions; furthermore, it appears that the addition of alumina decreases the number of nonbridging oxygens by means of alkali-aluminate "molecule" formation (see Fig. 4). A similar interpretation can be placed on some of the experimental data described under the next heading of this section.

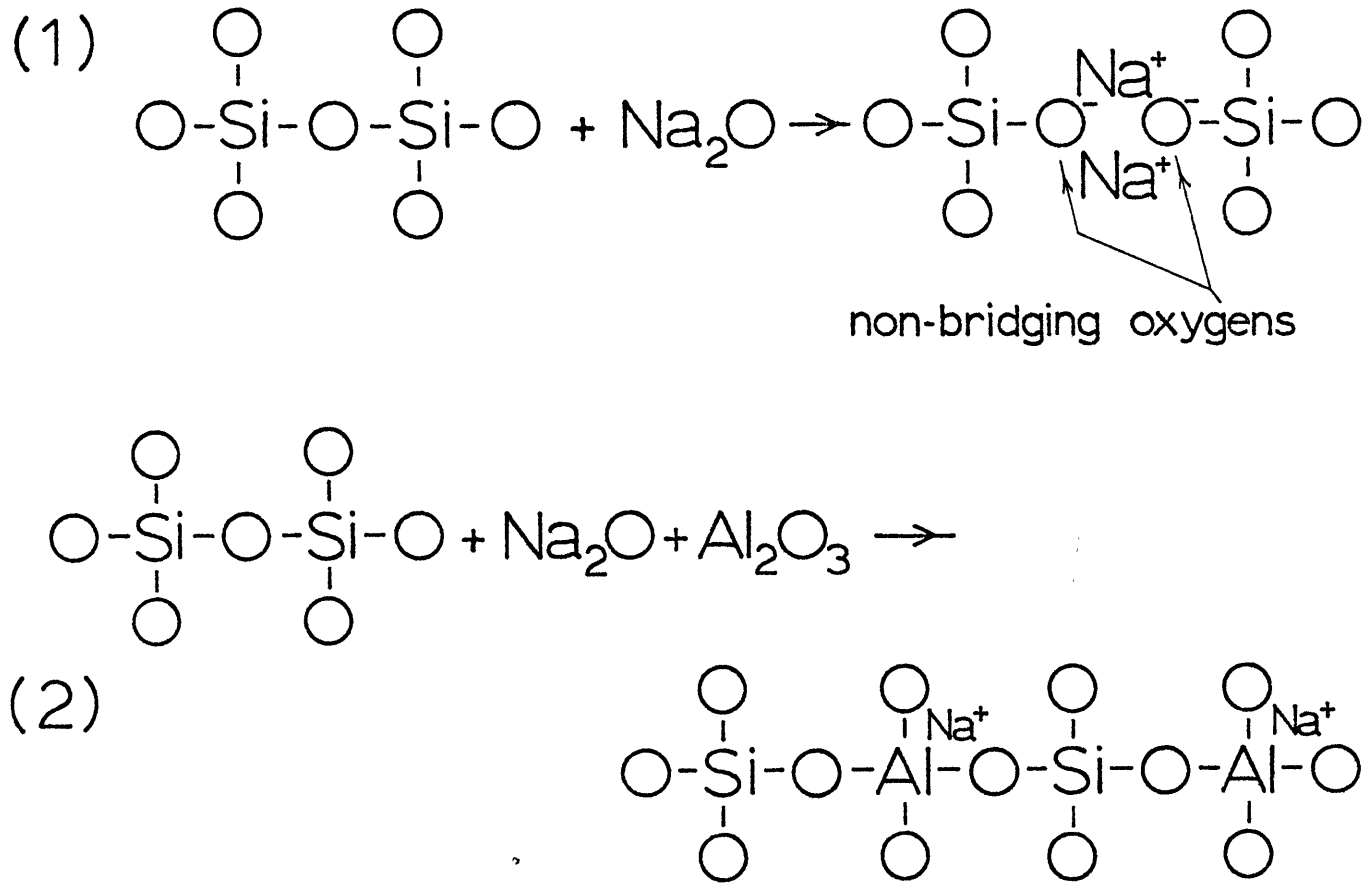


Figure 4. Schematic representation in two dimensions of 1) the creation of non-bridging oxygens by the introduction of Na into the SiO_2 network and 2) the ability of aluminum to restore the bridging in spite of the presence of alkali (from Sigel, 1971)

3. Experimental Studies of Glass and Melt Structure

Systematic experimental studies have yielded both direct and inferential knowledge on the nature of silicate melts, and have been particularly helpful in supplementing theoretical structural models. The topics that I will describe briefly below were selected to give the reader an overall view of the various experimental approaches to the problem of melt structure.

Aqeous dissolution.

The most direct glass structure determination was carried out by Lentz (1964). By dissolving sodium silicate glasses in acidic aqueous solutions, he was able to use gas chromatography to identify some of the discrete anions composing the glasses. The isolated silicate tetrahedron (SiO_4^{4-}) was the most common anion, followed in abundance by simple polymeric chains such as $Si_2O_7^{6-}$ and $Si_3O_{10}^{8-}$. Unfortunately, this type of study cannot readily be extended to other compositions because of the generally low solubility of silicate glasses in weak acidic solutions. Use of strong acid to decompose the glass would probably also break down the structural silicate units.

Ion exchange techniques.

Low-temperature ion exchange techniques have been used extensively to obtain indirect information on site types in glasses. The general experimental approach of these studies has been to equilibrate powdered glass with a bath of molten salt containing an exchanging cation. The experimental temper-

atures are low enough that the glass remains solid, and its silicate structure remains intact—in other words, equilibrium is reached between glass and salt only with respect to a pair of exchanging cations. The data obtained by this ion exchange method are summarized in Doremus (1973, chap. 14). Unfortunately, none of the glass compositions studied are geochemically relevant, and most of the data are for monovalent cations only. However, one important general conclusion can probably be extrapolated to complex geochemical systems: aluminum-bearing glasses tend to show a preference for large cations, while aluminum-free glasses prefer small cations (Eisenman, 1962). From a geochemical standpoint, this result might indicate that aluminous melts contain more sites favorable for occupation by large cations.

Systematic studies of physical properties.

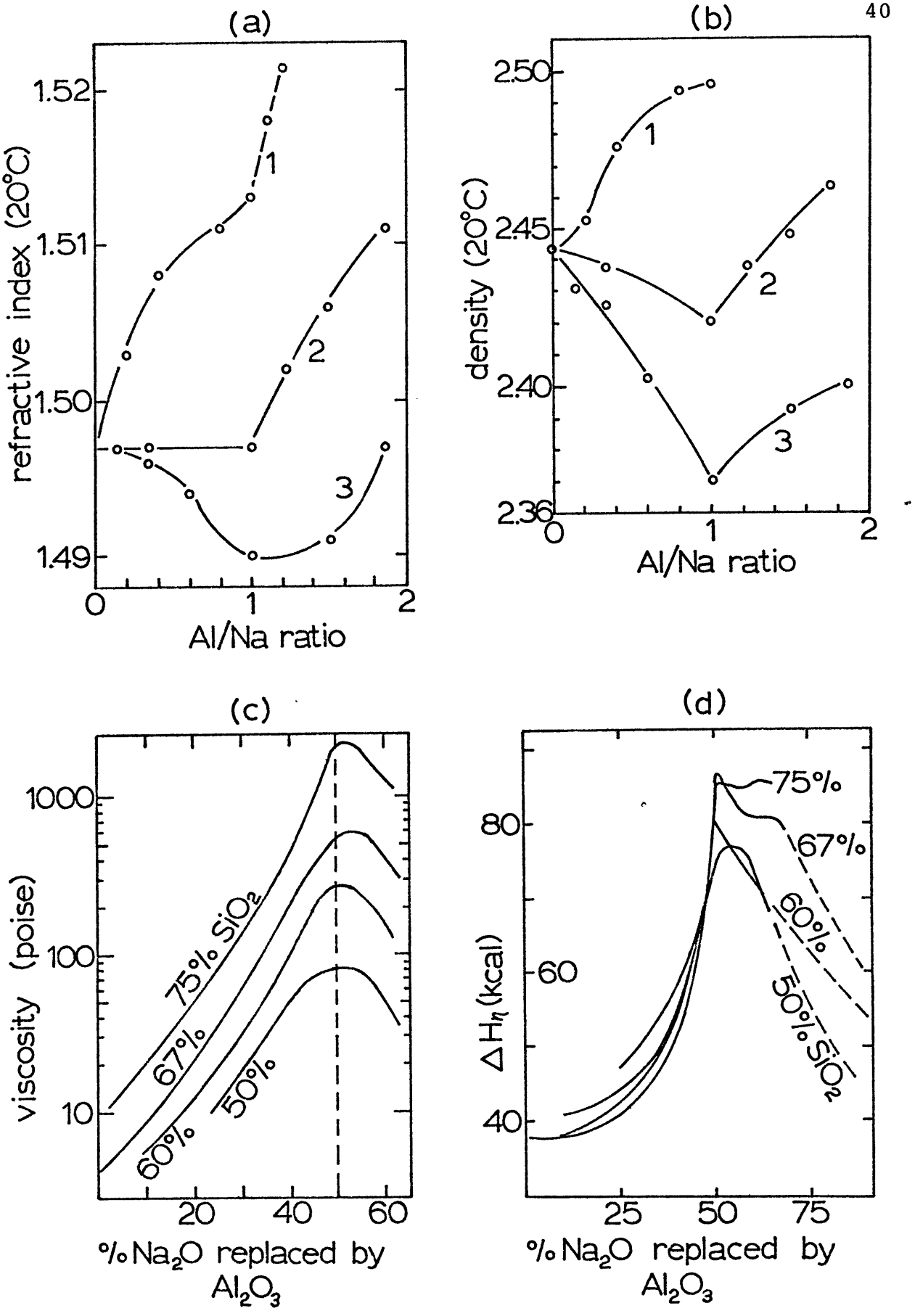
Systematic physical-property measurements on glasses in the system Na_2O-Al_2O_3-SiO_2 have provided unique insight into the structure of alkali aluminosilicate melts. The experiments of Day and Rindone (1962a,b) and Riebling (1966) demonstrated that, regardless of silica concentration, the Na/Al molar ratio plays an important role in the structure of these simple melts. The authors concluded that if Na/Al $\geq$ 1, all aluminum is in tetrahedral coordination with oxygen, and that these aluminate tetrahedra co-polymerize with the silicate network structure. An abundance of aluminum over sodium, on the other hand, results

in 6-coordinated aluminum, which does not participate in the network structure. Apparently, the presence of sodium cations in an aluminosilicate melt stabilizes aluminum in tetrahedral coordination. A 1:1 ratio of sodium:aluminum thus represents a maximum state of melt polymerization. This structural state is evidenced by abrupt changes in refractive index and density of the glasses, as well as peaks in viscosity and activation energy for viscous flow of the melts (Fig. 5).

The soda-alumina-silica system is the only system in which detailed, systematic physical property measurements have been made on melts and glasses. However, Schairer and Bowen (1955) measured refractive indices of glasses in the potash-alumina-silica system, and found striking maxima for glasses having a 1:1 molar ratio of K:Al. Thus, it appears that, at least for ternary silicate systems, the 1:1 alkali:aluminum ratio is generally important. Whether or not this conclusion can be extended to more complex systems containing divalent cations is not known.

Qualitative information on the nature of simple silicate melts can be deduced from the extensive physical property measurements of Bockris et.al. (1948, 1954, 1955, 1956). These authors determined ionic conductivity, viscosity, density, and expansivity of binary silicate melts of CaO, MgO, SrO, BaO, Na_2O, K_2O, and Li_2O. Their data are consistent with previously described models, in which the melt is composed of discrete anionic silicate complexes. Addition of a metal oxide to pure

Figure 5. Changes in physical properties of sodium aluminosilicate melts with the Na/Al atomic ratio: a) refractive index (Day and Rindone, 1962a); b) density (Day and Rindone, 1962a); c) viscosity at 1700°C (Riebling, 1966) and d) activation energy for viscous flow (Riebling, 1966). Note abrupt changes in refractive index and density curves, and peaks in viscosity and activation energy curves at the 1:1 ratio of Na:Al


(a)
refractive index (20°C)
1.52
1.51
1.50
1.49
0
1
2
Al/Na ratio
1
2
3
(b)
density (20°C)
2.50
2.45
2.40
2.36
0
1
2
Al/Na ratio
1
2
3
(c)
viscosity (poise)
1000
100
10
20
40
60
% Na2O replaced by Al2O3
75% SiO2
67%
60%
50%
(d)
ΔHη (kcal)
80
60
40
25
50
75
% Na2O replaced by Al2O3
75%
67%
60%
50% SiO2

molten silica appears to cause de-polymerization of the melt, such that at very basic compositions only the isolated SiO_4^{4-} ion remains intact.

Murase and McBirney (1973) measured several physical properties of natural silicate melts, and Kushiro et.al. (1976) extended viscosity measurements on simple (but geochemically important) melts to high pressure. The systematic accumulation of this sort of data should eventually supplement any natural melt structure models based on chemical considerations.

Systematic liquidus shifts.

Kushiro (1975) reached some general conclusions about the structure of silicate melts by observing changes in the liquidus diagrams of simple systems induced by incremental addition of minor chemical components. It was found that the addition of oxides of monovalent cations (H_2O, K_2O, Na_2O) caused the liquidus fields of less polymerized minerals to expand relative to adjacent phase fields of more polymerized minerals. Addition of oxides of polyvalent ($\geq$ 4) cations (TiO_2, P_2O_5, CO_2), on the other hand, tended to expand the liquidus fields of the more polymerized crystalline phases. Kushiro interpreted these results to mean that monovalent cations cause de-polymerization of complex silicate anions in the melt, while polyvalent cations promote polymerization. These conclusions seem consistent with Hess's (1970) statement that in binary silicate melts cations of high ionic potential push reaction (6) to the right.

Solubility of volatile components.

The interaction of volatile constituents with silicate melts is extremely important geochemically, and has recently been studied in some detail. Of specific interest here are proposed solution mechanisms for gases in silicate melts, because these bear directly on the nature of the melts. Uys and King (1963) examined water solubility in simple melts as a function of melt basicity, and proposed two solution mechanisms:

$$-\overset{|}{\underset{|}{Si}}-O-\overset{|}{\underset{|}{Si}}- + H_2O = -\overset{|}{\underset{|}{Si}}-OH + HO-\overset{|}{\underset{|}{Si}}- \qquad (9)$$

and

$$2\left(-\overset{|}{\underset{|}{Si}}-O^-\right) + H_2O = -\overset{|}{\underset{|}{Si}}-O-\overset{|}{\underset{|}{Si}}- + 2OH^- \qquad (10)$$

The variation of water solubility with melt composition is determined by the sum of the contributions from reactions (9) and (10). The experimental data suggest that the contribution of (9) decreases and (10) increases with melt basicity.

Mysen et.al. (1976) recently examined CO_2 solubility in simple and complex melts at high pressure, and found that CO_2 is considerably more soluble in basic than in acidic melts. Again, two mechanisms of solution appear to be operative: in acidic melts (e.g. albite), CO_2 dissolves primarily as gas molecules; in basic melts (e.g. melilite nephelinite), however, carbonate formation appears to be the important solution mechanism.

4. Concluding and Cautionary Remarks

Most of the melt-structure information and theoretical

models described in the preceding pages apply only to simple two- and three-component silicate systems. It is probably apparent at this point that even simple glass-forming melts are neither straightforward nor well characterized. The structure of molten silica is well known, and it seems clear that in general the addition of a second oxide de-polymerizes the silicate network structure. However, some oxides are more effective in this function than others, and in few cases is it possible to specifically characterize the de-polymerization process by identifying anionic complexes. Most models and experimental measurements give only a time- and space-averaged picture of melt structure.

None of the work described in this section dealt with temperature dependence of melt structure, yet in view of the pronounced effect of temperature on viscosity (Cukierman and Uhlmann, 1973; Kushiro et.al., 1976), it is obvious that the structure of a given melt is temperature-sensitive.

The question of temperature dependence of melt structure brings to mind the problem of extrapolating results obtained on glasses to high-temperature liquids. Riebling (1968) stated that "the structures, or distribution of different polyhedral species, of an oxide melt and its corresponding glass are not very different." He also recognized a predictive relationship between the density of a glass and that of a melt of the same composition, and concluded that the relative partial molar volumes of components in simple glasses are the same as in the

corresponding melts. Boon and Fyfe (1972), on the other hand, suggested that failure to quench in high-temperature coordination polyhedra of ferrous ions gave unexpected Mössbauer results on their glasses. It therefore seems risky to extrapolate low-temperature ion exchange data on site types in glasses to the molten state. My personal feeling is that the overall polymeric structure of a silicate melt is in most cases readily quenchable (this idea is compatible with the common definition of a glass as a supercooled liquid). However, it does not necessarily follow that high-temperature coordination polyhedra of non-glassforming cations will be quenched in. The quenchability of any structure in a melt is, of course, dependent on the composition of the melt. It is widely recognized that the kinetics of all transformations are far slower in silicic melts than in basic ones.

The validity of the experiments described in the following sections of this thesis depends only upon quenching in a high-temperature distribution of elements between phases, and not upon structural identity between a glass and its melt.

PART I. TWO-LIQUID PARTITION COEFFICIENTS: EXPERIMENTAL DATA AND GEOCHEMICAL IMPLICATIONS

1. Introduction

In recent years, the accumulation of experimental and analytical data on partitioning of elements among silicate phases has resulted in a general knowledge of the relative preference of different trace cations for crystalline compounds coexisting with silicate liquid. In most studies (e.g. Nagasawa and Schnetzler, 1971), differences among elements in their crystal-liquid partitioning behavior are attributed to varying compatibility of the respective cations in the rigid crystalline lattice under consideration. This approach is reasonable, because the radii of cations and the sizes of cationic sites in minerals are generally known. However, as recognized by Burns and Fyfe (1964), Whittaker (1967), and Banno and Matsui (1973), site availability in the silicate liquid must also influence the distribution of trace cations between minerals and coexisting liquid. Thus, the behavior of trace elements in magmas is not solely determined by the nature of the crystals, but also by the short-range structural characteristics of the melt phase. The preceding "previous work" section has established that the structure of molten silicate is composition-dependent; it is therefore reasonable to expect that the compatibility of trace cations in a melt will be influenced by the major element chemistry.

Part I of this thesis describes a series of partitioning experiments designed to investigate directly the relative site[1] availability in basic and acidic silicate melts by high-temperature equilibration of immiscible liquids in the system K_2O-FeO-Al_2O_3-SiO_2.

2. Experimental Philosophy and Objectives

The stable coexistence of acidic and basic silicate melts at reasonable magmatic temperatures provides a unique opportunity to examine the relative compatibility of trace cations in liquids of different bulk composition. The equilibrium distribution of trace elements between immiscible acidic and basic liquids should give qualitative information on the types of sites that are present in the two melts. To this end, I undertook an isothermal series of 1 atm doping experiments, involving systematic addition of trace and minor elements to immiscible 4-component liquids.

Bulk liquid compositions on the two-liquid boundary of the system K_2O-FeO-Al_2O_3-SiO_2 (Roedder, 1951) were selected for study (see Fig. 6 and Table 2). This system affords stable, low-temperature immiscibility between liquids that are relatively simple, yet broadly analogous to natural melts. The two liquids contain all of the major cation types present in magmas:

---

[1] The term "site" is used here to refer to an average structural position relative to oxygen and other cations in the melt.

Figure 6. Coexisting liquid compositions at 1180°C in the system K_2O-Al_2O_3-FeO-SiO_2. The molar ratio of total K_2O:total Al_2O_3 in all experiments is 1:1. However, immiscible liquids differentially partition these components, thus altering the 1:1 ratio in both liquids and necessitating the use of the sum (K_2O+Al_2O_3) to plot the diagram (see Table 2 for mole percentages of oxides in an immiscible liquid pair). Symbols: triangles, circles, and diamonds represent immiscible liquid pairs after 14 hours at temperature, starting as Lc+Fa+SiO_2 mechanical mixtures of intermediate composition; crosses, immiscible liquids resulting from 2-day equilibration of fragments of two glasses whose compositions lie outside of the immiscibility volume; squares, immiscible liquid compositions after 4-1/2 hours (inner pair) and 14 hours (outer pair), starting as an intermediate mechanical mixture of Lc, Fa, and SiO_2 glass; A and B are conjugate liquids A and B used for partitioning studies, obtained by melting MAJ2 mechanical mixture (run times up to 108 hours); plus sign, composition melting to a single liquid at 1180°C. Dashed line is the intersection of the 1180° isotherm with the two-liquid volume; dotted line is the approximate position of the tridymite liquidus at 1180°C; dot-dash line is the (nonisothermal) intersection of the immiscibility volume with the liquidus surface of the Lc-Fa-SiO_2 system (modified from Roedder, 1951). Most tie lines are omitted for the sake of clarity.

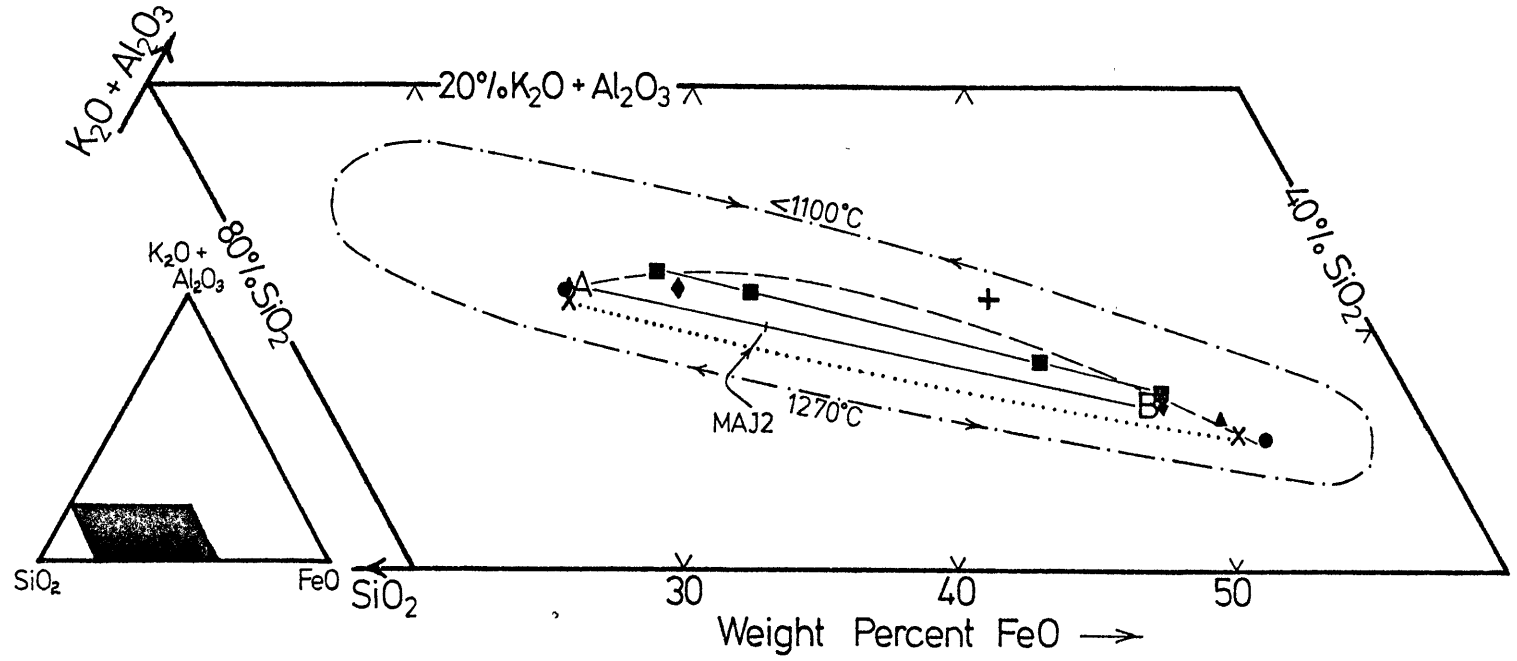

$K_2O + Al_2O_3$
20% $K_2O + Al_2O_3$
40% SiO_2
80% SiO_2
$K_2O + Al_2O_3$
≤1100°C
1270°C
A
B
MAJ2
SiO_2
FeO
SiO_2
30
40
50
Weight Percent FeO →

Figure 6

Table 2. Mole per cent oxides in immsicible acidic (A) and basic (B) liquids (see Fig. 6 and text) compared with some common igneous rocks. For natural rocks, oxides of divalent cations and alkali oxides are separately summed for comparison with FeO and K_2O, respectively, of liquids A and B.

	average dacite[a]		liquid A	average abyssal tholeiite[b]		average basalt[a]		liquid B
SiO_2	69.2		74.0	51.5		54.3		55.8
TiO_2	0.5		--	1.2		1.6		--
Al_2O_3	10.7		3.6	9.8		8.9		2.3
FeO[c]	4.6	Σ14.4	18.4	10.0	Σ34.7	10.4	Σ32.4	40.1
MgO	3.4		--	12.1		10.1		--
CaO	6.4		--	12.6		11.9		--
Na_2O	4.2	Σ 5.2	--	2.8	Σ 2.9	2.3	Σ 2.9	--
K_2O	1.0		4.0	0.1		0.6		1.8

[a] from Nockolds (1954)

[b] from Cann (1971)

[c] all Fe expressed as FeO

Si^{4+} (glass-former), Al^{3+}, divalent cation (Fe^{2+}), and alkali (K^{+}). When compared on a molar basis, the melt compositions differ appreciably from magmatic liquids only in their lesser alumina content (Table 2).

I examined the distribution of 14 trace or minor elements (Cs, Ba, Sr, Ca, Mg, La, Sm, Lu, Mn, Ti, Cr, Ta, Zr, and P) between the immiscible acidic and basic melts. This group represents a variety of geochemically "compatible" and "incompatible" elements whose cations have widely varied properties. All experiments were performed at the same temperature (1180°C) and pressure (1 atm), so that observed differences in partitioning behavior could be attributed solely to differences in cation properties.

In principle, the experiments described here are similar to previous solid glass-molten salt ion exchange studies described on page 36 of this thesis. My approach has the disadvantage of lacking a phase in which the activities of the exchanging ions are known. On the other hand, my experiments definitely represent high-temperature equilibrium, and the hazards of extrapolating site types from glasses to melt are absent.

3. Experimental and Analytical Methods

Starting materials.

Except where noted otherwise, starting materials for all experiments described in Part I consisted of mechanical mix-

tures of silica glass and synthetic leucite and fayalite. These compounds are stable to water adsorption, essentially stoichiometric, and comprise the endmember components of the pseudo-ternary system Lc-Fa-SiO_2, whose liquidus surface is intersected by the two-liquid volume of the K_2O-FeO-Al_2O_3-SiO_2 tetrahedron (Roedder, 1951). The silica glass, as well as the K_2CO_3, Al_2O_3, and Fe_2O_3 used in the synthesis of leucite and fayalite, were purchased from Spex Industries, Inc. The minimum purity of these chemicals was 99.9999+ per cent.

Leucite synthesis. Leucite was synthesized essentially by the method of Schairer and Bowen (1955). A $K_2O \cdot 4SiO_2$ glass was prepared first by melting down pre-weighed amounts of K_2CO_3 and SiO_2 over a period of 4 days, gradually raising the temperature of the mix from 750 to 1100°C. By this procedure, the weight loss due to CO_2 evolution was less than 1% more than the predicted value; the slight excess weight loss was assumed to be volatilized K_2O, which was replaced by adding the requisite amount of K_2CO_3. The glass was then crushed to a coarse powder, mixed with the required amount of Al_2O_3, and crystallized at 1200°C (with intermittent crushing and mixing) to leucite. The final product was inspected optically to assure complete crystallization, and an x-ray diffraction pattern was obtained.

Fayalite synthesis. Pure fayalite was prepared by solid-state reaction of wüstite and silica glass powder. Wüstite was obtained by careful hydrogen reduction of Fe_2O_3 at 600°C (a small

amount of Fe metal impurity usually resulted from this procedure, but this was readily removed magnetically). A final check of wüstite purity was made by x-ray diffraction. Wüstite and silica glass powder were then intermixed in proportions such that a ∿10% excess of iron oxide would remain after all silica went to form fayalite (I found that this procedure greatly reduced the fayalite synthesis time). The wüstite + SiO_2 mixture was placed in an alumina boat lined with platinum foil and heated in N_2 at 1000°C overnite. The resulting product was a greenish-yellow briquet speckled with black iron oxide. The briquet was ground in agate to a fine powder, returned to the N_2 furnace, and heated again at 1000°C overnight. This procedure was repeated two additional times, until unreacted SiO_2 was no longer visible under the microscope. At this point, the product consisted of ∿90% fayalite + ∿10% iron oxide. The iron oxide was reduced to metallic Fe by briefly heating the mixture in a gentle flow of H_2. A pure fayalite separate was obtained by grinding the mixture in agate to a fine powder, suspending the powder in acetone in a large watch glass, and pulling out the iron particles with a strong permanent magnet.

Experimental apparatus and run conditions.

Experiments were performed in vertical, platinum-wound, 1 atm quench furnaces, with temperature control apparatus reliable to better than ±2°C. The temperature was monitored with Pt/Pt10Rh thermocouples calibrated at the melting point of gold.

If the initial calibration of a new thermocouple was more than 1° off at 1063° (Au M.P. on Geophysical Laboratory scale), the thermocouple was re-welded and re-calibrated.

Charges of 20-40 mg were contained in pure iron capsules sealed in evacuated silica glass tubes (see Fig. 7). For a constant bulk composition, this capsule arrangement established the same low f_{O_2} for all experiments (∿iron-wüstite buffer, or $10^{-12.1}$ atm at 1180°C), and ensured that most iron in the silicate charges was ferrous[2]. Runs were quenched in 4-5 seconds by dropping the silica glass tubes into water.

Two minor problems were encountered in using the evacuated silica glass tube method: 1) during long runs (>2 days), small amounts of oxygen diffused through the glass tube wall; and 2) some K_2O was lost from the charges through volatilization into the vacuum space. Diffusion of oxygen through the glass tube was evidence by formation of fayalite on the outside of the iron capsule where it was in contact with SiO_2:

$$2Fe_{capsule} + O_{2\,diffusion} + SiO_{2\,tube} \rightarrow Fe_2SiO_{4\,fayalite}$$

This process appeared to have no effect on the experimental charge inside the iron capsule; it did, however, through local crystallization of the glass tubes, limit possible run duration to about 8 days.

The amount of K_2O volatilized during experimental runs

---

[2] Bowen and Schairer (1932) and Roedder (1951) found that iron-rich silicate melts in equilibrium with Fe metal contain a small percentage of Fe_2O_3 (usually about 2% of total iron is ferric).

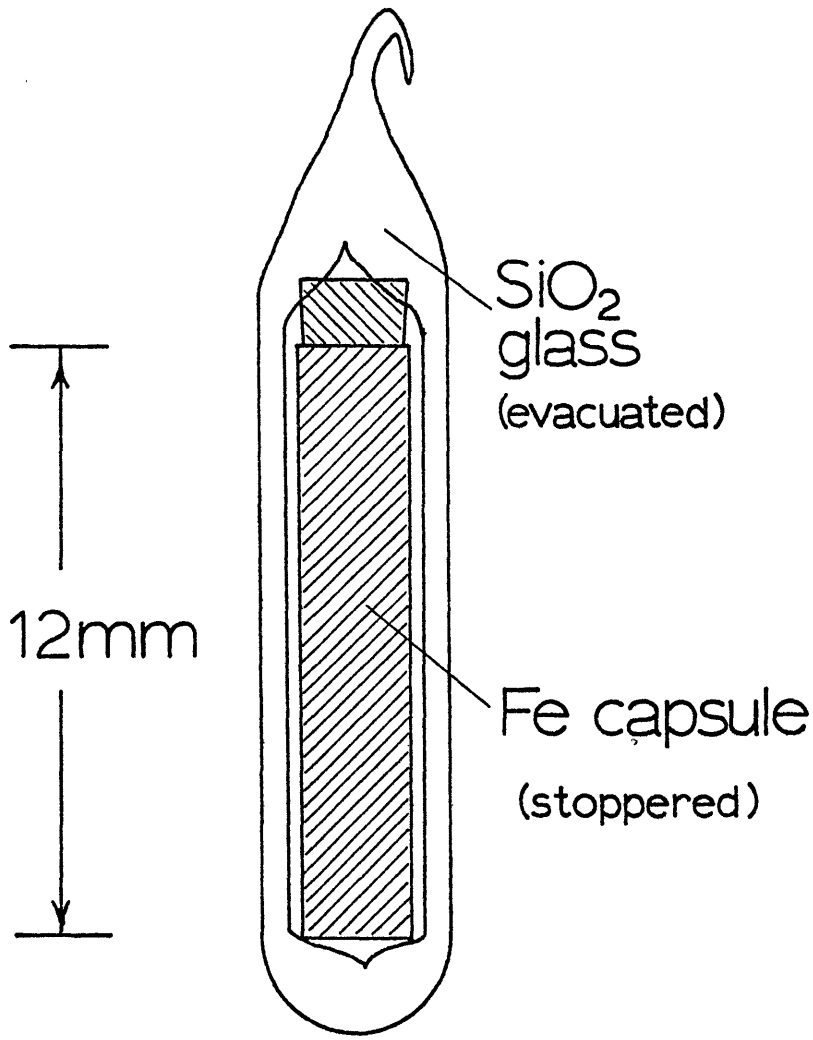


Figure 7. Container arrangement for two-liquid partitioning experiments: iron metal capsule enclosed in evacuated silica glass tube

could be gauged only by comparing microprobe analyses of the quenched charges with the starting compositions. No more than 5% of the total K_2O was lost during standard 4-day runs.

Preliminary experiments.

Low-temperature liquid immiscibility in the system K_2O-FeO-Al_2O_3-SiO_2 has been documented by Roedder (1951). However, his phase diagram provides little information about the shape and extent of the two-liquid volume except where it intersects the leucite-fayalite-silica liquidus surface. Preliminary experiments were performed in order to obtain an isothermal section through the two-liquid volume at 1180°C, and to examine the rate and mechanism of melting of Lc-Fa-SiO_2 mechanical mixtures to a two-liquid charge. The intersection of the two-liquid volume with the 1180° isotherm, delineated in Fig. 6, confirms the general shape of the two-liquid volume as deduced from Roedder's (1951) Lc-Fa-SiO_2 phase diagram. The system is not ternary, however, because immiscible liquids differentially partition K_2O and Al_2O_3, thus perturbing in the two liquids the 1:1 molar ratio of these oxides that characterizes a leucite component.

Beginning as Lc+Fa+SiO_2 mechanical mixtures, compositions within the two-liquid volume were found to melt completely and undergo phase separation in about 4 hours at 1180°C. However, the initial immiscible liquid compositions were less extreme (Fig. 6) than the equilibrium compositions obtained by maintaining temperature for an additional 8-10 hours. After 14 hours,

globules of the two liquids, each including the other, were as large as 400 μm in diameter (Fig. 8).

Partitioning experiments.

For two-liquid partitioning studies, a bulk composition (MAJ2; see Fig. 6) was selected that would yield an acidic liquid (liquid A) and a basic liquid (liquid B) in the ratio of 7:3[3] at 1180°C (see Fig. 6 and Table 2). A 40-gram batch of MAJ2 composition was mixed from the leucite, fayalite, and silica endmembers. A final adjustment to this bulk composition was made by adding a small amount of wüstite of known composition; this addition compensated for the iron lost from the silicate melt by the incongruent melting of fayalite to iron metal + liquid (Bowen and Schairer, 1932).

The MAJ2 composition was doped with a single minor element in amounts ranging between about 0.1 and 1 weight per cent. Except in P and Cs partitioning experiments, the minor element was added in oxide form and thoroughly premixed with the starting material by grinding in an agate mortar. Phosphorus was added and premixed in elemental form, and Cs as $CsNO_3$.

Although two-day run times were found sufficient to equilibrate the immiscible liquids at all examined concentrations of the alkaline earth elements, a standard run time of 4 days was

---

[3] I selected a 7:3 ratio for two reasons: 1) excellent large-scale phase separation was achieved; and 2) gravitational separation of the two phases during the runs was kept to a minimum.

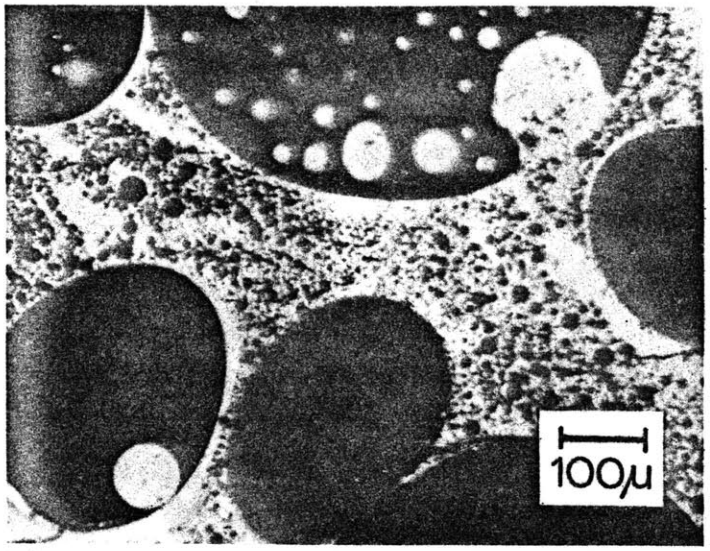


Figure 8. Immiscible liquids A (light) and B (dark), quenched from 1180°C after 4 days at temperature. Although not shown in this photograph, many charges contain a few crystals of tridymite, because the addition of small amounts of multivalent cations shifts the tridymite liquidus into the two-liquid volume

adopted. This run duration was insufficient only in the case of phosphorus, which, even after 7 days at 1180°C, showed inhomogeneous distribution within the two glass phases.

Analysis of charges.

The quenched two-glass charges were analyzed by electron microprobe for both major and trace or minor constituents. Major elements were determined first, using a fully automated Materials Analysis Company electron microprobe (Finger and Hadidiacos, 1972), operating at an accelerating voltage of 15 kV and a sample current of about 0.04 μA, with a beam spot of ∿6 μm diameter. Potassium volatilization under the electron beam during analysis was found to be insignificant. At least 3 replications on each glass phase of every charge was measured, in order to ensure major element equilibration and homogeneity, and to discern any effects of minor components on the bulk compositions of the coexisting liquids. Major element data for all experimental runs are summarized in Appendix I, which also includes a list of standards used for the analyses.

Trace and minor elements were determined by manual operation of the MAC electron microprobe. Tantalum and lutetium were excited by 20-kV electrons; all other elements were analyzed at 15 kV accelerating potential. The sample current was varied between 0.04 and 0.10 μA in order to maximize the count rate for a given element. Counting time per analysis spot ranged from 50 to 500 seconds (most were 100 or 200 seconds),

selected to give probable counting errors of better than 10% for all analysis spots except those on the lowest Ba, P, Ta, and Lu concentrations, which were about 15, 20, 20, and 25%, respectively. Appendix II lists counting times, peak-to-background ratios, counting errors, and standards for trace and minor element analyses. Background count rates for low-concentration elements were measured for 500 seconds (100 seconds each on 5 spots) on each phase of a blank two-glass sample of the same bulk composition as that used for partitioning experiments. Backgrounds determined by this procedure were found to be indistinguishable from those obtained by detailed peak scanning on the unknowns. Raw count data were compared to counts rates on synthetic standards (Appendix II) to obtain nominal concentration values. These nominal values were corrected for absorption and fluorescence effects by the method of Albee and Ray (1970), except in the cases of Ta and Lu, for which MAGIC (Colby, 1968) was used. Only in the case of Mg did the applied corrections affect the nominal values by more than 4%. For minor and trace elements, ten replicate spots were counted on each of the two glass phases in every charge.

Criteria for equilibrium and reversal of Ti experiments.

The primary criterion for equilibrium in all experiments was homogeneous distribution of the trace or minor element in both phases of the two-liquid charge, as indicated by low variance among ten replicate analysis points on each phase (see error bars in Figs. 9-14 and Table 3). The charge was

prepared for electron microprobe analysis by crushing to <0.5 mm fragment size, embedding the fragments in a 2x10 mm epoxy disk, and thin-sectioning the disk. This method insured that the entire charge was represented in the analysis, and that the polished surface of the section intersected at random any globule chosen for analysis.

The attainment of equilibrium was rigorously tested in titanium[4] experiments by approach from different directions. Separate glasses of liquid A and liquid B composition were prepared by fusing mixtures of Al_2O_3, SiO_2, and synthetic fayalite and potassium disilicate at 1350°C in iron capsules. A split of each mixture was doped with TiO_2 (∿0.25 and 0.38 wt.%, respectively, in compositions A and B) before fusion. Glass fragments (<0.5 mm) of Ti-bearing liquid A composition were then equilibrated at 1180°C with fragments of undoped liquid B for 4 days. Similarly, Ti-bearing B composition glass was equilibrated with undoped acidic glass. The results of these experiments are included in Fig. 11, which shows the excellent agreement of these reversal experiment results with each other and with the Ti partitioning data obtained using crystalline mechanical mixtures as starting material.

---

[4] Ti was selected for this purpose because, as a tetravalent cation, its diffusion rate should be slower than most other elements examined. Also, probable counting error is very low for Ti analysis.

4. Results and Interpretations

Partition coefficients.

The results of doping experiments on Cs, Ba, Sr, Ca, Mg, La, Sm, Lu, Mn, Ti, Cr, Zr, Ta, and P are presented in Figs. 9-14 and Table 3. The data may be compared with the qualitative predictions of Hess and Rutherford (1974), who stated that: 1) cations able to replace Si^{4+} in melts (e.g. Al^{3+}) and cations required for local charge balance in the copolymerization of AlO_4 and SiO_4 tetrahedra (alkalies, Ba^{2+}) would be enriched in the more acidic of two coexisting liquids; and that 2) cations of high field strength (charge/radius) would favor the basic melt if copolymerization with SiO_2 were not possible. The predictions of these authors are generally confirmed by the present data, except that barium behaves more like the other alkaline earth elements than like potassium. The two-liquid partition coefficient, here defined as

$$D_{B/A} = \frac{\text{concentration in Basic (Fe-rich) liquid}}{\text{concentration in Acidic (Si-rich) liquid}},$$

does not, however, show a simple dependence on cation field strength (Fig. 16).

Alkali and alkaline earth elements (Cs, Ba, Sr, Ca, Mg). The nearly equal distribution of the large alkaline earth elements (Ba, Sr) between acidic and basic melts (Fig. 9) suggests either that they do not occupy the same structural position in the melt as Fe^{2+}, or that substitution for Fe^{2+} is more

Table 3. Summary of two-liquid partitioning data

Element	Wt.-% in basic glass	σ (10 pts)	Wt.-% in acidic glass	σ (10 pts)	$D_{B/A}$	Element	Wt.-% in basic glass	σ (10 pts)	Wt.-% in acidic glass	σ (10 pts)	$D_{B/A}$
Cs	0.038	0.005	0.127	0.011	0.30	Sm	0.175	0.010	0.034	0.006	5.15
Cs	0.069	0.009	0.228	0.012	0.30	Sm	0.431	0.010	0.100	0.012	4.31
Cs	0.114	0.008	0.368	0.010	0.31	Sm	0.744	0.034	0.175	0.015	4.25
						Sm	0.984	0.032	0.233	0.023	4.22
Ba	0.101	0.020	0.063	0.022	1.60	Sm	1.144	0.050	0.273	0.012	4.19
Ba	0.142	0.012	0.087	0.015	1.63						
Ba	0.261	0.021	0.180	0.020	1.45	Mn	0.173	0.010	0.056	0.012	3.09
Ba	0.530	0.029	0.369	0.028	1.44	Mn	0.368	0.028	0.128	0.016	2.88
Ba	0.819	0.042	0.600	0.032	1.37	Mn	0.570	0.024	0.199	0.019	2.86
						Mn	0.742	0.016	0.256	0.021	2.90
Sr	0.20	0.03	0.15	0.02	1.33						
Sr	0.66	0.03	0.46	0.03	1.44	Cr	0.132	0.006	0.041	0.005	3.22
Sr	0.94	0.04	0.51	0.04	1.84	Cr	0.326	0.015	0.076	0.007	4.29
Ca	0.179	0.011	0.057	0.009	3.14	Ti	0.170	0.010	0.057	0.004	2.98
Ca	0.243	0.008	0.093	0.010	2.61	Ti[a]	0.193	0.008	0.063	0.003	3.06
Ca	0.350	0.008	0.151	0.010	2.32	Ti	0.260	0.007	0.086	0.005	3.02
Ca	0.429	0.011	0.186	0.009	2.31	Ti[a]	0.304	0.019	0.106	0.009	2.87
Ca	0.515	0.013	0.265	0.008	1.94	Ti	0.484	0.021	0.160	0.003	3.03
Ca	0.665	0.023	0.372	0.017	1.79	Ti	0.616	0.038	0.189	0.015	3.26
						Ti	0.766	0.030	0.231	0.013	3.32
Mg	0.139	0.011	0.065	0.006	2.14						
Mg	0.290	0.012	0.130	0.010	2.23	Zr	0.241	0.022	0.095	0.006	2.54
Mg	0.420	0.010	0.190	0.009	2.21	Zr	0.528	0.022	0.232	0.013	2.28
Mg	0.631	0.019	0.310	0.011	2.04	Zr	0.662	0.042	0.281	0.018	2.36
Mg	0.700	0.021	0.330	0.013	2.12	Zr	0.980	0.023	0.429	0.012	2.28
La	0.250	0.010	0.058	0.004	4.31	Ta	0.318	0.024	0.072	0.019	4.42
La	0.418	0.013	0.113	0.007	3.70	Ta	0.664	0.044	0.153	0.021	4.34
La	0.660	0.018	0.178	0.007	3.71	Ta	1.007	0.047	0.241	0.023	4.18
Lu	0.328	0.024	0.046	0.016	7.13	P	0.240	0.053	0.018	0.010	13.33
Lu	0.560	0.026	0.134	0.030	4.18	P	0.317	0.063	0.038	0.010	8.34

[a] Reversal experiments (see text)

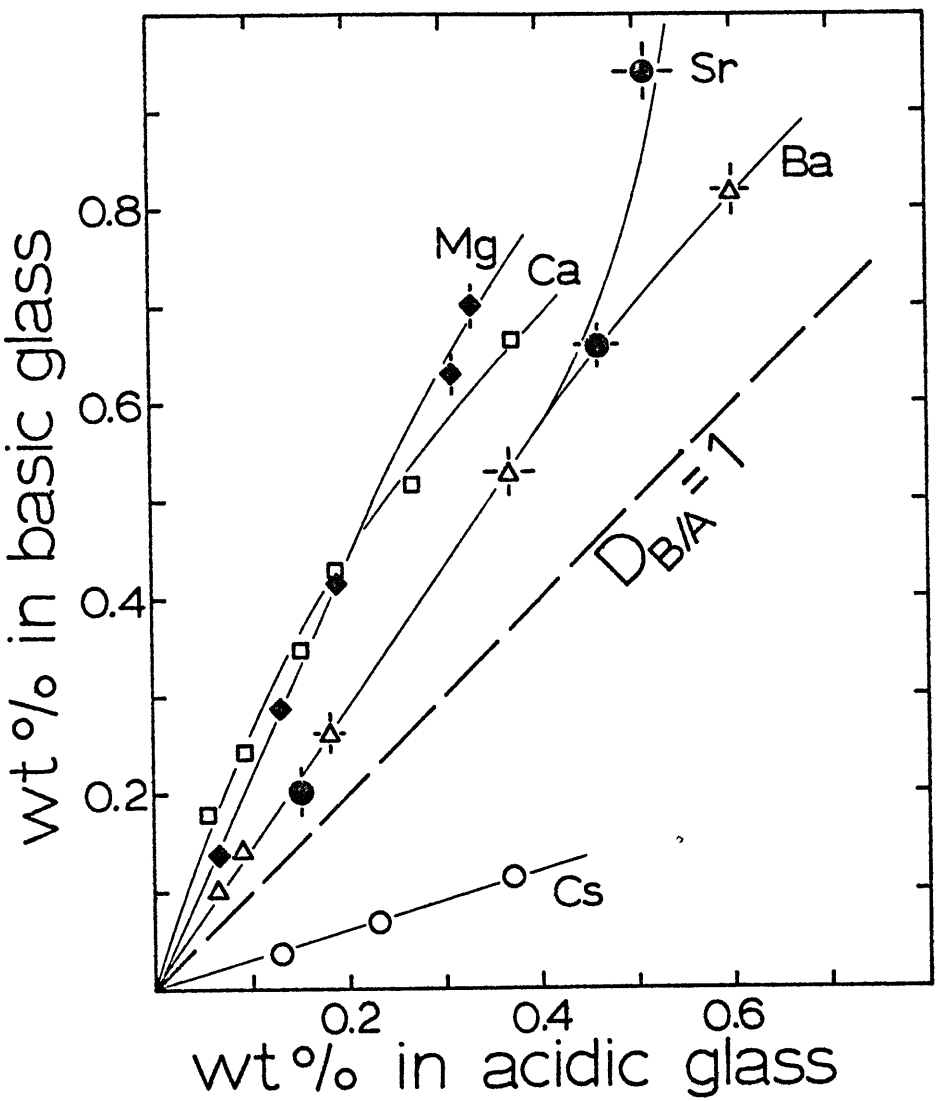


Figure 9. Graphical illustration of the distribution of trace and minor amounts of alkali and alkaline earth elements between liquids A and B at 1180°C. Error bars (±2 standard errors) show counting precision based on ten separate analysis spots on each glass phase (see text)

favorable in the acidic than in the basic melt. It is possible that more than one type of site is involved (e.g., both K^+- and Fe^{2+}-type sites). The smaller alkaline earth elements, on the other hand, probably assume structural roles very similar to that of Fe^{2+}, and are similarly partitioned between coexisting liquids (Fig. 9). In fact, the distribution of trace amounts of Mg between the two liquids is identical with the distribution of Fe, a major component of the system. The ratio of Mg/Fe in the two liquids is therefore the same, which implies complete interchangeability of Mg^{2+} and Fe^{2+} in silicate melts. At very low concentration, Ca^{2+} shows more enrichment in the basic melt than Mg^{2+}, indicating that Ca^{2+} does not so readily replace Fe^{2+} in the acidic melt.

The general trend of increasing enrichment in the acidic melt with increasing size of alkaline earth elements and Cs is evidence that acidic melts are more open-structured (or less efficiently packed on an atomic or molecular level) than basic melts. Such a structure might result from relative "inflexibility" of the more complex silica network shown by Hess (1970) to characterize acidic liquids.

Rare earth elements (La, Sm, Lu). The rare earth elements (REE) examined are enriched in the basic melt by a factor of 4 to 5 (see Fig. 10). As indicated by the error bars, the Lu data are subject to considerable uncertainty, but $D_{B/A}$ appears to increase slightly with decreasing ionic radius of the REE. The overall similarity in partitioning of La, Sm, and Lu sug-

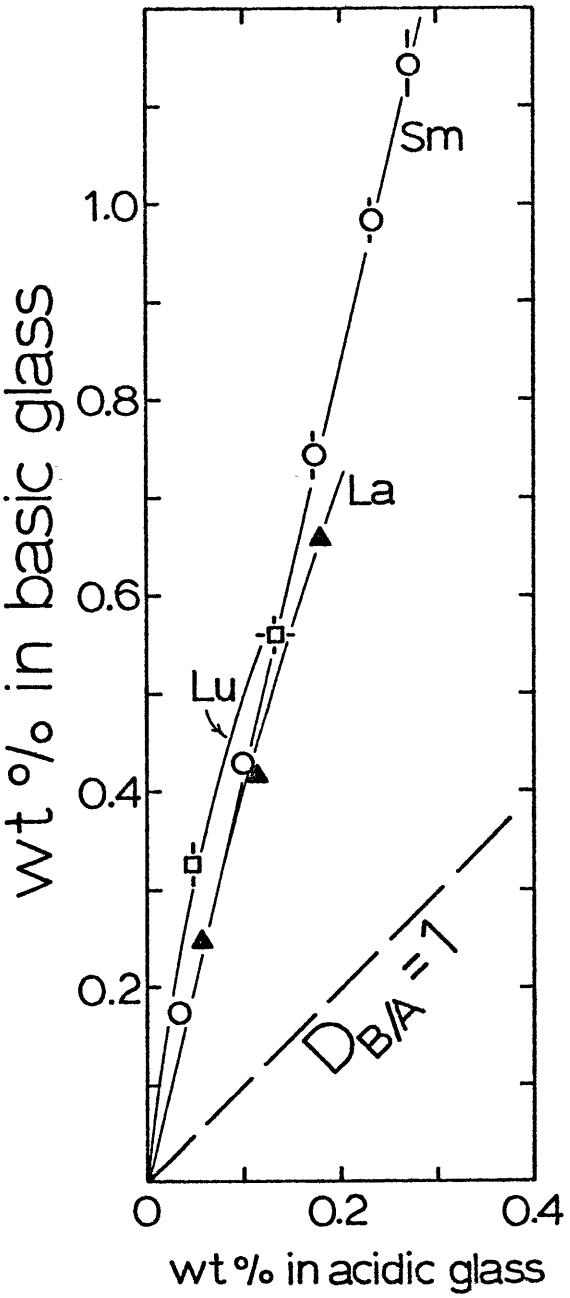


Figure 10. Partitioning of rare earth elements between liquids A and B at 1180°C. Error bars = ±2 standard errors

gests that the lanthanide contraction does not influence the structural position of REE in silicate melts. Because the REE are strongly enriched in Al-poor (basic) melt, it can be concluded that the REE cations are too large to replace Si^{4+} as glass-forming cations in the manner described by Day and Rindone (1962b) for Al^{3+}. Clearly, cation charge alone does not determine substitution behavior in silicate liquids.

Transition elements (Cr, Ti, Mn). The data presented in Fig. 11 for Cr, Ti, and Mn are incomplete as an examination of transition metal behavior in general, because two geochemically important elements, Co and Ni, were omitted in this initial study (these two elements are reduced in the presence of metallic iron capsules). The data obtained for Cr, Ti, and Mn are nonetheless interesting in their similarity: at low concentration (<2000 ppm metal in the basic melt), the partition coefficient ($D_{B/A}$) for all three elements is 3.0-3.3. Considering the differences in valence and octahedral site preference energy among the respective cations, this is a surprising result. A plausible inference is that site occupancy by transition metal ions is independent of charge in silicate liquids at high temperature. In other words, sites might exist in melts that can be filled by any cation of suitable size and bonding characteristics, regardless of valence.

An additional implication of the data in Fig. 11 is that two substitutions known to occur in crystalline silicates, $Cr^{3+} \rightleftarrows Al^{3+}$ and $Ti^{4+} \rightleftarrows Si^{4+}$ (Verhoogen, 1962), probably do not

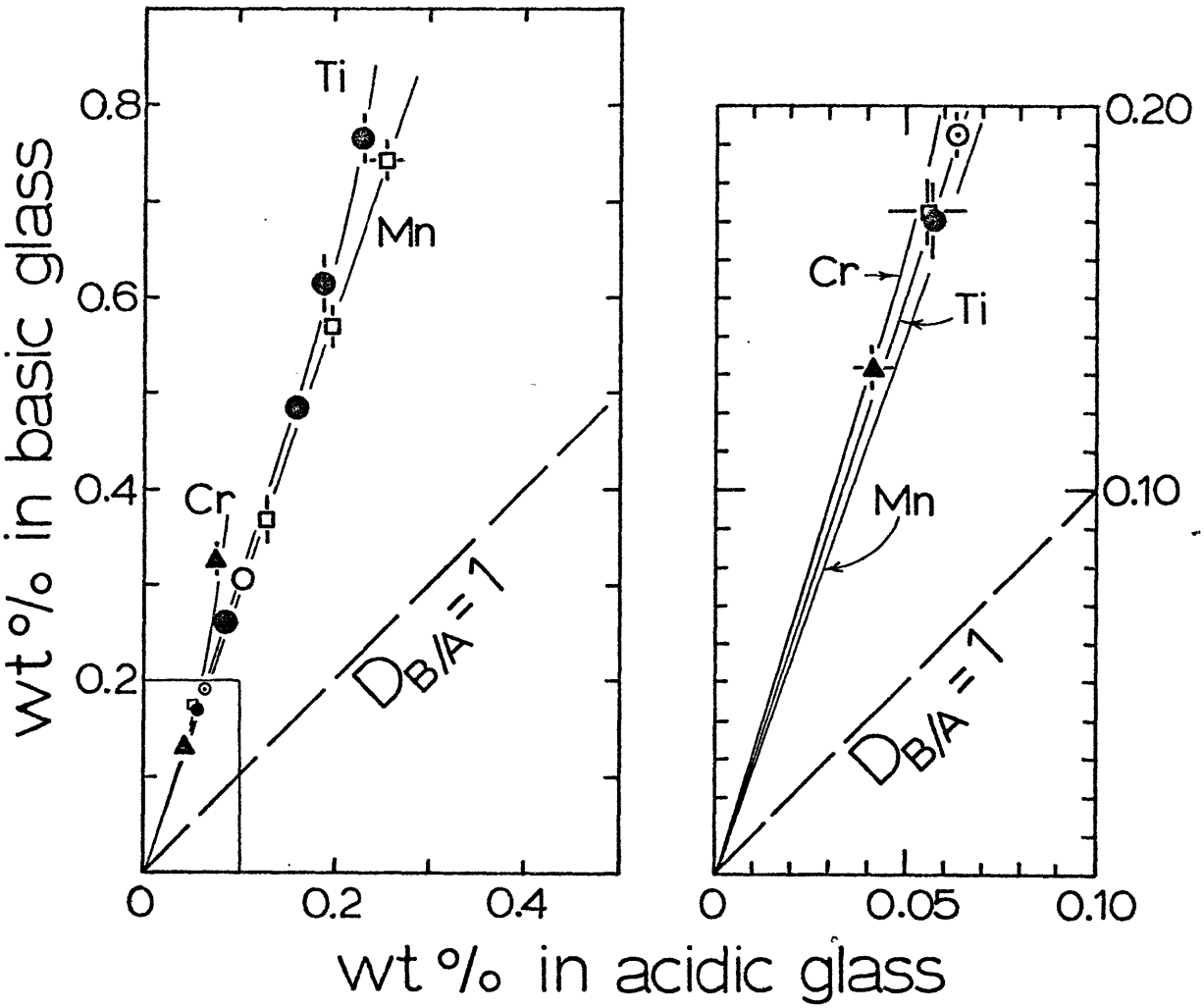


Figure 11. Partitioning of transition elements between liquids A and B at 1180°C. Only two data points were obtained for Cr because the melts were saturated with chromite at 0.32 wt% Cr in the basic melt (0.075% in the acidic melt). For titanium, solid circles represent partitioning values obtained using Lc+Fa+SiO_2 mechanical mixtures as starting material. The open-circle data point was obtained by equilibrating Ti-bearing B-composition glass fragments with undoped A-composition glass fragments. The dot-in-circle data point represents equilibrated glass fragments where all Ti was initially in the A-composition glass (see text). Error bars = ±2 standard errors

occur in liquids, because Cr and Ti are strongly depleted in the Al-, Si-rich (acidic) glass.

Highly-charged incompatible elements (P, Zr, Ta). Partitioning data for P, Zr, and Ta are summarized in Fig. 12. As previously mentioned, difficulty was encountered in equilibrating the immiscible liquids with respect to minor or trace amounts of phosphorus (this element is known to diffuse slowly in molten silicate [Doremus, 1973], probably because it exists as a large phosphate complex). Despite the inhomogeneity of phosphorus distribution (see error bars in Fig. 12), strong enrichment in the basic melt is obvious, and attests to the extreme incompatibility of this element in silicic liquids.

Like phosphorus, tantalum is assigned a valence of +5 in oxides and minerals, but in a two-liquid system tantalum shows less enrichment in the basic melt, again illustrating the subordinate role of cation valence to cation size and/or bond type in determining two-liquid partitioning behavior.

Zirconium, although tetravalent, is identical in ionic radius to Mg^{2+} (I.R. = 0.80Å for 6-fold coordination with oxygen [Whittaker and Muntus, 1970]), and is similarly partitioned between basic and acidic melts.

Effect of minor components on coexisting liquid compositions.

The addition of minor amounts of some oxides to immiscible liquids in the system K_2O-FeO-Al_2O_3-SiO_2 causes changes in the equilibrium major-element liquid compositions. Some elements

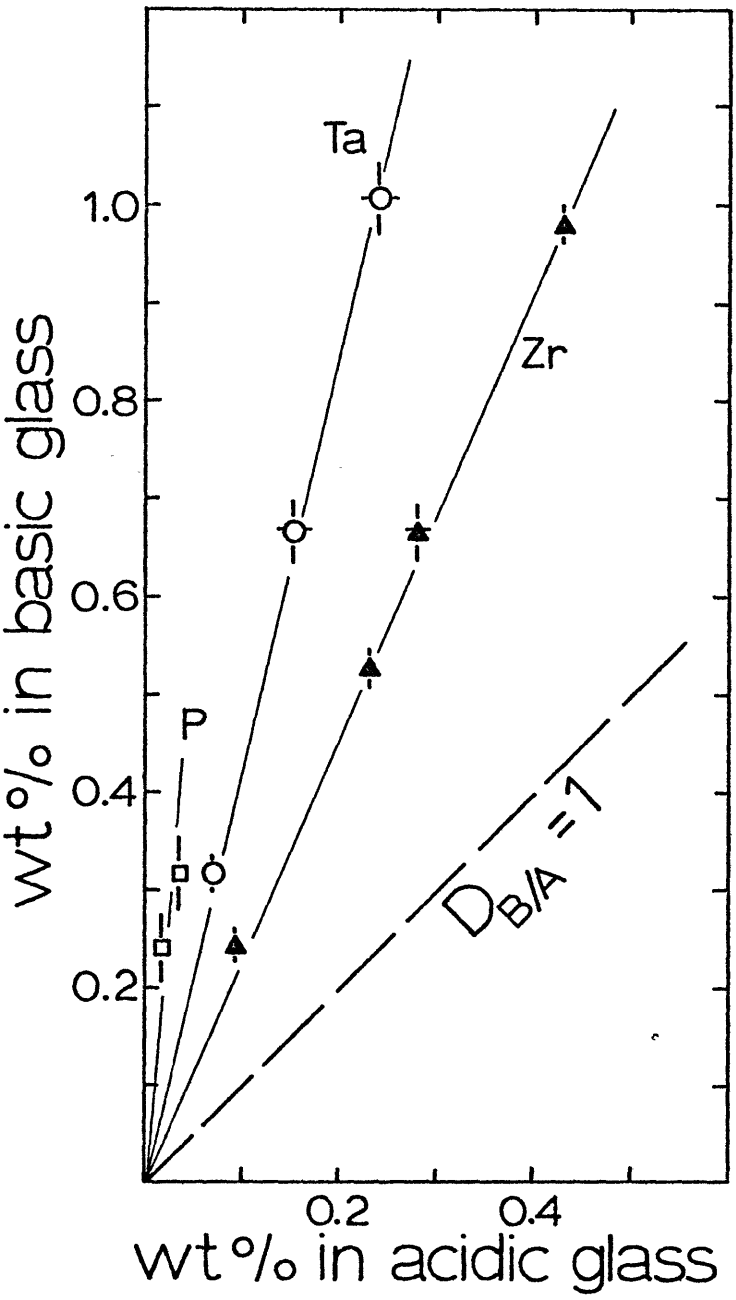


Figure 12. Partitioning of Ta, P, and Zr between liquids A and B at 1180°C. Error bars = ±2 standard errors. Large error bars on P data points reflect inhomogeneity in distribution of this element (see text)

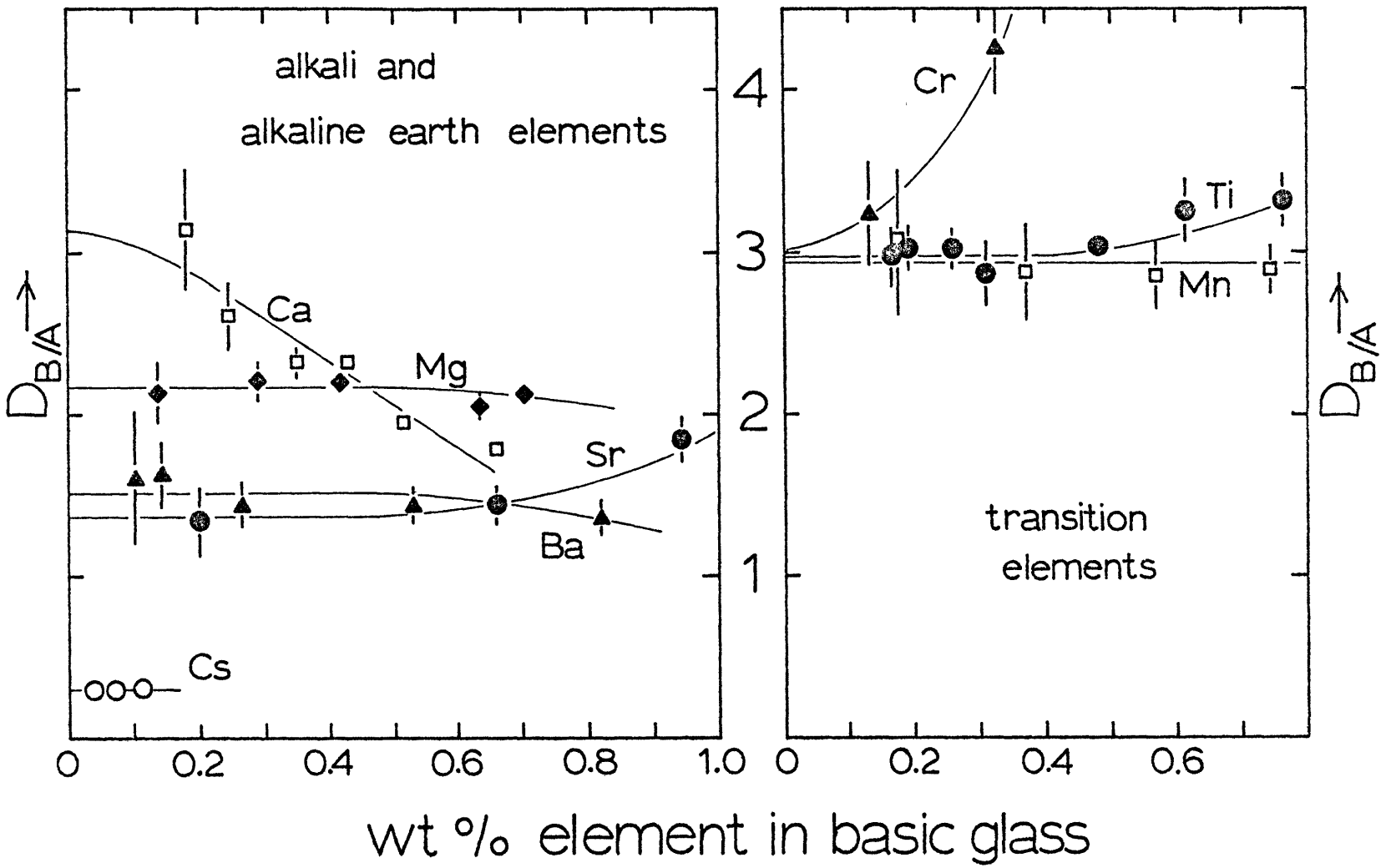


Figure 13. Two-liquid partitioning data for alkali, alkaline earth, and transition elements replotted (from Figs. 9 and 11) to show variation in $D_{B/A}$ with element concentration in basic glass. Error bars = ±2 standard errors

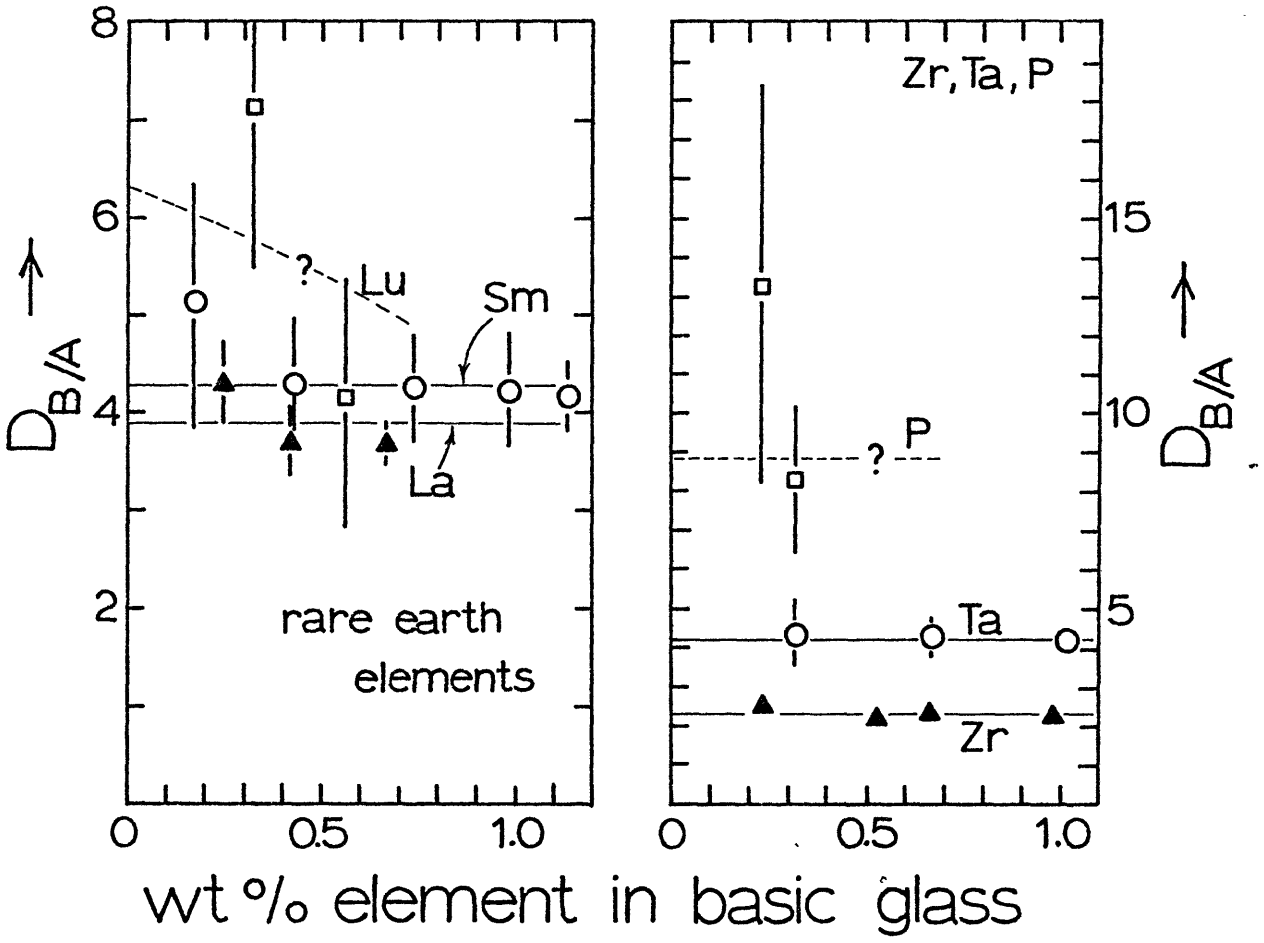


Figure 14. Two-liquid partitioning data for rare earth elements, Ta, Zr, and P replotted (from Figs. 10 and 12) to show variation in $D_{B/A}$ with concentration in basic glass. Error bars = ±2 standard errors

(Ti, Cr, REE, Ta, P) have the effect of broadening the miscibility gap, while most other elements cause slight convergence of the bulk compositions. These effects are potentially important to the prediction of immiscibility in magmas, and are therefore summarized in Fig. 15 for all elements examined in this study. Clearly, changes in immiscible liquid compositions must affect the minor- or trace-element partition coefficients, causing non-linearity in the data point trends of Figs. 9-14. As discussed in the next section, however, this nonlinearity is due at least in part to the breakdown of ideal dilute solution behavior.

5. Discussion

Systematics of two-liquid partitioning.

Hess and Rutherford (1974) suggested that high field-strength cations which are unable to assume tetrahedral coordination with oxygen are incompatible in highly-polymerized, silica-rich melts, and should therefore be partitioned into the more basic of two coexisting liquids. The validity of this hypothesis is supported by the common presence of stable two-liquid fields in binary silicate systems involving oxides of cations whose ionic potentials (charge/radius values) exceed about 1.5 (Glasser et.al., 1960). In the following paragraphs, the ideas of Hess and Rutherford are expressed as a general predictive model for trace element partitioning between basic and acidic liquids, which is subsequently tested against

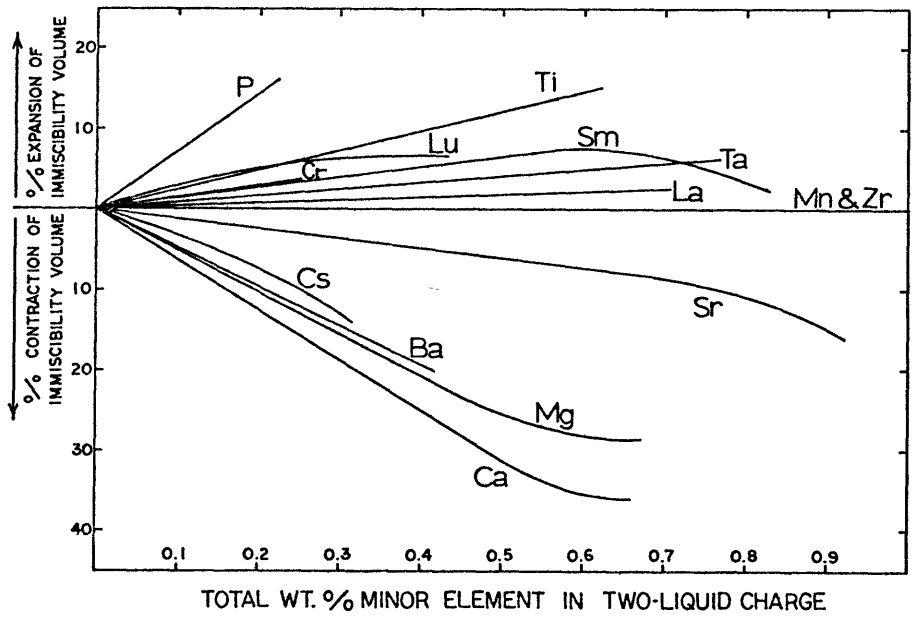


Figure 15. Graphical representation of the changes in equilibrium K_2O-Al_2O_3-FeO-SiO_2 liquid compositions induced by addition of a fifth component (designated by atomic symbol). Per cent expansion or contraction of immiscibility volume is gauged by FeO content of coexisting liquids, because the elongation of the immiscibility volume is directed almost toward the FeO endmember (Fig. 6)

the data obtained in this experimental study.

A basic melt, being less polymerized than an acidic one, contains more free oxygen ions and more oxygens linked to a single Si (Toop and Samis, 1962a,b). Consequently, there are more potential sites in a basic melt where high field-strength cations can be readily coordinated by oxygen. It is therefore not surprising that 13 of the 14 elements examined in this study are partitioned into the more basic of two coexisting liquids.

Following Hess and Rutherford (1974) and Levin and Block (1956), this "oxygen availability" argument could be used to predict relative two-liquid partition coefficients or relative compatibilities of different cations in a given silicate melt structure. In general: the greater the stabilization of a cation in its appropriate oxygen coordination polyhedron, the more it will be enriched in the more basic of two coexisting liquids. As a first approximation, cation-oxygen bond strength might be used as a relative measure of cation stabilization by an oxygen polyhedron. Assuming purely ionic bonding in silicate liquids, cation-oxygen bond energy is given by

$$\frac{2Ze^2}{R}$$

where Z = cation charge, e = the charge on an electron, and R = cation-oxygen interatomic distance. Cation stabilization in a polyhedron of oxygens, then, is proportional to Z/r (the ionic potential or field strength of the cation), where r is the cation radius.

The validity of these assumptions can be tested by plotting Z/r against the two-liquid partition coefficients obtained in this study (Fig. 16). The model successfully predicts that phosphorus (Z/r $\simeq$ 20) will be most enriched in the basic melt, and that cesium (Z/r $\simeq$ 0.5) will be least enriched, but for cations of field strength intermediate between these values, there is not a good correlation between $D_{B/A}$ and Z/r.

Possibly the weakest assumption in the predictive model proposed above is that cation-oxygen bonding in silicate melts is purely ionic. The charge/radius value, as a measure of ionic bond strength in the melt, cannot be expected to correlate well with the two-liquid partition coefficient for cations whose bond with oxygen is significantly covalent. The elements plotted in Fig. 16 can be classified (somewhat arbitrarily) by cation-oxygen bond type into two groups: those of >70% ionic character, and those of $\leq$65% ionic character. These two groups define two separate trends on a Z/r vs. $D_{B/A}$ plot (Fig. 16), each of which shows considerably less scatter than the data points on the whole. It is possible that the two trends outlined in Fig. 16 represent two different site types in the melt: one occupied by small, highly-charged cations whose bonding with oxygen is partially covalent and directional (P^{5+}, Ta^{5+}, Zr^{4+}, Cr^{3+}); the other by cations bound essentially by electrostatic forces (Cs^{+}, Ba^{2+}, Sr^{2+}, Mg^{2+}, Mn^{2+}, Ca^{2+}, La^{3+}, Sm^{3+}, Lu^{3+}).

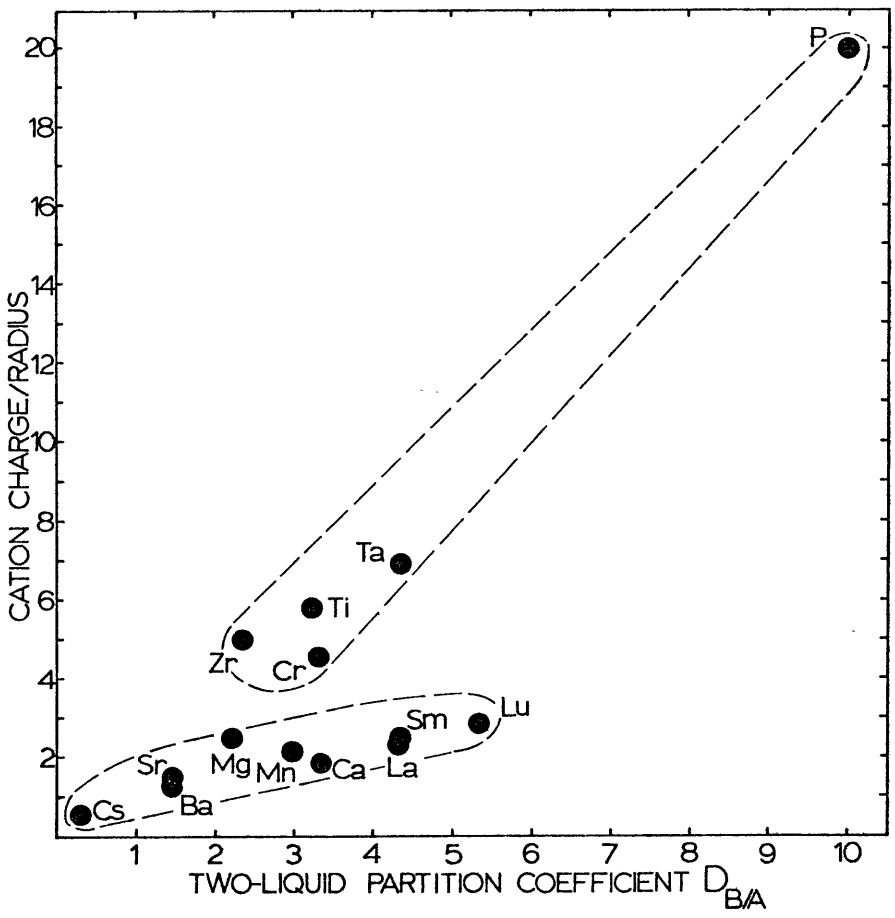


Figure 16. Plot of cation ionic potential (charge/radius) against the experimentally-determined two-liquid partition coefficient, $D_{B/A}$. Data points have been divided into two groups: the upper trend includes cations whose bonding with oxygen is $\leq$ 65% ionic; the remaining elements (lower trend) form bonds with oxygen of > 70% ionic character (see text). Ionic radii are those of Whittaker and Muntus (1970) for coordination determined by cation/oxygen radius ratio

Geochemical implications of two-liquid partitioning data.

Henry's Law. Henry's law states that the thermodynamic activity of a solute at low concentration can be approximated as a linear function of its concentration, i.e.:

$$a_i = K_i X_i \tag{11}$$

where a_i is the activity of a dilute component i in the solution, X_i is the concentration of component i, and K_i (termed the Henry's law constant) is constant, at a given temperature and bulk solvent composition, up to some maximum value of X_i. For two solutions A and B in equilibrium, each containing a small amount of component i, the following relation holds if i obeys Henry's law in A and B:

$$\Delta G_i^{A-B} = -RT\ln K_{eq} = -RT\ln a_i^B/a_i^A = -RT\ln \frac{K_i^B X_i^B}{K_i^A X_i^A} \tag{12}$$

where ΔG_i^{A-B} is the free energy charge associated with transferring a mole of i from A to B, when i is in its standard state in both phases, and K_{eq} is the equilibrium constant for the transfer reaction. Of major significance to partitioning studies is the fact that $K_{eq} = \frac{K_i^B X_i^B}{K_i^A X_i^A}$. For constant temperature and pressure, this implies that the partition coefficient, X_i^B/X_i^A, is constant as long as i obeys Henry's law in both A and B. Above a critical concentration level of i, a constant value of X_i^B/X_i^A cannot be expected, because the linear relation between a_i and X_i breaks down. From a geochemical viewpoint, it is of interest to know the concentration level to which Henry's law

is valid in silicate melts.

In addition to two-liquid partition coefficients, the data presented in Figs. 9-14 establish approximate limits of applicability of Henry's law for oxides dissolved in complex silicate melts. In general, the limit for a given element should correspond to the point where the plot begins to deviate from linearity (above which $D_{B/A}$ is no longer constant with increased concentration). At greater concentrations, Henry's law is no longer obeyed in one or both of the liquids (it is not possible to say in which). As discussed in the previous section, non-linearity in Figs. 9-14 may be caused by changes in major-element composition of the coexisting liquids. Information concerning Henry's law limits is nonetheless obtainable. The following observations are pertinent:

1) The definitely linear portions of the plots in Figs. 9-14 indicate Henry's law behavior in liquids A and B. Thus, Ba, Sr, Sm, Ti, Mn, Zr, and Ta show ideal dilute solution behavior up to at least 5000 ppm in the basic melt. Any curvature at higher concentration cannot be confidently attributed to the breakdown of Henry's law, because bulk liquid compositions do change.

2) Extreme curvature and apparent absence of a linear portion in a plot such as that of Ca (Fig. 9) probably indicates non-ideal behavior to very low concentration. Such curvature represents a factor-of-two decrease in $D_{B/A}$ over the composition interval studied, which is not likely to be induced by a 35%

narrowing of the liquid miscibility gap (Fig. 15).

3) Breakdown of Henry's law is indicated if the data plot for an element shows curvature opposite of that which would be caused by the observed change in major-element liquid compositions. For example, the data points for La (Fig. 10) suggest slight curvature to the right (decrease in $D_{B/A}$), yet the addition of La broadens the miscibility gap (Fig. 15).

Because of the difficulty in precisely establishing Henry's law limits for the elements studied, a complete inter-element comparison is not possible. However, there are some clear qualitative indications: 1) on an atom per cent basis, Mg^{2+} has the highest limit, probably because of its similarity in charge and radius to Fe^{2+}; and 2) most of the elements studied obey Henry's law in liquids A and B to concentrations well above those typically found in rocks. Because of the general compositional similarity of liquids A and B to natural melts (Table 2), I believe that these data are qualitatively applicable to natural systems, and might, in fact, be used in a general way to distinguish trace from minor elements in magmas.

Implications to solid-liquid partitioning.

It is commonly assumed in measuring and applying solid-liquid partitioning data that a trace element distribution coefficient is constant with changing liquid composition. Burns and Fyfe (1964), Banno and Matsui (1973), and Irvine (1974), among others, have recognized the fallacy of this assumption.

The present two-liquid partitioning data can be directly applied to this problem in a qualitative way. For example, Ba and Sr are only weakly partitioned into the basic liquid ($D_{B/A} \simeq 1.5$) at 1180°C, indicating that sites suitable for these ions are nearly as abundant in the silicic melt as in the less polymerized basic melt. By analogy, it is likely that natural intermediate to felsic liquids are almost as accommodating to the large alkaline earth ions as are basaltic liquids. Consequently, the distribution coefficients for Ba and Sr between a given solid phase and magmatic liquid should remain nearly constant with changing liquid composition (ignoring temperature dependence). However, this near-absence of liquid composition dependence would not be predicted for solid-liquid partitioning of transition metals, REE, Zr, Ta, and P. Figures 10-14 show that these elements are far more compatible in basic than in acidic liquids. Their solid-liquid partition coefficients would therefore increase with decreasing basicity of the melt in a fractional crystallization sequence. Cesium, on the other hand, would show progressively stronger enrichment in the melt phase of a fractionating magma.

The validity of the preceding argument is supported by the analytical data of Nagasawa and Schnetzler (1971) and Irving and Frey (1976), who found larger REE phenocryst-matrix partition coefficients in dacites than in more basic rocks, a result that is predictable from the data in Fig. 10. Clearly, natural systems are chemically and physically more complex than the 4-

component experimental charges used in this partitioning study. However, these experiments have demonstrated that cations show variable compatibility in melts of different composition (and structure). This sensitivity to liquid composition and structure must also be displayed in nature, although temperature and pressure effects may be superimposed. An important consequence to geochemistry is that constant solid-liquid partition coefficients cannot be generally assumed in trace element modelling of fractional crystallization processes. This consideration may be important for those elements whose solid-liquid partition coefficients are fairly close to 1.

Immiscibility in magmas.

Roedder and Weiblen (1971) suggested that fractionation of elements between immiscible silicate liquids could be an important process in the evolution of the lunar crust, noting in particular the potential significance of enrichment of incompatible elements in the more basic of two coexisting liquids. Such a pattern is opposite of that expected for contrasting magmas resulting from fractional crystallization processes, and if found in rocks, might be evidence for the occurrence of liquid immiscibility. The data in Figs. 9-14 indeed indicate that the operation of liquid immiscibility in nature would produce unusual trace element distributions; the REE, for example, would be enriched in an immiscible mafic melt. These data are therefore potentially useful for identifying instances of magma unmixing.

Considered in light of the present experimental data, a liquid-immiscibility origin for mafic-felsic associations such as basalt-rhyolite (Yoder, 1973) and alkali basalt-trachyte (Chayes, 1963) seems unlikely, because the rock types comprising the acidic members of these associations are typically enriched, not depleted, in indicative elements such as the rare earths (Haskin et al., 1968; Zielinski and Frey, 1970; Ewart et al., 1968). However, for the lamprophyric rocks, in which good textural evidence for immiscibility exists (Philpotts, 1971; Ferguson and Currie, 1971), the case for magma unmixing is not discredited by the partitioning data obtained in this study. Lamprophyres commonly show extreme enrichment in incompatible elements such as phosphorus (Turner and Verhoogen, 1960) that is not easily explained in these mafic to ultramafic rocks by conventional petrogenetic processes. The data in Figs. 9-14 indicate that such enrichment would be inherited by a basic melt originating as an immiscible fraction of a pre-existing magma. As emphasized by Bowen (1928), liquid immiscibility is a continuous process; thus, an isolated immiscible lamprophyric fraction of a magma would split upon further cooling into two liquid phases. The ocellar texture of many lamprophyres may therefore be correctly attributed to liquid immiscibility. If so, the partitioning of elements between felsic ocelli and lamprophyre matrix should resemble the two-liquid partitioning data presented in this paper. The data must, of course, be

applied qualitatively and with caution, considering especially the possible coexistence of one or more crystalline phases with the two liquids.

6. Concluding Remarks

This study of trace- and minor-element partitioning between coexisting silicate liquids was conceived primarily as an investigation of relative compatibilities of widely varying cation types in silicate melts. Acidic melts have sites that can accept large cations such as Cs^{+}, Ba^{2+}, and Sr^{2+}; in general, the compatibility of a cation in an acidic melt decreases as the charge/radius ratio of the cation increases. The higher percentage of nonbridging oxygen ions in basic melts favors the incorporation of trace cations that form strong bonds with oxygen. These conclusions are consistent with previous concepts of silicate melt structure.

In addition to supplementing and supporting existing structural models of silicate melts, the experiments described in Part I of this thesis have shown that the compatibility of a trace element in the melt phase of a magma may be an important geochemical consideration. In particular, it is now clear that solid-liquid partition coefficients must depend on liquid composition. As evidenced by the degree of fractionation between immiscible melts, this dependence is stronger for some elements than others. Crystal-liquid partitioning of the large alkaline earth elements (Ba and Sr) should be insensitive to composition-

al variation of the liquid phase. The distribution of these elements between crystals and liquid is therefore a promising area for temperature measurement applications. At the other extreme, crystal-liquid partitioning of an element such as P will depend strongly on melt composition; in this case, any reported partition coefficient value for a solid-liquid pair can only be taken as representative of that specific liquid composition.

In spite of the rapidly-expanding volume of partitioning data for natural crystal-liquid pairs, it has not generally been possible to discern and evaluate melt-composition effects because unknown variables such as temperature and pressure are also contained in most of the data. Part I of this thesis has shown that melt-composition effects on solid-liquid partitioning must in fact be expected. In Part II, I will attempt to separate the effects of melt composition and temperature on the partitioning of a single element (Mn) between forsterite and a wide variety of geologically-relevant liquid compositions.

PART II. PARTITIONING OF MANGANESE BETWEEN FORSTERITE AND SILICATE LIQUID: THE EFFECT OF LIQUID COMPOSITION

1. Introduction.

Silicate melts are characterized by a complex structure that varies extensively with melt composition. This structural variation occurs both on a "short-range" scale, involving changes in oxygen coordination of cations (Day and Rindone, 1962b; Burns and Fyfe, 1964), and with respect to the overall polymeric nature of the melt (Toop and Samis, 1962a,b; Hess, 1970, 1975). Silicate melts of different bulk composition thus have different inherent structures. It is therefore reasonable to expect that the chemical potential of a dilute species in a melt will be sensitive to bulk compositional changes. In Part I of this thesis, I demonstrated directly that most trace cations show a preference for basic relative to acidic melts, which implies that the energy states or activities of these cations are lower in basic liquids. I also discussed the implications of my data to solid-liquid partitioning of trace elements in geochemical systems: in short, solid-liquid partition coefficients must depend on liquid composition, because the compatibility of a trace cation in a melt depends on the structure (and hence on the composition) of the melt.

Part II of this thesis describes a series of experiments designed to obtain detailed information on the effect of liquid

compositional variations on the distribution of Mn between forsterite and silicate melts. In previous partitioning studies (e.g. Drake and Weill, 1975; Longhi et al., 1976), variations of solid-liquid partition coefficients with melt composition have been treated by defining equilibrium constants that contain composition-dependent activity terms for the exchanging cations. Because of the complexity and variability of melt structure, defining cation or oxide activities is difficult, especially if large variations in melt composition must be considered. Thus, the equilibrium-constant approach does not always succeed in eliminating melt-composition dependence of trace element partitioning, probably because it does not satisfactorily account for structural changes in the melt.

The experimental results reported here suggest that the silicon:oxygen atomic ratio is a fundamental structural parameter of silicate melts which can be used to separate melt-composition from temperature effects on trace element partitioning between olivine and complex silicate liquids.

2. Experimental and Analytical Methods.

Selection of compositions

In addition to geological relevancy, an important requirement in choosing a system for these studies was a large primary phase volume of a pure crystalline phase, where the composition of liquid in equilibrium with crystals could be varied extensively. The Fo-Ab-An system (Fig. 17) was selected as a

starting point. In this system, forsterite is the liquidus phase over a large portion of the diagram, and coexists at equilibrium with liquids ranging from very basic to nearly pure albite liquid. Because the solid solution of monticellite in forsterite is small for olivine coexisting with Fo-Ab-An liquids, the olivine composition remains essentially constant with gross variations in melt composition. Observed changes in partitioning of a trace element between olivine and liquid should therefore be attributable either to temperature or melt composition differences; the effect of slight variations in olivine composition can be ignored (the CaO content of forsterite in the experiments described below ranges from 0.04 to 0.4 wt. %; see Table 4b).

I decided to examine the partitioning of manganese because this element showed a 3 to 1 preference for basic relative to acidic melt in my previous two-liquid partitioning studies. Manganese should therefore show fairly strong melt-composition dependence in olivine-liquid partitioning. Manganese is a suitable element for the additional reason that its distribution between forsterite and melt is fairly close to 1:1 (based on observed partition coefficients in glassy rocks). Thus, electron microprobe analysis for Mn in both olivine and coexisting glass is precise and accurate at concentration levels resembling those in natural rocks.

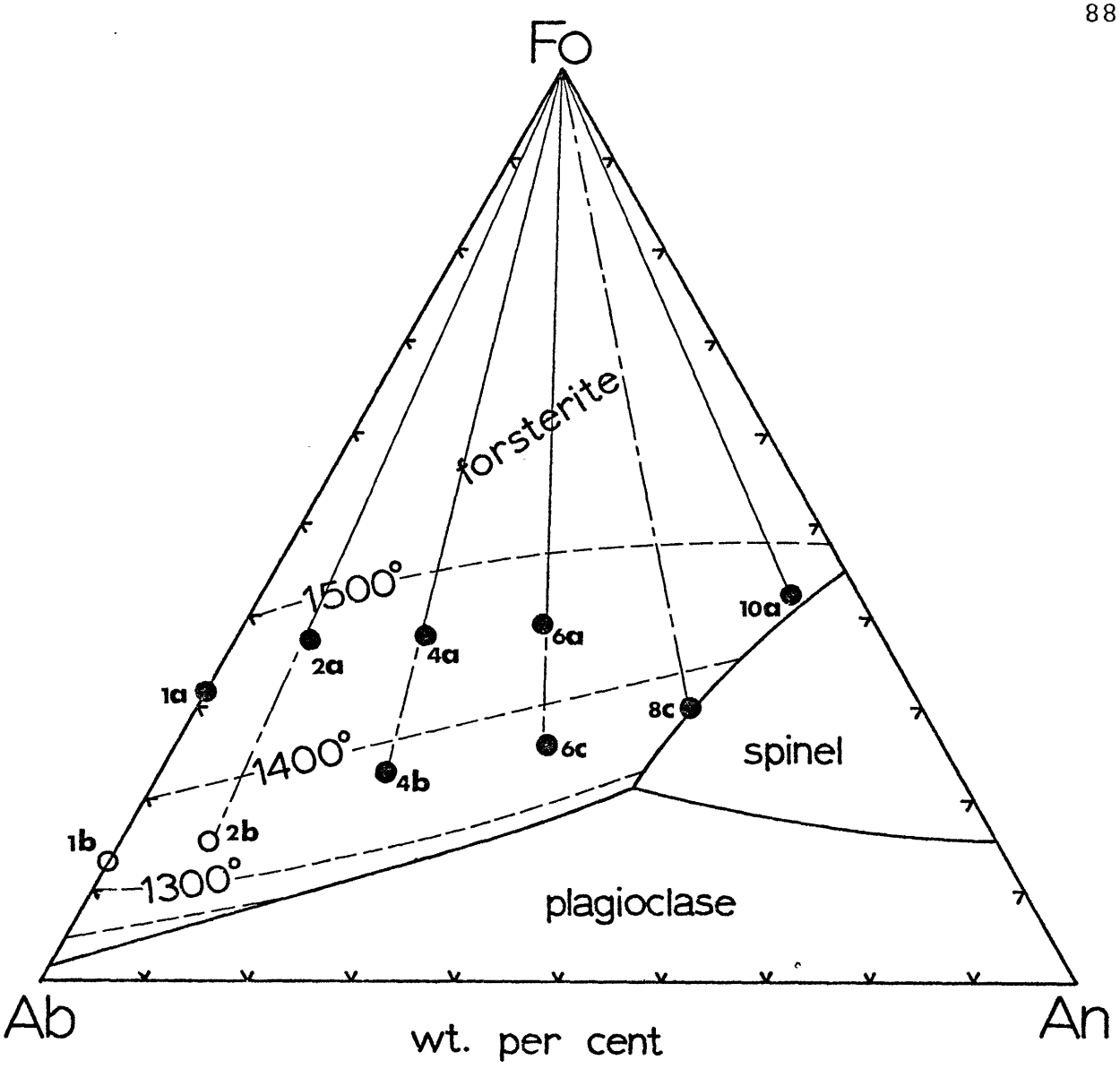


Figure 17. Liquidus diagram of the system forsterite-albite-anorthite (after Schairer and Yoder, 1966). Circles indicate compositions of Fo-Ab-An glasses in equilibrium with forsterite crystals at 1350 and 1450°C (solid circles are electron microprobe analyses; open circles are compositions estimated from this phase diagram). Run numbers for some of the manganese partitioning experiments are denoted by small bold type. Glass analyses for these and other runs are summarized in Table 4.

Specific techniques

Starting materials. Starting materials consisted of oxide mixes, except that the albite endmember was pre-synthesized by the method of Schairer and Bowen (1956). Forsterite and anorthite compositions were prepared by calcining pre-weighed mixes of reagent grade $MgCO_3$ + SiO_2 and $CaCO_3$ + Al_2O_3 + SiO_2, respectively. Starting compositions were prepared in two-gram batches by weighing in the required amounts of the three endmember compositions and grinding under acetone for 30 minutes in an agate mortar. 200-mg splits were doped with Mn by weighing in the desired amount (usually ∿0.2 wt. %) of spectroscopic grade MnO.

Apparatus and run conditions. All experiments were performed in a platinum-wound, 1-atm quench furnace with temperature control equipment reliable to better than ±1°C. Temperature was monitored by a Pt/Pt10%Rh thermocouple, calibrated at the melting points of Au and Ni (in vacuo).

Unless noted otherwise, the 10 to 20-mg charges were contained in platinum capsules that were welded shut to prevent sodium volatilization during the runs. The capsules were lowered into a furnace already at run temperature, held at temperature for 2-5 days (see following section), and quenched by dropping into water. This procedure resulted in equidimensional forsterite crystals ranging in size from 10 to 70 μm (higher temperatures and basic melts favored larger crystals).

Preliminary experiments

Criteria for equilibrium. In order to determine suitable run durations for the Mn partitioning experiments, systematic preliminary runs were made and analyzed in detail. A starting composition of $Fo_{50}Ab_{25}An_{25}$, doped with ∿0.5 wt. % Mn, was run at 1250° and 1450° for 2 days. The same composition was then re-run at the same temperatures for a duration of 4 days. The observed partition coefficients for experiments run at the same temperature were not significantly different (Table 5), although the variance among replicate Mn analysis spots was slightly higher for the shorter (2-day) run at 1250°. Figure 18 shows a Mn concentration profile obtained by traversing a 50-μm forsterite crystal in the charge held for 2 days at 1450°. There is no suggestion of disequilibrium.

The following standard run times were adopted for all partitioning experiments: 1450°-2 days; 1350°-3 days; 1300°-4 days; 1250° and below - 5 days. The equilibration of any given charge was judged by the observed variance in replicate Mn analysis spots on forsterite and glass. In most cases, this variance is close to that expected from counting errors (Table 5).

The effect of oxygen fugacity. The possible effect of oxygen fugacity on the oxidation state of Mn in the melt was examined by duplicating 2 partitioning experiments in platinum and molybdenum capsules. When sealed in an evacuated silica glass tube, a molybdenum capsule buffers the contained charge at an f_{O_2}

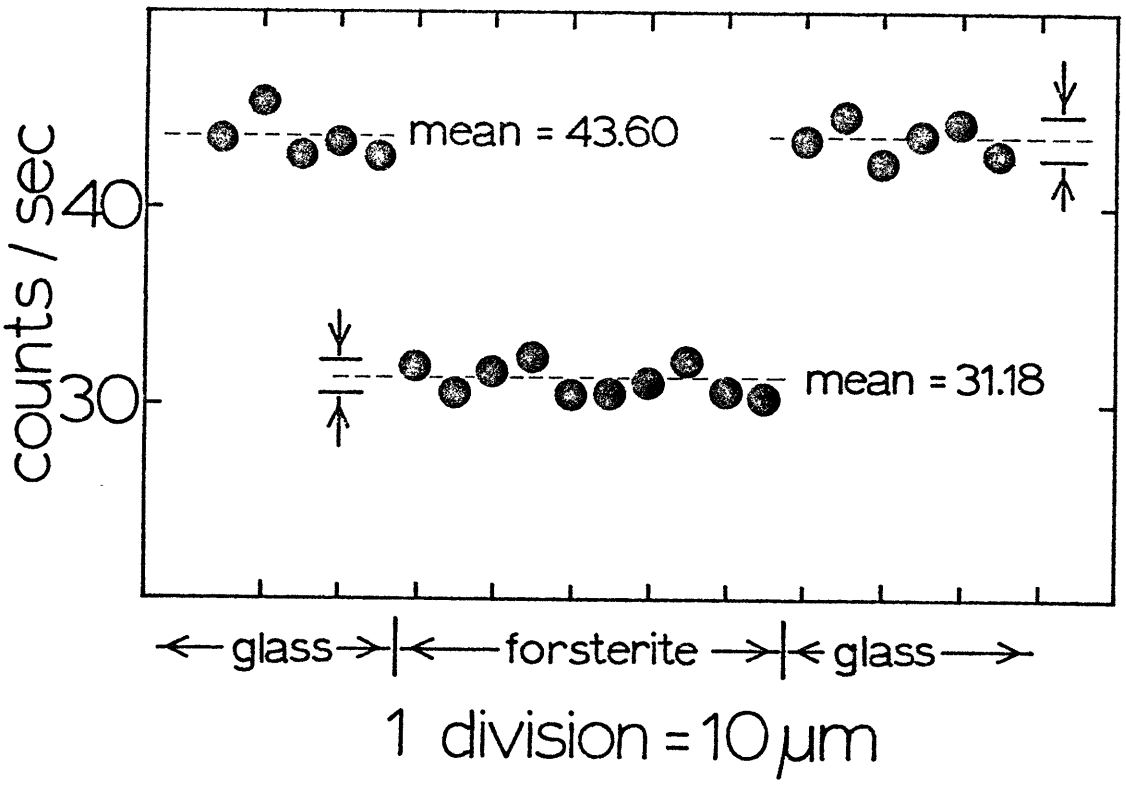


Figure 18. Electron microprobe traverse across a 50μm forsterite crystal in run number 6R1 (see Table 4). Total seconds counted on each analysis spot = 100. 1σ counting error for each spot is indicated by $\frac{\downarrow}{\uparrow}$

very close to the iron-wüstite curve (Biggar, 1970). The platinum capsules, on the other hand, were welded shut in air, creating highly oxidizing conditions inside the capsules during the runs. However, the extreme difference in f_{O_2} for the two capsule types did not appear to affect the oxidation state of Mn in the melt, because partition coefficients for runs duplicated in the two containers were the same within experimental error (see Table 5). This coincidence of partition coefficient values indicates that Mn ions in silicate melt are predominantly divalent even under very oxidizing conditions. If a significant amount of a higher oxidation state were present in the runs made in platinum, the observed forsterite-liquid partition coefficients would be low relative to those measured in charges of the same composition run in molybdenum (assuming that Mn ions of charge >2 would not be incorporated into forsterite).

Molybdenum capsules were not adopted for general use in these experiments because sodium volatilization into the vacuum space enclosed by the SiO_2 glass tube is a serious problem. Also, the molybdenum capsule + glass tube arrangement can only be used over 1400°C for very short (1-2 hour) runs.

Concentration dependence of partition coefficients. Mysen (1975) has demonstrated that the distribution of Ni between olivine and silicate melt depends on the amount of Ni present in the system, even at very low Ni concentrations. The data of Leeman (1974) suggest no such concentration dependence for

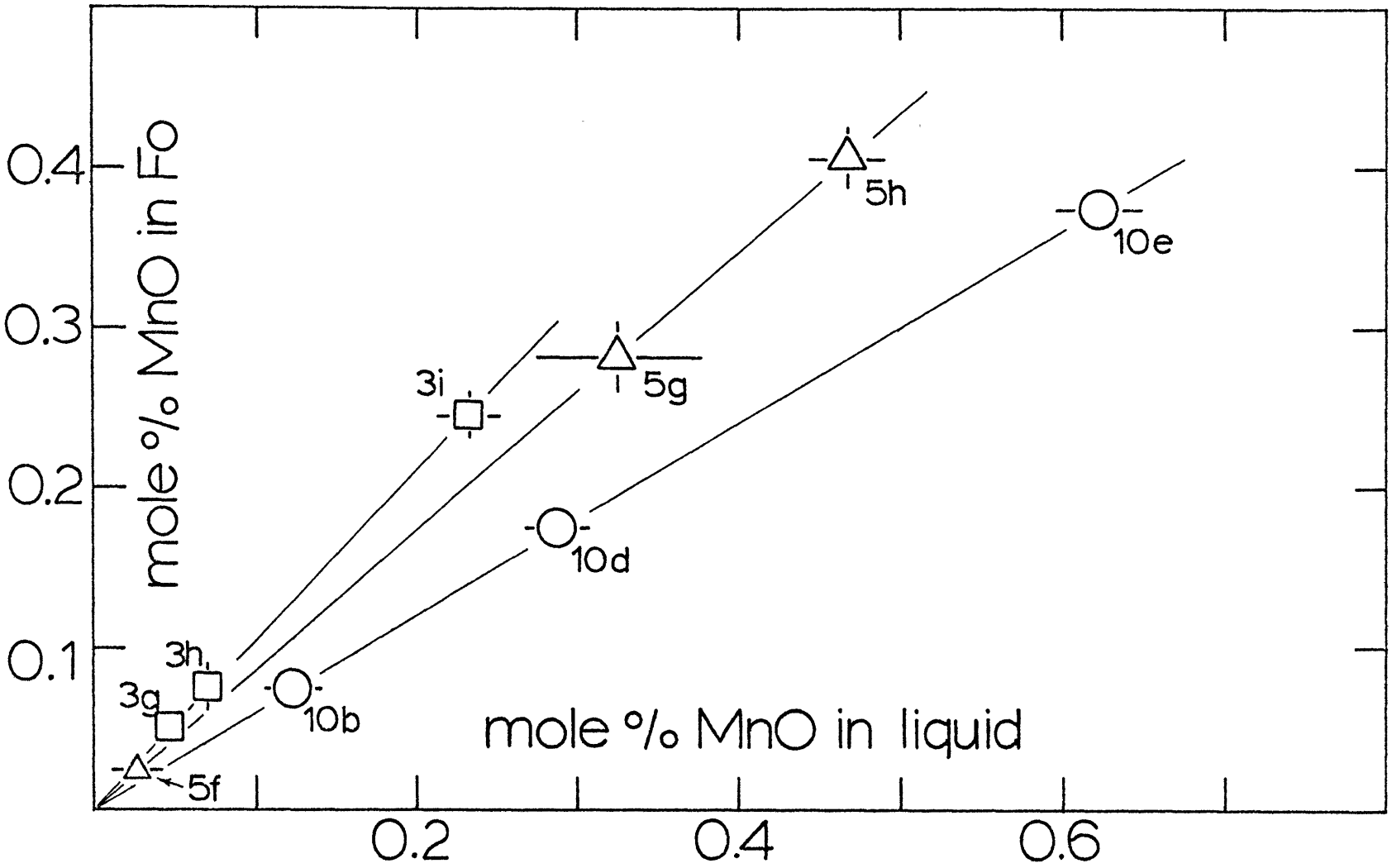


Figure 19. Experimental results showing lack of dependence of forsterite/liquid partitioning of Mn on the concentration of Mn in the charge (see text)

either Ni or Mn partitioning between olivine and melt at the concentration level used in this work (∿0.2 wt. % Mn). As a check for concentration dependence of Mn partitioning in the specific compositions used in this study, I ran several experiments at different Mn concentrations in the range 0.05 to 0.5 wt. % Mn. The results of these experiments (Fig. 19) indicate that Mn partition coefficients are independent of Mn concentration up to at least 0.6 % MnO in forsterite.

Scope of partitioning experiments.

An initial group of Mn partition coefficients was measured for forsterite-liquid pairs along four isotherms (1450, 1350, 1300, 1250°C) on the liquidus surface of the Fo-Ab-An system (Fig. 17, Table 4). In order to establish more general validity for the model proposed later in this paper, liquid compositions were not confined to the Fo-Ab-An composition plane [such liquids may in fact be structurally unique because they contain a stoichiometric plagioclase component, possibly analogous to the important 1:1 ratio of Na:Al in sodium aluminosilicate melts (Day and Rindone, 1962b)]. Four additional isothermal series of runs were therefore made, in which the starting compositions contained a 35% excess of CaO relative to Fo-Ab-An compositions (see Table 4 for glass analyses). As noted in Table 5, some charges contained plagioclase or spinel as well as forsterite. Several runs were also made in which forsterite coexisted with synthetic melts of iron-free "basaltic" composi-

tion (iron was replaced by magnesium on a molar basis). One of these glasses approximates an alkali basalt, and contains 4.07% TiO_2 and 1.77% K_2O (Table 4); this composition is well removed even from the SiO_2-Al_2O_3-MgO-CaO-Na_2O system.

Analysis of charges.

Both major element compositions and manganese partition coefficients were determined by electron microprobe. For major element analysis, the M.I.T. Materials Analysis Company electron microprobe was used in automated mode (Finger and Hadidiacos, 1972), operating at an accelerating voltage of 15 kV and a sample current of about 0.02 μA. On forsterite crystals, a beam spot of about 2 μm diameter was used. Positioning of the beam on very small crystals was facilitated by the blue fluorescence of pure forsterite. For glass analyses, a 6-μm beam spot was used unless the polished surface of the charge was very crowded with crystals, in which case a smaller beam was required. Sodium volatilization under the electron beam was found to be a serious problem in Fo-Ab-An glasses near the Fo-Ab sideline; compositions reported for these glasses are estimates from the published phase diagram of Schairer and Yoder (1966; see Table 4 and Fig. 17).

The low concentrations of Mn used in this study necessitated detailed peak and background determinations for this element. Improved count rates were achieved by increasing the sample current to ∿0.045 μA, and total accumulated counts were

Table 4a. Major element analyses and Si/O ratios of glasses in experimental runs. Analyses are listed in order of decreasing Si/O except for Fe-free basalt compositions MAR4 and OIB4. Bulk compositions of even-numbered runs are in the Fo-Ab-An plane; odd-numbered runs have excess CaO in the bulk composition (see text).

(1250°C)

run no.	3j			4e			5e		
	wt%	σ	mole %	wt%	σ	mole %	wt%	σ	mole %
SiO_2	63.33	0.83	66.6	61.25	0.99	64.0	56.46	1.15	58.7
Al_2O_3	20.55	0.11	12.7	21.71	0.13	13.4	20.67	0.06	12.7
MgO	6.45	0.06	10.1	8.14	0.12	12.7	8.63	0.22	13.4
CaO	4.62	0.11	5.2	5.10	0.07	5.7	8.57	0.08	9.5
Na_2O	5.29	0.07	5.4	3.88	0.08	3.9	5.66	0.42	5.7
MnO	0.14		0.1	0.29		0.3	0.11		0.1
total	100.38	Si/O=0.347		100.37	Si/O=0.335		100.10	Si/O=0.319	

run no.	6f			7g			9e		
	wt%	σ	mole %	wt%	σ	mole %	wt%	σ	mole %
SiO_2	54.61	0.19	57.0	53.68	0.41	54.7	48.04	0.48	48.7
Al_2O_3	23.21	0.09	14.3	20.19	0.08	12.1	18.84	0.22	11.3
MgO	9.96	0.07	15.5	10.03	0.23	15.2	11.59	0.16	17.5
CaO	7.84	0.06	8.8	11.98	0.06	13.1	17.69	0.18	19.2
Na_2O	4.32	0.18	4.4	4.75	0.05	4.7	3.42	0.08	3.4
MnO	0.20		0.2	0.25		0.2	0.17		0.1
total	100.14	Si/O=0.307		100.88	Si/O=0.306		99.75	Si/O=0.284	

run no.	MAR4			OIB4		
	wt%	σ	mole %	wt%	σ	mole %
SiO_2	53.37	0.64	54.6	51.99	0.24	54.0
TiO_2	1.57	0.05	1.2	4.07	0.08	3.2
Al_2O_3	18.15	0.06	10.9	19.54	0.21	12.0
MgO	10.63	0.12	16.2	9.50	0.12	14.7
CaO	12.28	0.08	13.5	9.35	0.06	10.4
Na_2O	2.90	0.09	2.9	3.91	0.12	3.9
K_2O	0.29	0.01	0.2	1.77	0.05	1.2
MnO	0.27		0.2	0.23		0.2
total	99.46	Si/O=0.307		100.36	Si/O=0.300	

Table 4a (continued).
(1300°C)

run no.	3g,3h,3i			4d			5f,5g,5h		
	wt%	σ	mole %	wt%	σ	mole %	wt%	σ	mole %
SiO_2	63.20	0.54	65.2	61.33	0.29	61.9	56.46	0.06	57.5
Al_2O_3	20.11	0.30	12.2	20.62	0.13	12.3	19.20	0.19	11.5
MgO	8.82	0.12	13.6	10.38	0.03	15.6	10.83	0.05	16.4
CaO	4.42	0.03	4.9	4.99	0.08	5.4	7.97	0.04	8.7
Na_2O	4.00	0.10	4.0	4.75	0.21	4.7	5.91	0.23	5.8
MnO	see table 5			0.19		0.2	see table 5		
total	100.55	Si/O=0.344		102.26	Si/O=0.332		100.37	Si/O=0.319	

run no.	6e			8e			9j		
	wt%	σ	mole %	wt%	σ	mole %	wt%	σ	mole %
SiO_2	53.91	0.34	54.6	49.56	0.32	50.5	47.19	0.54	47.9
Al_2O_3	21.74	0.06	13.0	22.69	0.13	13.6	21.52	0.29	12.9
MgO	12.60	0.10	19.1	13.96	0.15	21.2	13.80	0.24	20.9
CaO	7.82	0.06	8.5	10.53	0.15	11.5	15.20	0.30	16.5
Na_2O	4.66	0.19	4.6	2.86	0.03	2.8	1.88	0.12	1.9
MnO	0.23		0.2	0.35		0.3	0.26		0.2
total	100.96	Si/O=0.302		99.95	Si/O=0.284		99.85	Si/O=0.275	

Table 4a (continued).
(1350°C)

run no.	1b[a]			2b[a]			3d		
	wt%	σ	mole %	wt%	σ	mole %	wt%	σ	mole %
SiO_2	64.8	---	66.7	62.8	---	64.9	59.60	1.77	60.1
Al_2O_3	16.5	---	10.0	17.9	---	10.9	18.06	0.05	10.7
MgO	8.6	---	13.2	8.6	---	13.2	12.13	0.06	18.2
CaO	--	---	--	1.6	---	1.8	4.04	0.05	4.4
Na_2O	10.1	---	10.1	9.1	---	9.1	6.79	0.05	6.6
MnO	0.24		0.2	0.13		0.1	0.13		0.1
total	---	Si/O≃0.36		---	Si/O≃0.35		100.75	Si/O=0.331	

run no.	4b			5d			6c		
	wt%	σ	mole %	wt%	σ	mole %	wt%	σ	mole %
SiO_2	58.73	0.40	58.9	54.07	0.99	54.6	53.89	0.94	54.3
Al_2O_3	17.20	0.49	10.2	18.16	0.13	10.8	19.06	0.19	11.3
MgO	13.44	0.20	20.0	14.34	0.11	21.6	14.89	0.11	22.4
CaO	4.35	0.02	4.7	7.45	0.17	8.1	7.11	0.05	7.7
Na_2O	6.48	0.10	6.3	4.98	0.12	4.9	4.52	0.13	4.4
MnO	0.09		0.1	0.18		0.2	0.22		0.2
total	100.29	Si/O=0.328		99.18	Si/O=0.310		99.69	Si/O=0.306	

run no.	7j			8c			91		
	wt%	σ	mole %	wt%	σ	mole %	wt%	σ	mole %
SiO_2	50.05	0.48	50.2	49.33	0.46	49.6	45.63	0.16	45.6
Al_2O_3	20.09	0.10	11.9	20.88	0.46	12.4	20.84	0.11	12.3
MgO	15.27	0.08	22.8	16.87	0.27	25.3	16.82	0.16	25.1
CaO	11.02	0.06	11.8	9.47	0.03	10.2	14.39	0.14	15.4
Na_2O	3.42	0.10	3.3	2.55	0.20	2.5	1.71	0.05	1.7
MnO	0.29		0.2	0.31		0.3	0.16		0.1
total	100.14	Si/O=0.288		99.41	Si/O=0.284		99.55	Si/O=0.268	

[a] compositions estimated from Fo-Ab-An phase diagram (see text)

Table 4a (continued).

(1350°C)

run no.	10b,10d,10e		
	wt%	σ	mole %
SiO_2	47.41	0.39	47.2
Al_2O_3	21.05	0.10	12.4
MgO	17.41	0.08	25.8
CaO	12.62	0.14	13.5
Na_2O	0.90	0.04	0.9
MnO	see table 5		
total	99.39	Si/O=0.275	

(1450°C)

run no.	1a			2a			3f		
	wt%	σ	mole %	wt%	σ	mole %	wt%	σ	mole %
SiO_2	60.39	1.31	58.6	58.52	0.23	56.4	55.42	0.99	53.6
Al_2O_3	13.45	0.18	7.7	13.34	0.14	7.6	14.08	0.21	8.0
MgO	18.21	0.16	26.3	20.22	0.18	29.0	20.40	0.29	29.4
CaO	---	--	--	1.29	0.02	1.3	3.36	0.03	3.5
Na_2O	7.91	0.12	7.4	6.11	0.12	5.7	5.82	0.16	5.5
MnO	0.39		0.3	0.15		0.1	0.29		0.2
total	100.35	Si/O=0.336		99.63	Si/O=0.328		99.37	Si/O=0.316	

run no.	4a			5c			6a		
	wt%	σ	mole %	wt%	σ	mole %	wt%	σ	mole %
SiO_2	55.61	0.46	52.5	52.33	0.74	50.3	52.04	0.16	49.1
Al_2O_3	14.46	0.03	8.0	14.68	0.24	8.3	16.34	0.08	9.1
MgO	22.00	0.18	31.0	21.55	0.14	30.9	22.95	0.06	32.3
CaO	3.59	0.08	3.6	6.27	0.09	6.5	5.92	0.03	6.0
Na_2O	5.30	0.12	4.9	4.34	0.08	4.0	3.86	0.05	3.5
MnO	0.25		0.2	0.19		0.2	0.26		0.2
total	100.91	Si/O=0.311		99.36	Si/O=0.301		101.37	Si/O=0.293	

Table 4a (continued).
(1450°C)

run no.	7f			9c			10a		
	wt%	σ	mole %	wt%	σ	mole %	wt%	σ	mole %
SiO_2	48.85	0.85	47.2	44.45	0.23	42.9	45.38	0.28	43.3
Al_2O_3	16.55	0.21	9.4	17.73	0.00	10.1	19.93	0.02	11.2
MgO	21.56	0.08	31.0	23.11	0.46	33.2	24.19	0.26	34.4
CaO	9.25	0.09	9.6	12.13	0.14	12.5	10.27	0.05	10.5
Na_2O	2.98	0.17	2.8	1.30	0.04	1.2	0.77	0.05	0.7
MnO	0.24		0.2	0.19		0.2	0.13		0.1
total	99.43	Si/O=0.284		98.91	Si/O=0.263		100.67	Si/O=0.261	

Table 4b. Analyses (weight % oxides) of forsterite in selected experimental charges.

run no.	2a	10a	3d	7j	10d	4d	8e	7g
T°C	(1450)	(1450)	(1350)	(1350)	(1350)	(1300)	(1300)	(1250)
SiO_2	41.91	41.64	42.24	42.42	42.53	42.61	42.41	42.18
MgO	57.57	57.74	58.50	58.18	58.08	58.09	58.07	58.03
CaO	0.04	0.36	0.14	0.34	0.34	0.15	0.26	0.40
total	99.52	99.74	100.88	100.94	100.95	100.85	100.73	100.61
				cations/4 oxygens				
Si	0.988	0.980	0.982	0.986	0.988	0.991	0.987	0.984
Mg	2.022	2.027	2.028	2.017	2.013	2.013	2.016	2.020
Ca	0.000	0.009	0.003	0.008	0.008	0.003	0.006	0.009
total	3.011	3.016	3.014	3.011	3.009	3.007	3.009	3.013

increased by counting 50 to 200 seconds on each spot. Background count rates were determined at an offset of 0.294° 2θ (LiF analyzing crystal) on either side of the Mn K_α peak. By linear extrapolation of these two values, a background count rate under the peak was obtained and subtracted from the count rate on the peak. In a single charge, ten replications of this procedure were done on forsterite crystals and ten on glass to obtain a Mn partition coefficient. Calculated correction factors (Albee and Ray, 1970) for Mn in forsterite and the glasses analyzed in this study were found to be nearly identical, so correcting the raw count data was for the most part unnecessary. To obtain an absolute amount of Mn in either phase, the count rate was compared to a Mn-bearing ilmenite standard and corrected for fluorescence and absorption differences between standard and unknown.

3. Results

The results of the manganese partitioning experiments are summarized in Table 5 and Figs. 20-24. The symbol $D_{Mn}^{Fo\text{-}liq}$ is used throughout to refer to a mole per cent partition coefficient, defined as $\frac{\text{mole \% MnO in Fo}}{\text{mole \% MnO in Liq}}$ (Fig. 22 is replotted using the conventional weight per cent partition coefficient so that the diagram may be more readily compared with natural system data).

Variation of $D_{Mn}^{Fo\text{-}liq}$ with melt composition is obvious for all four isothermal series of experiments, but is less prominent

Table 5. Summary of forsterite-liquid partitioning data for Mn.

run number	T°C	run duration (h)	MnO in forsterite				MnO in glass				partition coeff MnO in Fo/MnO in gl		
			weight %	mole %	σ (%), 10 pts	1σ counting error (%)	weight %	mole %	σ (%), 10 pts	1σ counting error (%)	weight ratio	mole ratio	2 std errors (%)
1a	1450	57	0.319	0.212	2.3	2.0	0.388	0.318	4.0	3.3	0.822	0.667	2.9
2a	1450	53	0.114	0.076	5.8	2.6	0.149	0.121	5.6	2.2	0.765	0.627	5.1
3f	1450	47	0.199	0.133	6.1	3.4	0.286	0.234	3.0	2.8	0.695	0.568	4.3
4a	1450	53	0.169	0.113	10.3	3.3	0.247	0.197	5.9	2.7	0.684	0.573	7.5
5c	1450	49	0.122	0.081	4.8	2.7	0.185	0.151	3.9	3.1	0.659	0.536	3.9
6a	1450	53	0.162	0.108	7.6	7.0	0.255	0.204	6.1	5.6	0.635	0.529	6.2
7f	1450	47	0.148	0.099	5.6	3.9	0.239	0.195	3.8	3.4	0.619	0.508	4.3
9c	1450	49	0.120	0.080	6.4	2.7	0.192	0.157	3.3	3.0	0.625	0.510	4.6
10a	1450	53	0.079	0.053	9.1	3.1	0.125	0.101	4.6	2.4	0.632	0.525	6.4
1b	1350	72	0.386	0.256	8.5	2.4	0.238	0.207	6.0	3.2	1.622	1.237	6.6
2b	1350	68	0.173	0.115	3.7	3.5	0.130	0.113	6.8	3.9	1.331	1.018	4.9
3d	1350	72	0.152	0.101	3.2	4.0	0.132	0.113	3.9	5.2	1.152	0.895	3.2
4b	1350	68	0.095	0.064	8.6	4.8	0.093	0.079	10.6	4.9	1.022	0.808	8.6
5d	1350	72	0.164	0.109	7.2	6.5	0.181	0.155	10.8	8.4	0.906	0.705	8.2
6c	1350	91	0.192	0.128	10.8	3.4	0.215	0.183	5.3	3.2	0.893	0.699	7.6
7j	1350	75	0.248	0.165	3.1	5.8	0.290	0.246	2.9	5.3	0.855	0.672	2.7

Table 5 (continued).

run number	T °C	run duration (h)	MnO in forsterite				MnO in glass				partition coeff MnO in Fo/MnO in gl		
			weight %	mole %	σ (%), 10 pts	1σ counting error (%)	weight %	mole %	σ (%), 10 pts	1σ counting error (%)	weight ratio	mole ratio	2 std errors (%)
8c	1350	91	0.244	0.163	5.9	3.0	0.310	0.264	4.0	3.4	0.787	0.617	4.5
9l[a]	1350	75	0.125	0.083	8.4	6.3	0.161	0.136	5.5	5.5	0.776	0.612	6.4
10b[a]	1350	68	0.109	0.073	9.2	7.3	0.144	0.122	7.1	6.6	0.757	0.598	7.3
10d[a]	1350	75	0.261	0.174	4.6	5.1	0.341	0.288	3.6	4.5	0.765	0.604	3.7
10e[a]	1350	75	0.563	0.375	2.2	2.9	0.738	0.623	2.0	2.1	0.763	0.602	1.9
3g	1300	115	0.073	0.050	10.3	7.7	0.052	0.046	9.6	6.9	1.404	1.087	8.9
3h	1300	146	0.112	0.075	8.4	4.5	0.079	0.069	7.1	5.2	1.418	1.087	7.0
3i	1300	92	0.365	0.244	2.6	3.3	0.255	0.223	4.4	4.0	1.431	1.094	3.2
4d	1300	92	0.241	0.160	5.1	4.5	0.188	0.161	4.1	5.1	1.282	0.998	4.1
5f[b]	1300	115	0.035	0.023	16.5	11.1	0.032	0.027	26.8	11.3	1.094	0.852	19.9
5g[b]	1300	146	0.422	0.281	3.8	3.2	0.376	0.323	7.5	3.3	1.122	0.868	5.3
5h[b]	1300	92	0.613	0.407	1.9	2.7	0.544	0.467	2.2	2.3	1.127	0.871	1.8
6e	1300	92	0.239	0.159	5.3	4.5	0.233	0.200	4.9	4.6	1.026	0.795	4.6
8e[a]	1300	92	0.315	0.210	4.0	4.0	0.348	0.301	3.2	3.8	0.905	0.698	3.2
9j[a]	1300	92	0.252	0.168	7.3	4.4	0.261	0.224	3.5	4.3	0.964	0.750	5.1
3j	1250	144	0.243	0.162	5.3	5.5	0.136	0.121	8.3	6.9	1.789	1.339	6.2

Table 5 (continued).

run number	T°C	run duration (h)	MnO in forsterite				MnO in glass				partition coeff MnO in Fo/MnO in gl		
			weight %	mole %	σ (%), 10 pts	1σ counting error (%)	weight %	mole %	σ (%), 10 pts	1σ counting error (%)	weight ratio	mole ratio	2 std errors (%)
4e[b]	1250	144	0.444	0.295	7.2	4.3	0.293	0.260	5.5	5.3	1.515	1.135	5.7
5e[b]	1250	138	0.149	0.099	5.3	3.9	0.109	0.096	8.8	4.5	1.367	1.038	6.5
6f[b]	1250	144	0.234	0.156	8.9	4.6	0.202	0.178	5.1	5.0	1.158	0.876	6.5
7g[b]	1250	118	0.300	0.200	4.8	2.7	0.246	0.213	8.8	3.0	1.220	0.938	6.3
9e[b]	1250	118	0.195	0.130	9.1	5.4	0.171	0.146	8.2	5.8	1.140	0.888	7.7
MAR4	1250	125	0.310	0.207	4.9	4.0	0.266	0.231	5.7	4.3	1.165	0.896	4.8
OIB4	1250	125	0.280	0.187	6.6	4.8	0.228	0.202	4.1	4.5	1.228	0.926	4.9
runs in molybdenum capsules (see text)													
7e(Mo)[c]	1350	79	0.291	0.194	4.3	3.5	0.343	0.291	3.7	3.0	0.847	0.665	3.6
4f(Mo)[c]	1250	127	0.417	0.277	3.8	4.0	0.273	0.242	2.7	4.6	1.527	1.144	2.9
equilibration experiments (see text)													
6R1	1450	50	0.391	0.261	3.5	2.5	0.610	0.488	3.1	2.2	0.641	0.534	3.0
6R2	1250	50	0.587	0.391	11.9	2.9	0.501	0.441	5.5	2.9	1.172	0.886	8.3
6R3	1450	99	0.363	0.242	2.7	2.6	0.576	0.461	2.2	2.2	0.630	0.525	2.2
6R4	1250	99	0.524	0.349	5.2	3.0	0.450	0.397	4.3	3.0	1.164	0.879	4.3

[a] charges contain spinel as well as Fo [b] charges contain plag as well as Fo

[c] except for some sodium loss, 7e(Mo) and 4f(Mo) glasses are the same as 7j and 4e, resp.

at high temperature. For example, at 1450° $D_{Mn}^{Fo\text{-}liq}$ varies between 0.51 and 0.67 over a composition range of 48.9 to 60.4 wt. % SiO_2; at 1350°, $D_{Mn}^{Fo\text{-}liq}$ ranges from 0.62 to 0.90 over approximately the same SiO_2 composition interval. In general, Mn is more strongly partitioned into olivine at lower temperatures, although the melt composition effect causes considerable overlap in partition coefficient values for different isothermal series of experiments. This overlap is emphasized in Fig. 20, which reveals a general temperature dependence of $D_{Mn}^{Fo\text{-}liq}$, but is useless, for example, as a thermometer calibration plot.

If the assumption is made that Mn partitioning between olivine and melt can be represented by the exchange reaction

$$MnO_{melt} + MgSi_{0.5}O_{2\,olivine} \rightleftarrows MnSi_{0.5}O_{2\,olivine} + MgO_{melt}, \quad (13)$$

an equilibrium constant of the following form may be written:

$$K = \frac{[MgO_{melt}]\,[Tph_{ol}]}{[Fo_{ol}]\,[MnO_{melt}]} \quad (13a)$$

where the bracketed symbols refer to activities (Tph=tephroite). Because forsterite is nearly pure, $[Fo_{ol}] \approx 1$; $[Tph_{ol}]$ can probably be approximated as a mole fraction, X_{Tph}^{ol} (if the forsterite-tephroite solution is ideal), or as the product of a Henry's law constant and X_{Tph}^{ol}. In either case, equation (13a) reduces to:

$$[MgO_{melt}]\,\frac{[Tph_{ol}]}{[MnO_{melt}]} = \text{constant} \quad (13b)$$

for any fixed temperature and pressure. Difficulty arises in

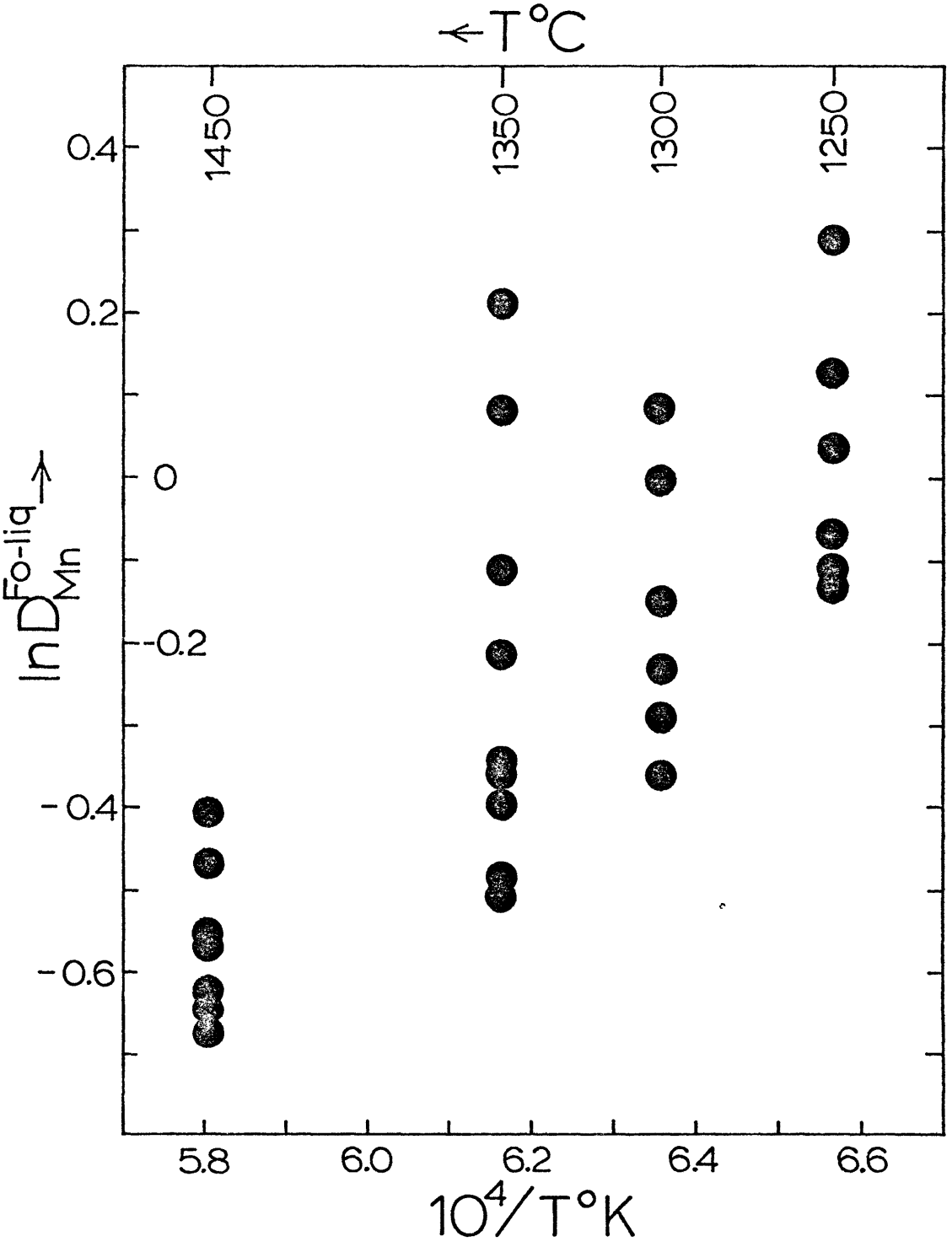


Figure 20. $\ln D_{Mn}^{Fo\text{-}liq}$ vs. reciprocal absolute temperature for all Mn partitioning experiments

defining $[MgO_{melt}]$ and $[MnO_{melt}]$, but as a first approximation the respective molar oxide concentrations could be used. Because the ratio $[Tph_{ol}]/[MnO_{melt}]$ is then essentially a molar partition coefficient, D_{Mn}^{Fo-liq} should vary linearly with $[MgO_{melt}]^{-1}$. This plot is attempted in Fig. 21, which shows a good, nearly linear correlation between D_{Mn}^{Fo-liq} and the reciprocal of the molar MgO concentration in the melt. However, the plot does not succeed in removing the overlap of D_{Mn}^{Fo-liq} values for the different isothermal series of experiments. For practical purposes, only one line or curve is defined by the diagram, when in fact, since K should vary with temperature, four lines of different slope representing the four isotherms should be revealed. There are two possible reasons for the failure of this plot to produce the desired (and expected) results: 1) K is not sufficiently temperature-dependent that Fig. 21 is sensitive to changes in its value; and 2) the activities of MgO and MnO in the melt are not well approximated by their mole fractions. In view of the data of Leeman (1974), which shows more than a factor of two change in D_{Mn}^{ol-liq} for basaltic compositions over the temperature interval 1250-1450°C, the first of the above possibilities does not seem likely. Thus, a better representation of oxide activities in the silicate melt is probably required.

The method of Drake (1972) for estimating oxide activities

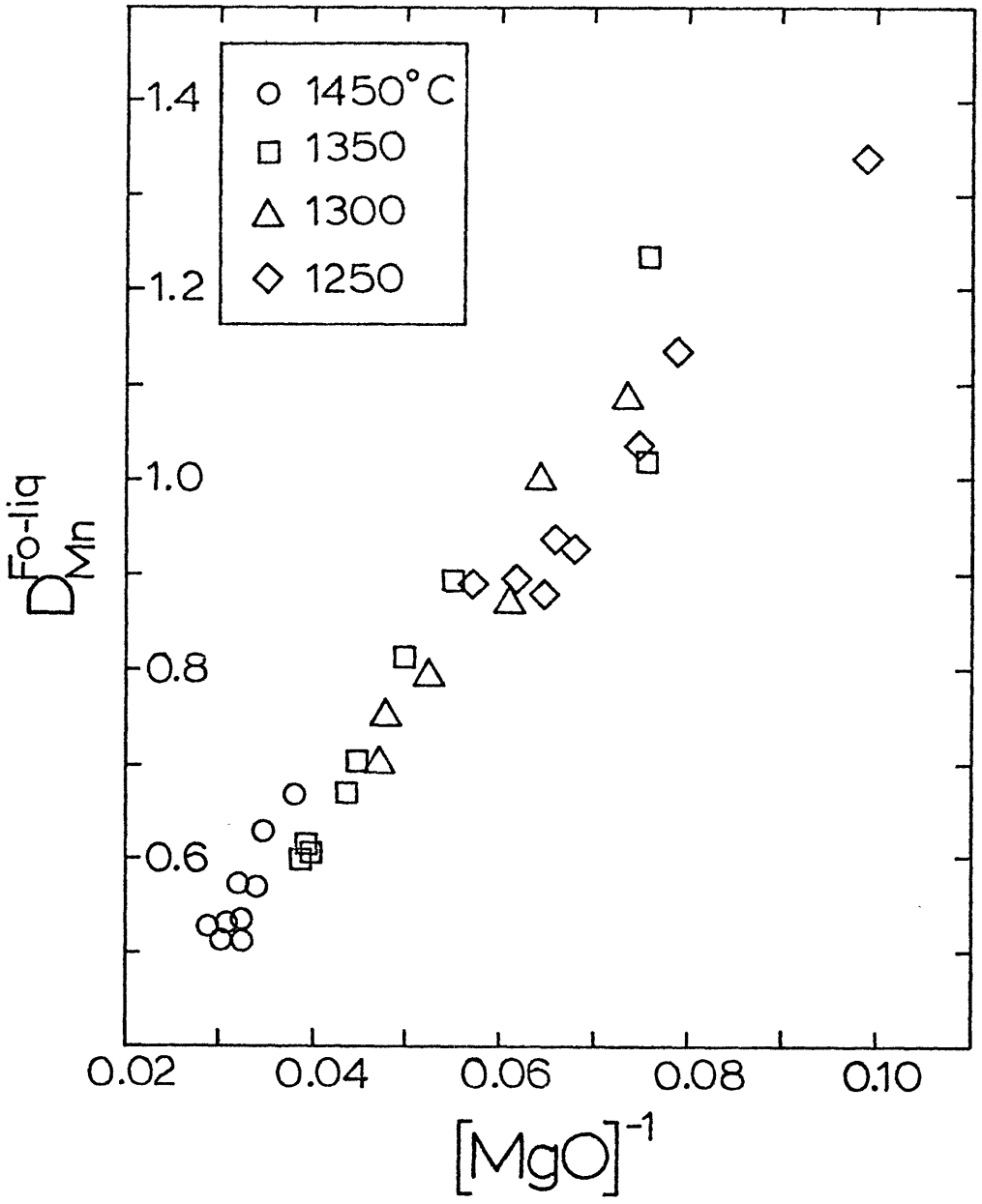


Figure 21. D_{Mn}^{Fo-liq} vs. reciprocal molar MgO concentration in the melt (see text for explanation)

in the melt was used to calculate K values from equation (13a)[5] for forsterite-liquid pairs examined in this study. The results are presented in Fig. 22, which shows a good general dependence of K upon temperature, but again the range of K values at any one temperature is quite large relative to the total variation.

The limited success of the thermodynamic models described above led me to consider an alternative approach to the problem of melt-composition dependence of manganese partitioning. As suggested in Part I of this thesis, the relative compatibility of trace cations in melts of different bulk composition is influenced by the inherent structural differences between the melts. It might therefore be possible to correlate observed changes in partitioning behavior with variation in some compositional parameter that represents the average structural characteristics of the melt. This approach is broadly analogous to that of Pearce (1964) and Mysen et al. (1976), who correlated the solubility of CO_2 in silicate melts with melt basicity (defined as $\frac{\Sigma \text{ basic oxides}}{\Sigma \text{ acidic oxides}}$). Similarly, Morris and Haskin (1974) were able to correlate changes in the redox equilibrium of Eu in silicate melts with the (silicon+aluminum):oxygen ratio of the melts.

Unsuccessful attempts were made to correlate $D_{Mn}^{Fo\text{-}liq}$ with melt basicity and with (Si + Al)/O. In these attempts, as in Fig. 21, fairly good overall correlations between the composition parameters and $D_{Mn}^{Fo\text{-}liq}$ resulted; however, temperature and melt composition effects on $D_{Mn}^{Fo\text{-}liq}$ were not resolved.

---

[5] Note that Drake's (1972) method, described briefly on p. 23 of this thesis, gives the same K_D values for equation (13a) as those obtained assuming that the activities of MgO and MnO are equal to their molar oxide concentrations.

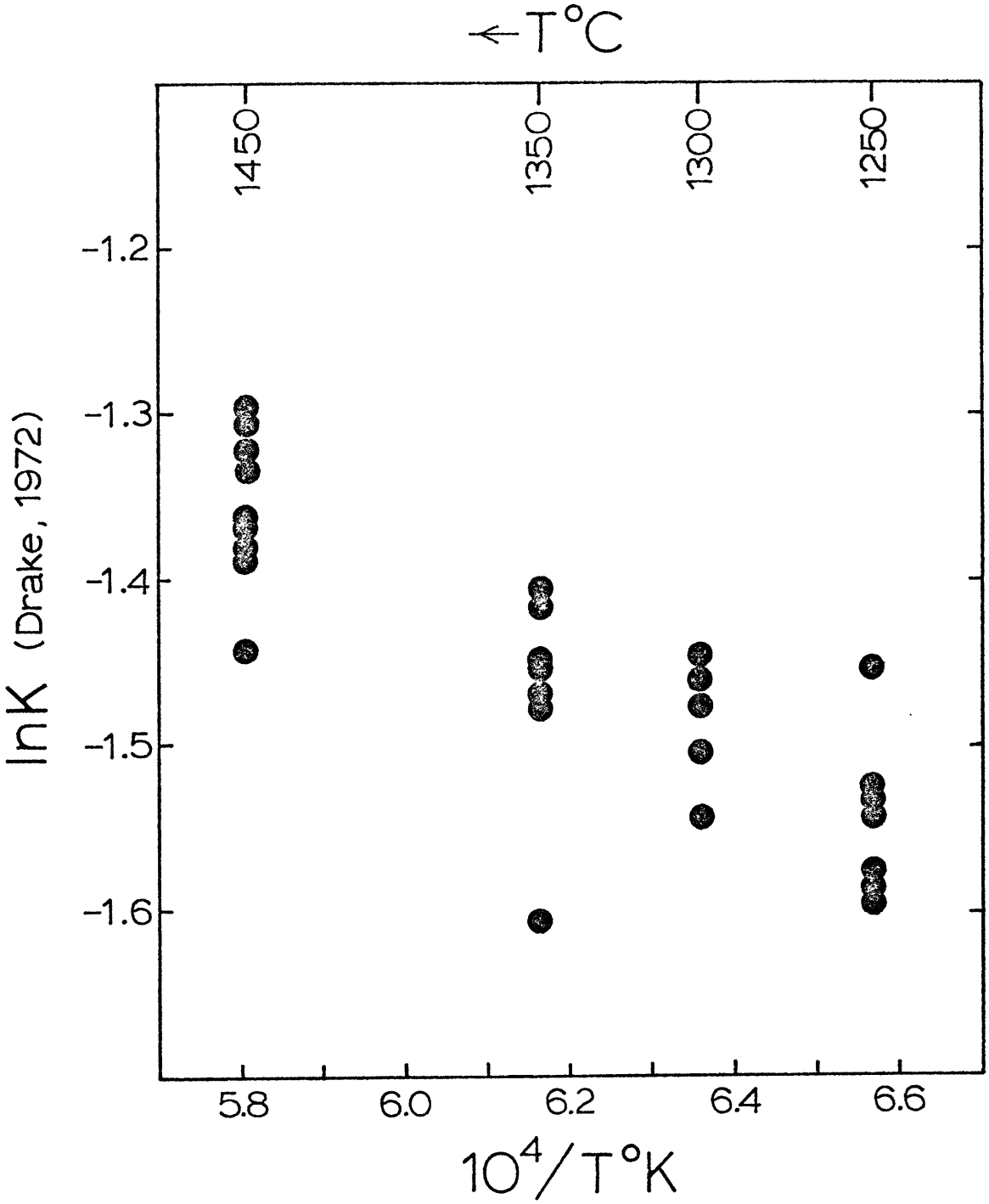


Figure 22. lnK vs. reciprocal absolute temperature for all Mn partitioning experiments. K is the equilibrium constant for reaction (13) (see text), calculated using the method of Drake (1972) to approximate oxide activities in the melt

In Fig. 23, the manganese partitioning data are plotted against the silicon: oxygen atomic ratio of the melts. In this diagram, four constant-temperature trends are readily distinguished. Thus, the plot separates the dependence of D_{Mn}^{Fo-liq} on melt composition from that on temperature. It should be noted that a variety of liquid compositions is represented on this diagram: the solid symbols are SiO_2-Al_2O_3-MgO-CaO-Na_2O melts, some of which are in the Fo-Ab-An plane; and the "B's" are synthetic iron-free basaltic compositions (see Table 4). The total range of SiO_2 content of the glasses is 44.5 to 65.0 wt. %. The silicon:oxygen atomic ratio thus appears to be a general and dominating influence on the compatibility of trace or minor amounts of Mn in silicate melts.

Figure 23 can be replotted to show the temperature-dependence of D_{Mn}^{Fo-liq} for constant values of Si:O in the melt. In general, a log-linear relation between D_{Mn}^{Fo-liq} and reciprocal absolute temperature should be expected, and is certainly apparent in Fig. 24, although the plot systematically changes slope for different values of Si:O.

4. Discussion

Implications for silicate melt structure.

The success of a melt composition parameter such as Si:O in explaining solid-liquid partitioning data implies that this ratio has significance to the structure of silicate melts. In some way, the Si:O ratio probably reflects the extent of melt

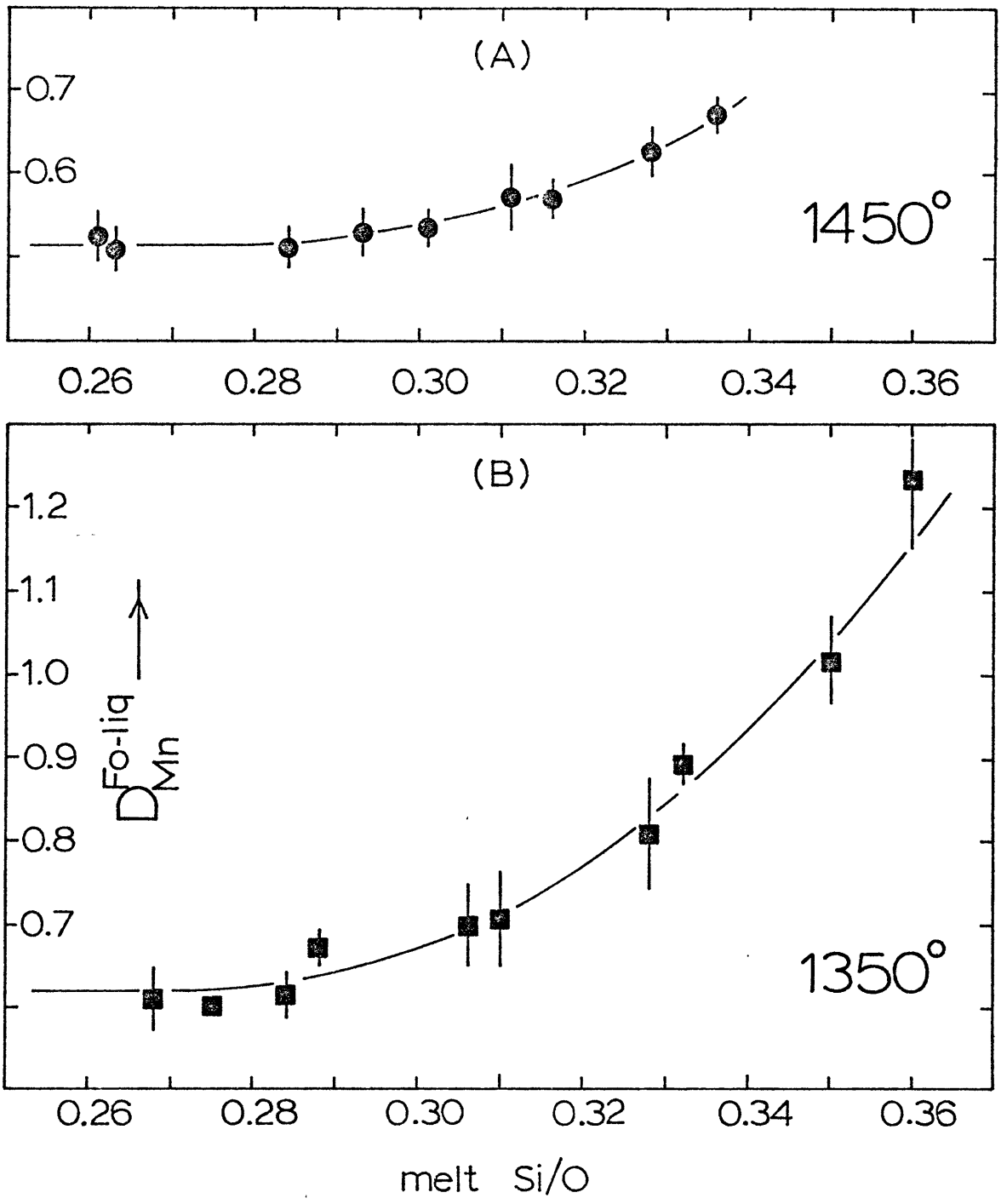


Figure 23 (A and B). D_{Mn}^{Fo-liq} vs. the Si/O ratio of the melt for runs made at 1450 and 1350°C, respectively. Error bars are ±2 standard errors of the mean; curves are visually fit to the data

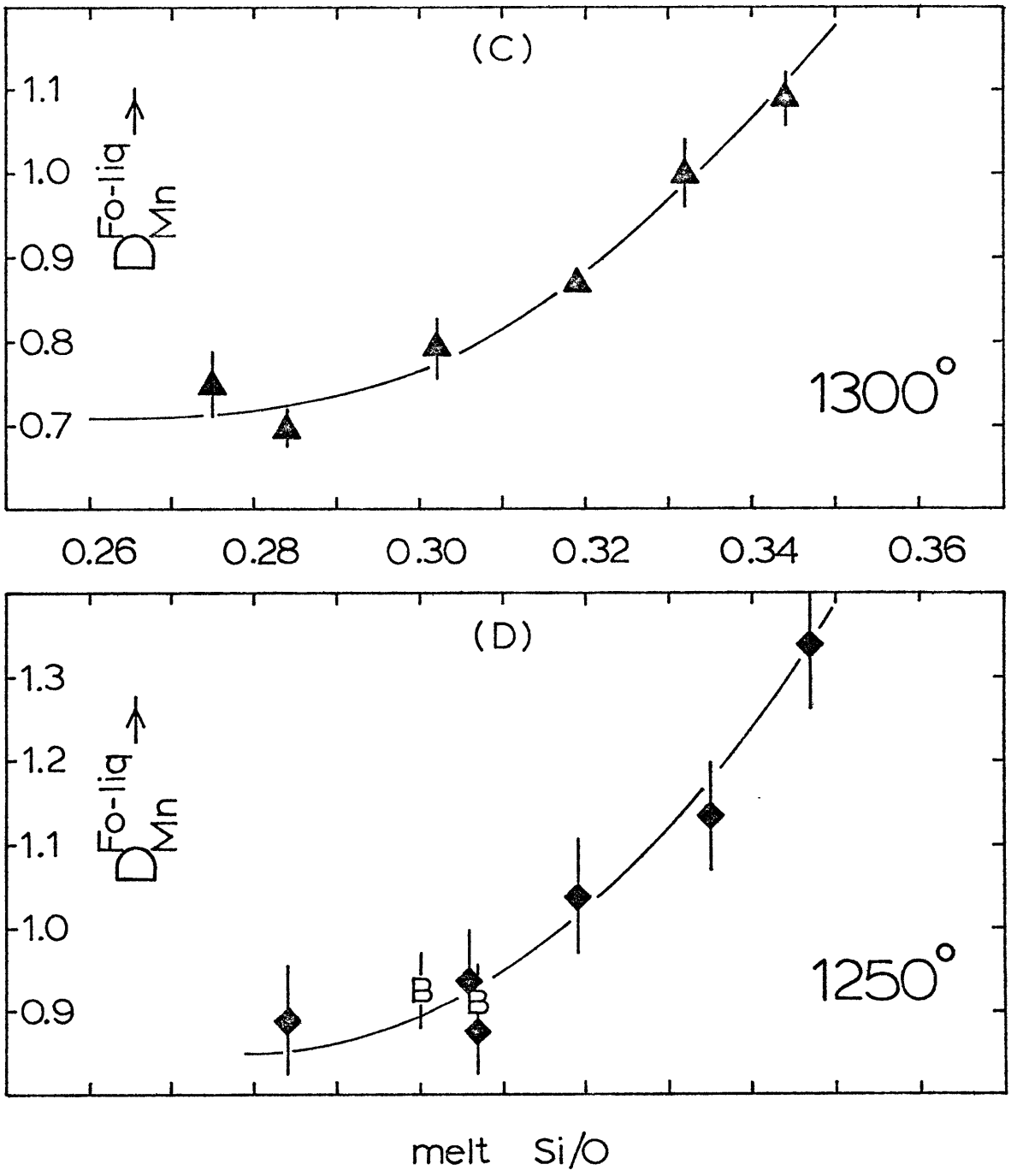


Figure 23 (C and D). D_{Mn}^{Fo-liq} vs. the Si/O ratio of the melt for runs made at 1300 and 1250°C, respectively. Error bars are ±2 standard errors of the mean; curves are visually fit to the data

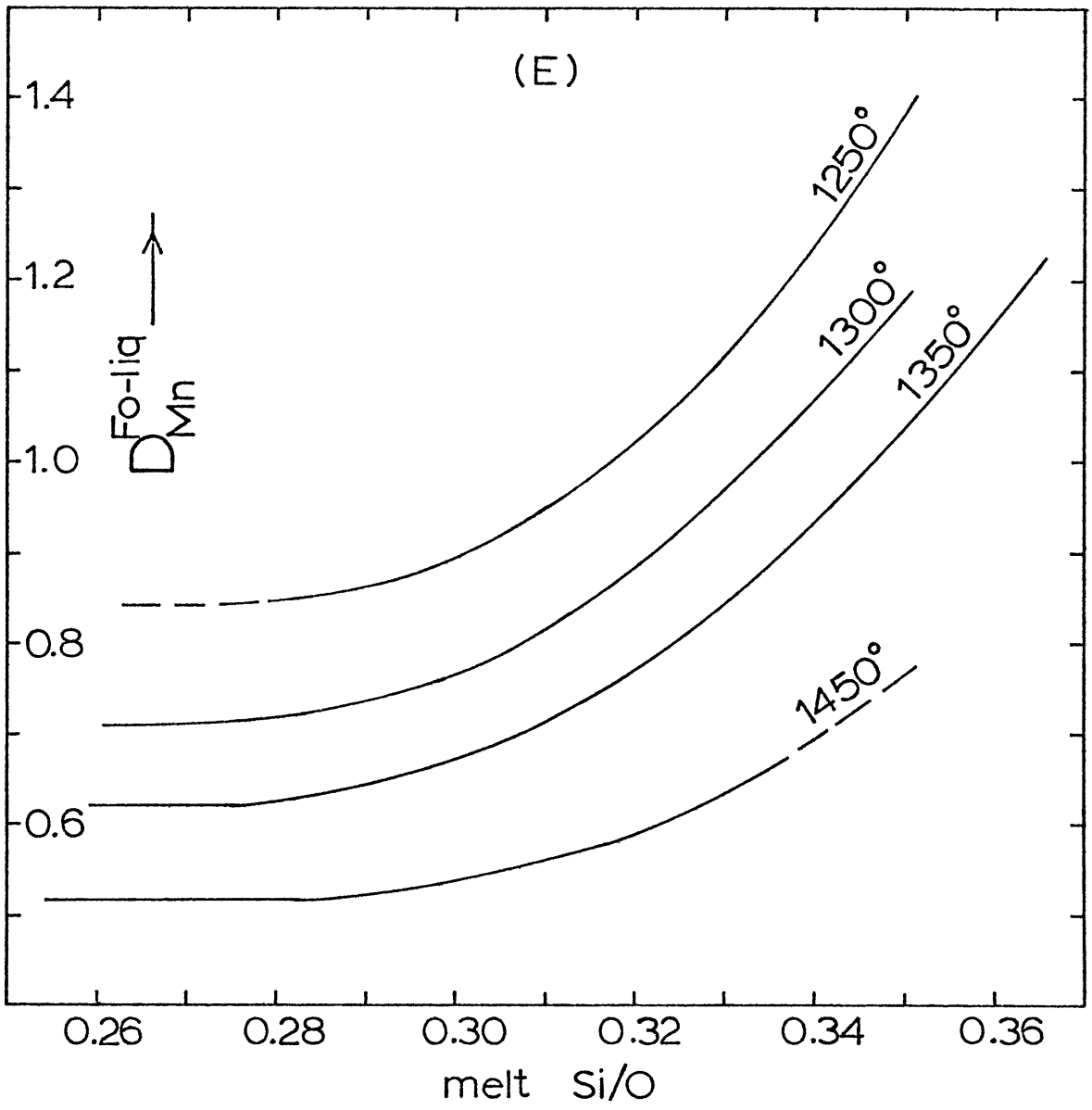


Figure 23 (E). Composite diagram of curves from Figs. 23 (A)-23 (D)

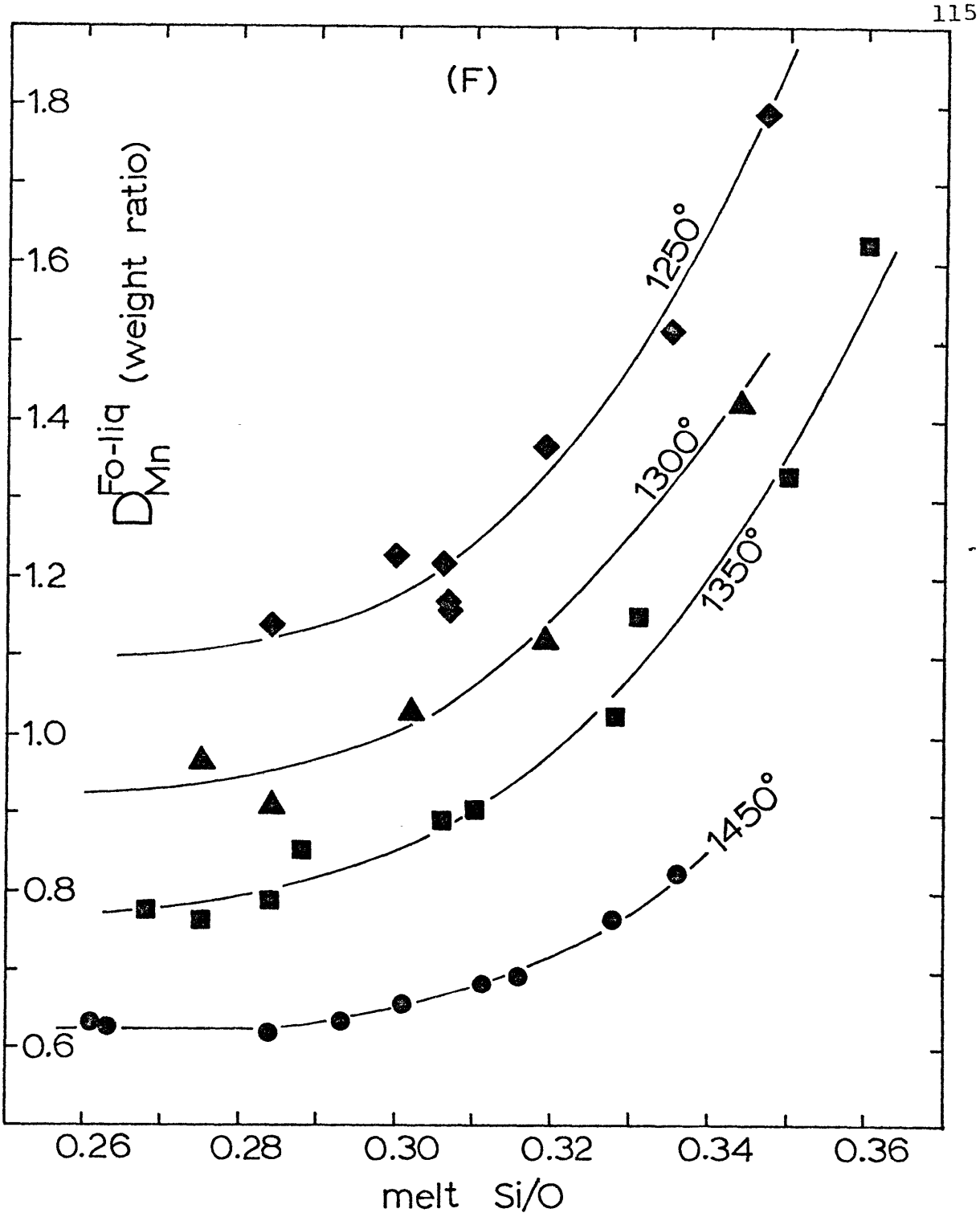


Figure 23 (F). Mn partitioning data plotted against melt Si/O using the conventional weight ratio partition coefficient ([wt% MnO in Fo]/[wt% MnO in glass])

polymerization, as suggested by the similarity in general shape of the curves in Fig. 23 to the proposed melt polymerization curve of Toop and Samis (1962a; see Fig. 26). In the following paragraphs, some simple theoretical considerations on the structure of silicate melts are invoked to support the validity of the Si:O ratio as a general structural parameter.

Pure molten SiO_2, which has a Si:O value of 0.5, is a completely polymerized, 3-dimensional network of silicate tetrahedra (Mozzi and Warren, 1969). Complete polymerization is in fact dictated by the Si:O stoichiometry and the requirement that each silicon be surrounded by four oxygens. All oxygens are therefore bridging oxygens, bonded to two silicon atoms. If a metal oxide is dissolved in pure molten silica, the total Si:O value of the melt falls below 0.5, and complete polymerization is no longer required to maintain the 4-fold coordination of each silicon by oxygen. In this manner, nonbridging oxygen ions are created in the melt as an oxide is added to pure SiO_2. The number of nonbridging oxygens created does not depend upon the identity of the oxide, but only upon the number of oxygen ions introduced into the melt. This conclusion is supported by the infrared reflectance spectra of binary silicate glasses, which have absorption features attributable to nonbridging oxygen ions that are remarkably similar for alkali and alkaline earth silicate glasses of the same Si:O atomic ratio (Simon, 1960). Thus, at least for binary $MO-SiO_2$ or M_2O-SiO_2 liquids, the proportion of nonbridging to total oxygen ions appears to

be largely determined by the Si:O ratio.

If the Si:O ratio of a melt provides a general measure of the proportion of nonbridging oxygen ions, then the observed correlation between D_{Mn}^{Fo-liq} and Si:O can be rationalized. Levin and Block (1957) pointed out that for silicate melts, as for complex ionic crystals, Pauling's rules for structural stability are probably applicable. The first of Pauling's rules states (in part) that each cation is surrounded by anions that form a coordinated polyhedron. Manganese ions in a silicate melt are thus coordinated by oxygen anions. More important, however, is the fact that the coordinated oxygen ions cannot be "saturated" or bonded to two silicons - they must be nonbridging or free oxygen anions. The stability or energy state of Mn^{2+} ions in a melt is therefore influenced by the availability of nonbridging oxygen ions to form coordination polyhedra. Hence, because melts of lower Si:O have more nonbridging oxygens, Mn^{2+} is more stable in basic melts. This greater stability (lower chemical potential) is evidenced by lower D_{Mn}^{Fo-liq} values for forsterite coexisting with basic melt.

The relative difference in energy states of Mn^{2+} ions in melts of different Si:O can be quantified using information contained in Fig. 24. Because Mn is present at Henry's law concentration in both forsterite and liquid, a relation of the following form describes the temperature dependence of D_{Mn}^{Fo-liq}:

$$\ln D_{Mn}^{Fo-liq} = - \Delta\bar{G}^{\circ}/RT + \text{constant} \qquad (14)$$

which can be rewritten

$$\ln D_{Mn}^{Fo\text{-}liq} = -\frac{\Delta\bar{H}^\circ}{RT} + \frac{\Delta\bar{S}^\circ}{R} + \text{constant} \qquad (14a)$$

In these equations, $\Delta\bar{G}^\circ$, $\Delta\bar{H}^\circ$, and $\Delta\bar{S}^\circ$ refer to molar energy changes associated with the transfer of Mn from liquid to forsterite when Mn is in its standard state in both phases. Because the standard states are undefined, the energy quantities have no specific meaning, but they can be used for comparative purposes. From equation (14a) it is clear that the slopes of the lines in Fig. 24 are equal to $-\Delta\bar{H}^\circ/R$ for Mn partitioning between forsterite and melts of various Si:O ratios. Calculated values for $\Delta\bar{H}^\circ$ (Fig. 24) show that the transfer of Mn from liquid to forsterite is 4.2 kcal/mole more exothermic for acidic melts (Si:O = 0.35) than for basic melts (Si:O = 0.29). A higher energy state for Mn ions in acidic melts is thus indicated.

An interesting feature of Fig. 23(e) is that for melt Si:O values below about 0.28, $D_{Mn}^{Fo\text{-}liq}$ is independent of melt composition. Apparently, Mn^{2+} ions are equally compatible in all very basic melts. It is therefore likely that the 0.28 Si:O ratio has some structural significance for silicate liquids, perhaps indicating the composition at which polymeric units become completely dissociated (when bridging oxygens are essentially absent). According to Huggins et al. (1943), the specific silicate anionic species in a simple glass can be predicted from the Si:O ratio. The predictions of this model, summarized in Table 6, indicate that isolated silicate tetrahedra begin to

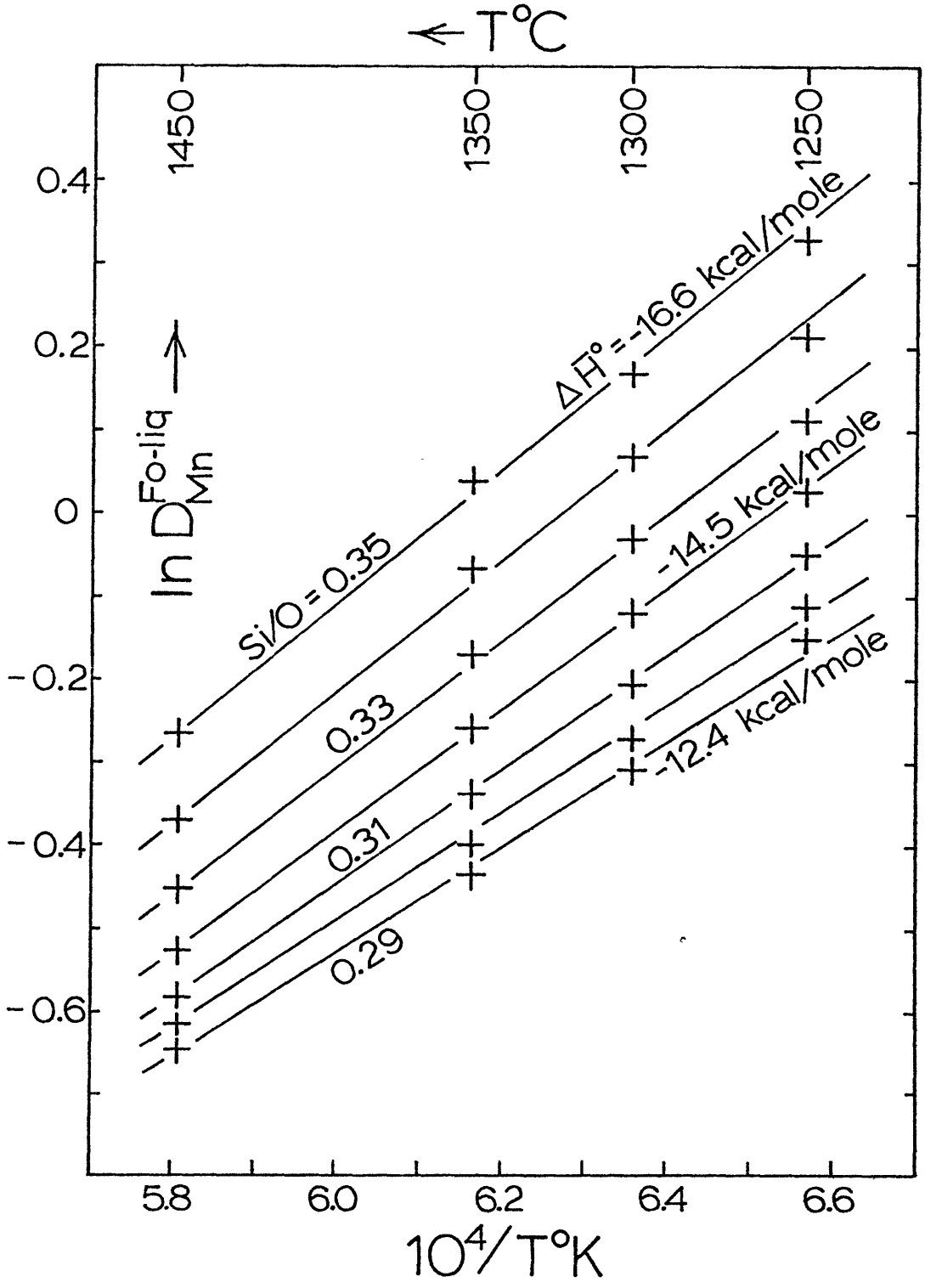


Figure 24. $\ln D_{Mn}^{Fo-liq}$ vs. reciprocal absolute temperature for melts of constant Si/O. The crosses are not error bars, but represent the intersection of vertical, constant-Si/O lines with the isothermal curves in Fig. 23(E)

Table 6. Anionic structures present in simple silicate glasses of varying SiO_2 concentration (and Si/O), according to Huggins, et.al.(1943).

mole % SiO_2	Si/O ratio	anionic structures
33	0.250	single SiO_4^{4-} tetrahedra
33-40	0.250-0.286	SiO_4^{4-} and $Si_2O_7^{6-}$
40	0.286	$Si_2O_7^{6-}$
40-50	0.286-0.333	longer chains and rings
50	0.333	rings and/or infinitely long chains
50-66	0.333-0.400	chains and sheets with or without rings
66	0.400	infinite 2-dimensional sheets
66-100	0.400-0.500	sheets and 3-dimensional network
100	0.500	3-dimensional network

appear in melts having Si:O values less than 0.286 - almost exactly the composition at which $D_{Mn}^{Fo\text{-}liq}$ ceases to vary with Si:O.

The above coincidence suggests a thermodynamic formalism that may represent the partitioning of Mn between forsterite and melt more accurately than previous treatments. Electrical conductivity measurements have established the strongly ionic nature of silicate liquids (Bockris et al., 1948). It is therefore reasonable to write a reaction like

$$2Mn^{2+}_{(melt)} + SiO_4^{4-}{}_{(melt)} \rightleftarrows Mn_2SiO_4{}_{olivine} \qquad (15)$$

to describe Mn partitioning between olivine and melt. This reaction has an equilibrium constant

$$K_{eq} = \frac{[Mn_2SiO_4]^2_{olivine}}{[Mn^{2+}]^2_{melt}[SiO_4^{4-}]_{melt}} \qquad (15a)$$

where the bracketed symbols represent activities. In this representation, the Mn partition coefficient is a function of the activity of a specific silicate anion (SiO_4^{4-}) in the melt. The activity of SiO_4^{4-} is, as usual, difficult to express. However, if the model of Huggins et al. (1943) is correct in predicting the proliferation of individual SiO_4^{4-} units at Si:O values less than 0.286, the Temkin (1945) ionic fraction concept might be called upon. In very basic melts, where SiO_4^{4-} is the dominant anionic species, Temkin's anionic fraction or activity of SiO_4^{4-} will be close to 1. Unless the Si:O ratio exceeds $\sim$0.28 and more complex anions begin to form in signifi-

cant amounts, $[SiO_4^{4-}]$ will be essentially independent of melt composition. Thus, it seems reasonable that in very basic melts D_{Mn}^{Fo-liq} should also be independent of melt composition, as observed in Fig. 23(e).

Geochemical implications.

Melt composition effects in natural systems. The experimental data obtained in this study firmly establish the importance of melt compositional variation to the partitioning of trace elements between olivine and liquid in a magma. From Fig. 23 (e and f), it is obvious that melt composition effects increase in significance with decreasing basicity of the melt. In ultrabasic magmas, for example, melt composition has no influence on olivine-liquid partitioning. In basaltic magmas, which have Si:O values ranging between $\sim$0.290 and 0.315, chemical composition has a minor effect on the compatibility of trace elements in the melt. For andesitic (Si:O $\gtrsim$ 0.32-0.35) and more siliceous magmas, melt composition becomes extremely important. It should of course be noted that the temperature range covered by the experiments in this study is for the most part above normal magmatic temperatures. However, if the data are extrapolated to lower temperatures, the influence of melt composition on D_{Mn}^{Fo-liq} appears only to increase.

Other transition elements. In the experiments described in Part I of this thesis, I found that three transition elements - Mn, Ti, and Cr - were identically partitioned between immiscible

acidic and basic melts at 1180°C (all three elements were enriched in the basic melt by a factor of 3 to 1; see Fig. 11). I would therefore predict that the partition coefficients for Cr and Ti between forsterite and melt would show the same dependence on melt composition as $D_{Mn}^{Fo\text{-}liq}$. The absolute values of $D_{Cr}^{Fo\text{-}liq}$, $D_{Ti}^{Fo\text{-}liq}$, and $D_{Mn}^{Fo\text{-}liq}$ would certainly differ, but the observed factor-of-two change in $D_{Mn}^{Fo\text{-}liq}$ along the 1350° isotherm in Fig. 23(e) would also occur for $D_{Cr}^{Fo\text{-}liq}$ and $D_{Ti}^{Fo\text{-}liq}$. Hart et al. (unpublished data) have in fact verified this two-fold change in the partitioning of nickel for the same forsterite-liquid pairs that define the 1350° isotherm in Fig. 23(e).

Geothermometry. I specifically omitted iron from the bulk compositions used in this study because I wished to maintain a constant olivine composition over a range of temperature and melt composition. The absence of iron from charges invalidates immediate application of Fig. 24 as a geothermometer for olivine-bearing volcanic rocks; the effect of iron on manganese partitioning between olivine and melt has not been evaluated. However, some insight into the applicability of my data to natural systems can be gained by comparing my results with those of other workers on iron-bearing natural and synthetic compositions.

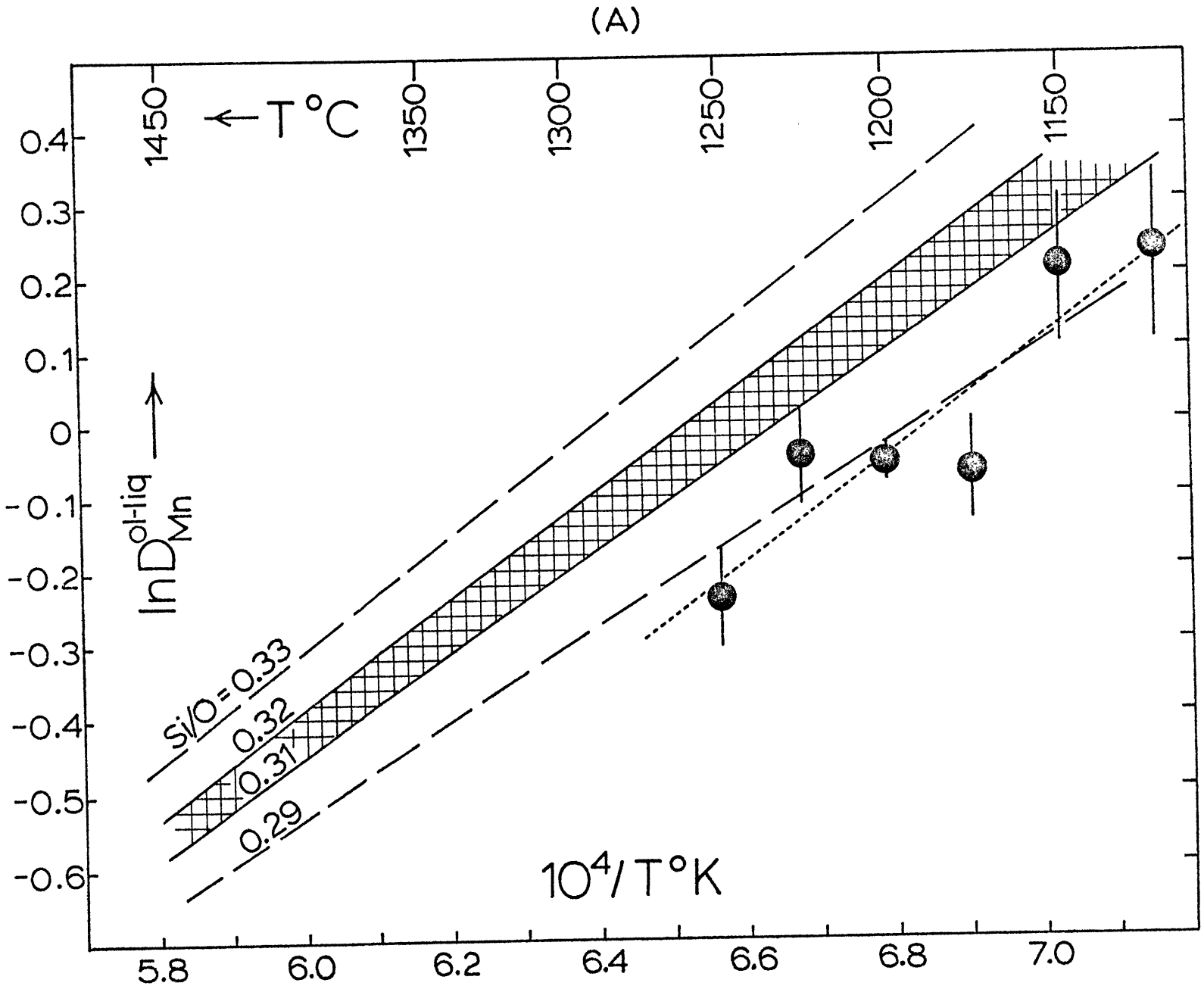
Duke (1976) measured six values for $D_{Mn}^{ol\text{-}liq}$ over the temperature range 1125-1250°C. His liquid compositions range in molar MgO/(MgO + FeO) from 0.895 to 0.338, and his olivines from $Fo_{95.4}$ to $Fo_{61.0}$ (Table 7a). In Fig. 25(a), Duke's data

are compared with constant-Si/O, ln D vs. 1/T lines from Fig. 24. His partition coefficients are somewhat lower than would be predicted from my iron-free temperature calibration, but the slope of the plot is similar. There does not appear to be a systematic effect on D_{Mn}^{ol-liq} caused by the decrease in MgO/(MgO + FeO) with decreasing temperature. If used directly as a geothermometer for natural systems, my ln D vs. 1/T calibration would give temperatures about 50°C higher than Duke's calibration.

In Fig. 25 (b), the manganese partitioning data of Leeman (1974) are compared with those obtained in the present study. Leeman's glass compositions have molar MgO/(MgO + total Fe as FeO) values ranging from 0.804 to 0.284; these glasses coexist with olivines ranging from $Fo_{96.7}$ to $Fo_{50.2}$ (Table 7b). The slope of the line defined by Leeman's data points is considerably steeper than that of the present study and that of Duke (1976). This steeper slope cannot be completely accounted for by the changing Si/O ratios of the glasses, which fall in a fairly narrow range between 0.288 and 0.321 (Table 7b). The most likely explanation for the discrepancy between my data and Leeman's is that the different slopes are due simply to a difference in thermodynamics between iron-bearing and iron-free systems. A better assessment of this possibility could be made if Duke's data covered a larger temperature range. In terms of slope on a ln D vs. 1/T plot, Duke's data are more in accord with mine than with Leeman's. Another factor which may be of

Figure 25(a). Comparison of manganese partitioning data (mole ratio) for iron-bearing compositions (Duke, 1976) with iron-free system data obtained in this study. Constant Si/O lines are from Fig. 24, extended to lower temperature. All six of Duke's liquid compositions have Si/O values between 0.312 and 0.317 (Table 7a), so his data points ideally should plot in the crosshatched area of the diagram. Error bars are ±2 sigma; dotted line is a least-squares fit to Duke's six data points.

(b) Manganese partitioning data of Leeman (1974) compared with the present study. Leeman's data (solid circles) represent glasses having a wide range of Mg/Fe ratios, but the Si/O values are confined to a fairly narrow range (0.288 to 0.321; see Table 7b). Dashed constant-Si/O lines (0.29 and 0.32) from Fig. 24 are drawn in for reference. Open triangles are Duke's (1976) data points, which define the dotted line. Solid line is a least-squares fit to Leeman's data; error bars are ±2 sigma. See text for discussion


(A)
T°C
1450
1350
1300
1250
1200
1150
0.4
0.3
0.2
0.1
0
-0.1
-0.2
-0.3
-0.4
-0.5
-0.6
$\ln D_{Mn}^{ol\text{-}liq}$
Si/O=0.33
0.32
0.31
0.29
$10^4/T°K$
5.8
6.0
6.2
6.4
6.6
6.8
7.0

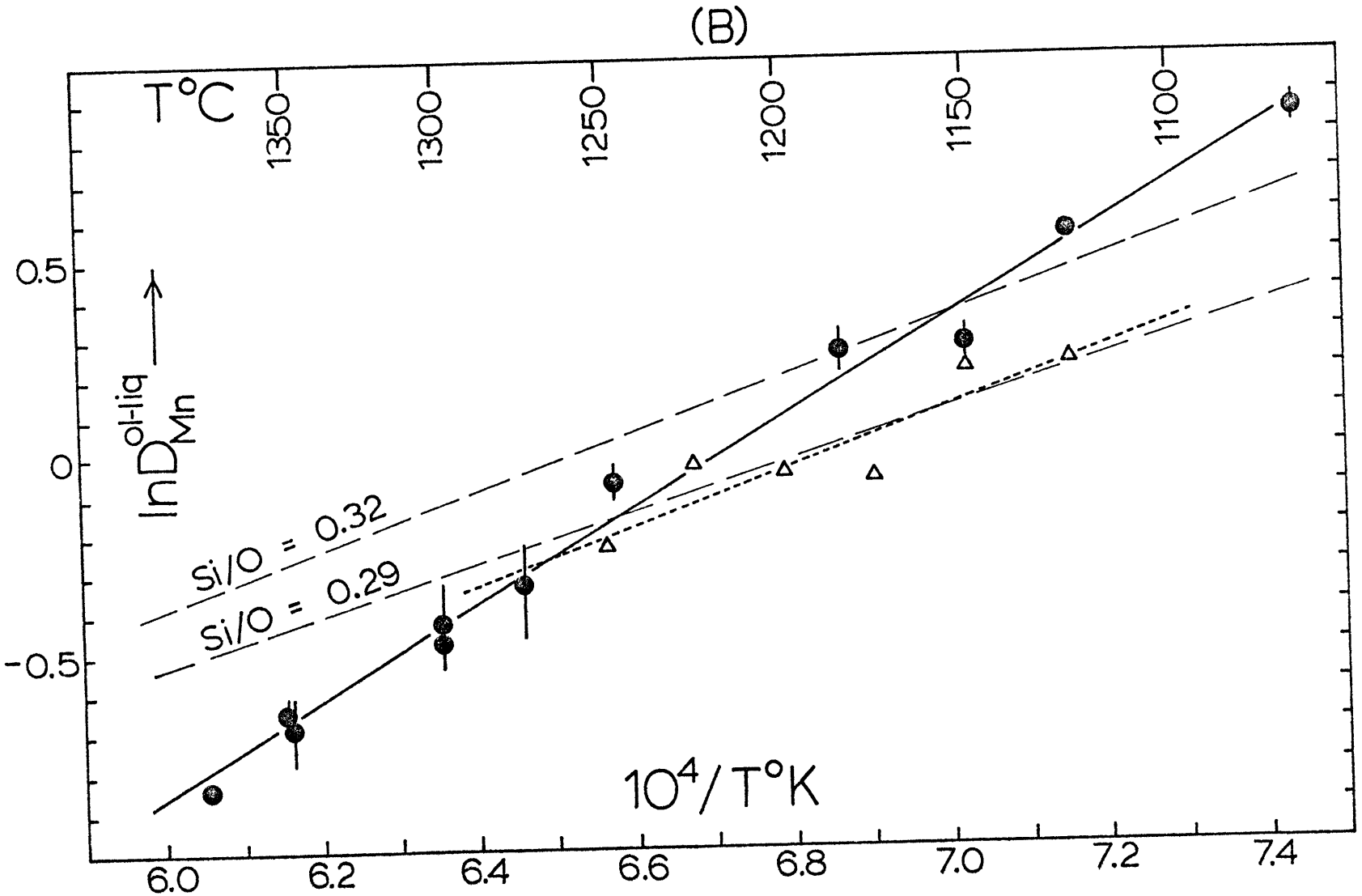

(B)
T°C
1350
1300
1250
1200
1150
1100
0.5
0
-0.5
$\ln D_{Mn}^{ol\text{-}liq}$
Si/O = 0.32
Si/O = 0.29
$10^4/T°K$
6.0
6.2
6.4
6.6
6.8
7.0
7.2
7.4

Table 7(a). Summary of coexisting glass and olivine compositions and Mn partitioning data for iron-bearing charges of Duke (1976)

Run no.	97		100		95		103		101		105	
T^oC	1250		1225		1200		1175		1150		1125	
log f_{O2}	-9.7		-10.0		-10.3		-10.8		-11.0		-11.4	
Liquid Compositions												
	wt%	mole %	wt%	mole %	wt%	mole %	wt%	mole %	wt%	mole %	wt%	mole %
SiO_2	54.1	54.0	52.5	53.2	52.6	54.4	51.6	53.7	51.3	53.4	50.7	53.6
Al_2O_3	14.1	8.3	14.8	8.8	16.1	9.8	13.1	8.0	12.5	7.7	13.2	8.2
FeO[a]	2.4	2.0	3.7	3.1	5.6	4.8	12.0	10.5	16.4	14.3	17.1	15.1
MgO	11.4	17.0	10.5	15.9	8.0	12.3	7.1	11.0	6.2	9.6	4.9	7.7
CaO	15.1	16.1	14.1	15.3	12.6	14.0	12.3	13.7	11.2	12.5	10.6	12.0
Na_2O	2.7	2.6	3.6	3.5	4.6	4.6	2.9	2.9	2.5	2.5	3.2	3.3
total	99.8		99.2		99.5		99.0		100.1		99.7	
Si/O	0.316		0.312		0.313		0.317		0.316		0.315	
Olivine Compositions												
mole %	$Fo_{95.4}$		$Fo_{93.8}$		$Fo_{90.7}$		$Fo_{80.2}$		$Fo_{67.8}$		$Fo_{61.0}$	
D_{Mn}^{ol-liq}[b] (±2σ)	0.787±.05		0.960±.06		0.946±.02		0.937±.06		1.237±.12		1.264±.14	

[a] all Fe as FeO

[b] mole ratio = (mole% MnO in olivine)/(mole% MnO in glass)

Table 7(b). Summary of coexisting glass and olivine compositions and Mn partitioning data for iron-bearing charges of Leeman (1974)

run no.	T1		T3		T4	
$T^{o}C$	1184		1300		1352	
log f_{O2}	-7.1		-1.6		-1.1	
GLASS ANALYSES*						
	wt%	mole%	wt%	mole%	wt%	mole%
SiO_2	48.39	52.49	46.28	50.79	45.62	49.33
TiO_2	3.08	2.51	1.01	0.83	0.98	0.80
Al_2O_3	15.20	9.72	10.53	6.81	9.88	6.30
Fe_2O_3	3.31	1.35	11.41	4.71	10.75	4.37
FeO	8.62	7.82	2.61	2.39	2.47	2.23
MgO	7.18	11.61	12.95	21.18	15.65	25.22
CaO	9.82	11.41	9.60	11.29	8.81	10.21
Na_2O	2.49	2.62	1.51	1.61	1.18	1.23
K_2O	0.55	0.38	0.33	0.23	0.24	0.17
MnO	0.10	0.09	0.16	0.15	0.15	0.14
total	98.74		96.39		95.73	
Si/O	0.296		0.291		0.288	
OLIVINE ANALYSES**						
SiO_2	39.32	33.51	42.19	33.53	41.98	33.65
MgO	41.27	52.41	54.17	64.17	53.68	64.13
FeO	19.60	13.97	3.33	2.21	3.22	2.16
MnO	0.16	0.12	0.14	0.09	0.11	0.07
total	100.35		99.83		98.99	
D^{ol-liq}_{Mn} (molar)	1.29±.07		0.62±.01		0.52±.02	

Table 7(b). (continued)

run no.	T5		T8		T9		T10	
T^oC	1248		1125		1151		1378	
log f_{O2}	-6.3		-7.9		-7.5		-4.8	
GLASS ANALYSES*								
	wt%	mole%	wt%	mole%	wt%	mole%	wt%	mole%
SiO_2	48.72	52.43	50.48	56.81	47.62	52.63	46.97	47.61
TiO_2	1.85	1.50	3.93	3.33	3.72	3.09	2.03	1.55
Al_2O_3	12.41	7.87	11.49	7.62	12.75	8.30	10.01	5.98
Fe_2O_3	3.24	1.31	3.29	1.39	4.18	1.74	3.95	1.50
FeO	8.09	7.28	8.21	7.73	10.87	10.05	8.80	7.46
MgO	9.01	14.45	4.43	7.43	5.82	9.59	16.38	24.75
CaO	11.08	12.78	8.95	10.79	9.27	10.98	8.99	9.76
Na_2O	1.84	1.92	2.46	2.68	2.66	2.85	1.14	1.12
K_2O	0.48	0.33	1.28	0.92	0.93	0.66	0.27	0.18
MnO	0.14	0.13	0.11	0.10	0.12	0.11	0.10	0.09
total	96.88		95.96		97.94		98.64	
Si/O	0.304		0.321		0.299		0.290	
OLIVINE ANALYSES**								
SiO_2	40.01	33.74	36.56	33.29	38.48	33.45	40.06	33.29
MgO	45.34	56.99	32.52	44.09	38.33	49.66	47.44	58.75
FeO	12.97	9.15	22.46	17.10	23.02	16.73	8.25	5.72
MnO	0.17	0.12	0.24	0.18	0.20	0.15	0.05	0.04
total	98.49		99.03		100.03		99.10	
D_{Mn}^{ol-liq} (molar)	0.93±.04		1.74±.02		1.32±.05		0.43±.01	

Table 7(b). (continued)

run no.	T11		T12		T15		T17	
T°C	1275		1350		1071		1300	
log f_{O2}	-5.9		-7.2		-8.8		-5.8	
GLASS ANALYSES*								
	wt%	mole%	wt%	mole%	wt%	mole%	wt%	mole%
SiO_2	48.66	50.90	49.74	49.72	48.75	54.70	49.15	50.81
TiO_2	2.50	1.97	2.31	1.74	3.65	3.08	2.45	1.91
Al_2O_3	11.43	7.04	10.42	6.14	12.23	8.08	11.88	7.24
Fe_2O_3	3.63	1.43	1.16	0.44	4.04	1.71	2.91	1.13
FeO	8.50	7.43	8.81	7.36	12.09	11.35	7.47	6.46
MgO	10.76	16.77	15.71	23.40	3.06	5.12	11.81	18.20
CaO	10.96	12.28	10.07	10.79	8.72	10.48	10.62	11.76
Na_2O	1.80	1.82	0.59	0.57	3.18	3.46	2.07	2.07
K_2O	0.42	0.28	0.14	0.09	2.47	1.77	0.50	0.33
MnO	0.08	0.07	0.07	0.06	0.28	0.27	0.11	0.10
total	98.74		99.02		98.47		98.97	
Si/O	0.300		0.301		0.308		0.300	
OLIVINE ANALYSES**								
SiO_2	40.18	33.34	40.65	33.25	35.13	33.28	40.67	33.54
MgO	47.08	58.23	49.16	59.93	23.49	33.17	47.86	58.83
FeO	12.07	8.38	9.93	6.79	41.55	32.92	10.97	7.57
MnO	0.07	0.05	0.04	0.03	0.78	0.62	0.09	0.06
total	99.40		99.78		100.95		99.59	
D_{Mn}^{ol-liq}	0.72±.10		0.50±.04		2.35±.08		0.65±.07	

* all glasses contain less than 0.1% NiO+CoO, except T8, which contains 1.33% CoO

** all olivines contain less than 1.5% CaO+NiO+CoO, except T8 (7.25% CoO) and T10 (3.30% NiO)

Table 8. Comparison of temperatures obtained from the calibration lines of Duke (1976), Leeman (1974), and this study over a reasonable range of basalt liquidus temperatures. The Si/O = 0.30 line from my calibration was used

$\ln D_{Mn}^{ol-liq}$ (mole ratio)	T°C		
	Duke	Leeman	Watson
-0.2	1242	1244	1287
-0.1	1215	1235	1253
0.0	1186	1214	1219
0.1	1158	1197	1187
0.2	1131	1180	1158
0.3	1107	1162	1130
0.4	1083	1145	1100

importance is that some of Leeman's glass analyses are not particularly good, often totalling only about 96%. This low total is probably not due to a uniform analytical problem with all elements, but to inaccurate values for one or two elements; this inaccuracy could have an appreciable effect on calculated composition parameters such as Si/O.

For temperature measurement applications, the overall agreement among the data of Duke (1976), Leeman (1974), and this study is fairly good: in the temperature range ∿1100-1250°C (a reasonable range of basaltic rock liquidus temperatures), the three calibrations give the same results within ∿50° (see Table 8); furthermore, temperatures obtained from my calibration line fall in between those of Duke and Leeman over the temperature range ∿1100-1200°C.

5. Concluding Remarks

In this work, I have taken a strictly empirical approach to the problem of melt composition dependence of crystal-liquid partition coefficients. I propose the use of the silicon: oxygen atomic ratio as a general liquid structure parameter primarily because it satisfies the experimental data, although simple melt structure considerations do lend support to its validity. It should be noted that the use of the Si:O ratio to predict average anionic species in glasses (Huggins et al., 1943) is by no means universally accepted. Mackenzie (1960), for example, feels that this model is unacceptable because it does not account for discontinuous physical-property changes

that occur in silicate melts as metal oxide is added to molten SiO_2. The model of Huggins et al. is not entirely consistent with that of Toop and Samis (1962a), either. However, in dealing with the compatibility of trace elements in a melt, the proportion of nonbridging to total oxygen ions might well be the most important consideration. The Si:O ratio may determine this proportion independently of the actual silicate anions that form. For example, the proportion of nonbridging oxygens (and the Si:O ratio) could be the same for a melt containing a 50/50 mix of long and short polymeric chains as for a melt containing all medium-length chains. Although the average chain length for the two melts might be identical, their physical properties would undoubtedly differ. The equivalent availability of nonbridging oxygens in the two melts would make dissolved Mn^{2+} ions equally compatible.

Because natural melts (and the melts examined in this study) contain large amounts of Al_2O_3, the effect of this oxide on the production of nonbridging oxygens should be considered briefly. Aluminum is generally regarded as a network-forming cation (e.g. Flood and Knapp, 1968; Bottinga and Weill, 1972) because it can assume tetrahedral coordination and polymerize with silicate tetrahedra (Day and Rindone, 1962b). In complex melts, therefore, the presence of Al_2O_3 might be expected to result in fewer nonbridging oxygens, as depicted schematically by Sigel (1971, see Fig. 4). However, because each AlO_4 unit in a polymer chain has an excess -1 charge, one of the oxygens in

the unit is still available for coordination by another cation. Consequently, in terms of compatibility of trace cations, the effect of adding Al_2O_3 to a silicate melt may be similar to that of adding a network-modifying oxide that produces nonbridging oxygens. Hence, the generality of the simple Si:O ratio as an "oxygen availability" indicator is not destroyed by the presence of Al_2O_3.

In natural melts, H_2O and CO_2 can be significant constituents, especially if considered on a mole per cent basis. The effect of these components on crystal-liquid partition coefficients is unknown, but if their dissolution mechanisms produce nonbridging oxygens (see Uys and King, 1963; Mysen et al., 1976 for discussion), it is possible that the applicability of the Si:O ratio can be extended to hydrous, CO_2-bearing melts.

In any case, the empirical use of the Si:O ratio to eliminate melt composition dependence in the partitioning of manganese between olivine and volatile-free melt seems more satisfactory than previous equilibrium constant approaches.

SUMMARY AND SYNTHESIS, WITH SOME SPECULATIONS

This final section summarizes the most important results and implications of the experimental data presented in the preceding sections of this thesis. Where relevant, I will briefly discuss how my work has augmented existing knowledge, and where, specifically, it supports or discredits previous theories or models. Although this section is subdivided into separate headings "melt structure" and "geochemistry," it should be noted that this distinction of topics is somewhat artificial, because geochemically significant effects are ultimately caused by melt structural influences.

1. Melt Structure

The results of experiments on the distribution of trace elements between coexisting acidic and basic melts lead to the following conclusions about the relative short-range structural characteristics of complex silicate liquids: 1)basic liquids have more sites suitable for trace cations whose oxygen coordination number in minerals is typically six or less; and 2) acidic melts have sites that can accomodate large monovalent cations well, and large divalent cations to some degree. The first conclusion is entirely compatible with melt structure models that predict a lesser degree of polymerization (hence more nonbridging oxygens) in basic melts (e.g. Toop and Samis, 1962a,b). Conclusion (2) above is consistnet with the observation of Eisenman (1962)

that glasses containing aluminum show a greater preference for large cations than do aluminum-free melts. Doremus (1973, Chap. 3) also pointed out that alkali ions in particular appear to be bonded to single nonbridging oxygens in glasses; thus, a large number of nonbridging oxygens is not required to coordinate each large alkali cation in an acidic melt.

The structural position occupied by a cation in a silicate liquid appears to be largely influenced by its ionic radius. This conclusion is suggested by the similarity in two-liquid partitioning of Zr^{4+} and Mg^{2+}, for example, which are identical in size. The rare earth elements probably all occupy the same type of site in silicate melts, because the partitioning behavior of La^{3+}, Sm^{3+}, and Lu^{3+} is similar. This site is almost certainly different from that of the much smaller Al^{3+} ion.

Like the rare earth elements, the transition elements examined in the two-liquid partitioning study (Ti, Cr, Mn) probably all assume the same structural position in melts (at least at trace element levels), because the distribution of these three elements between acidic and basic melts is nearly identical at low concentration.

Partitioning data for Mn between pure forsterite and a range of silicate melt compositions give some insight into the long-range or overall polymeric characteristics of the melts. In a qualitative way, the curves in Fig. 23(e) represent relative polymerization states of the various melts studied [compare Fig. 23(e) with Fig. 26]. Melts having Si/O

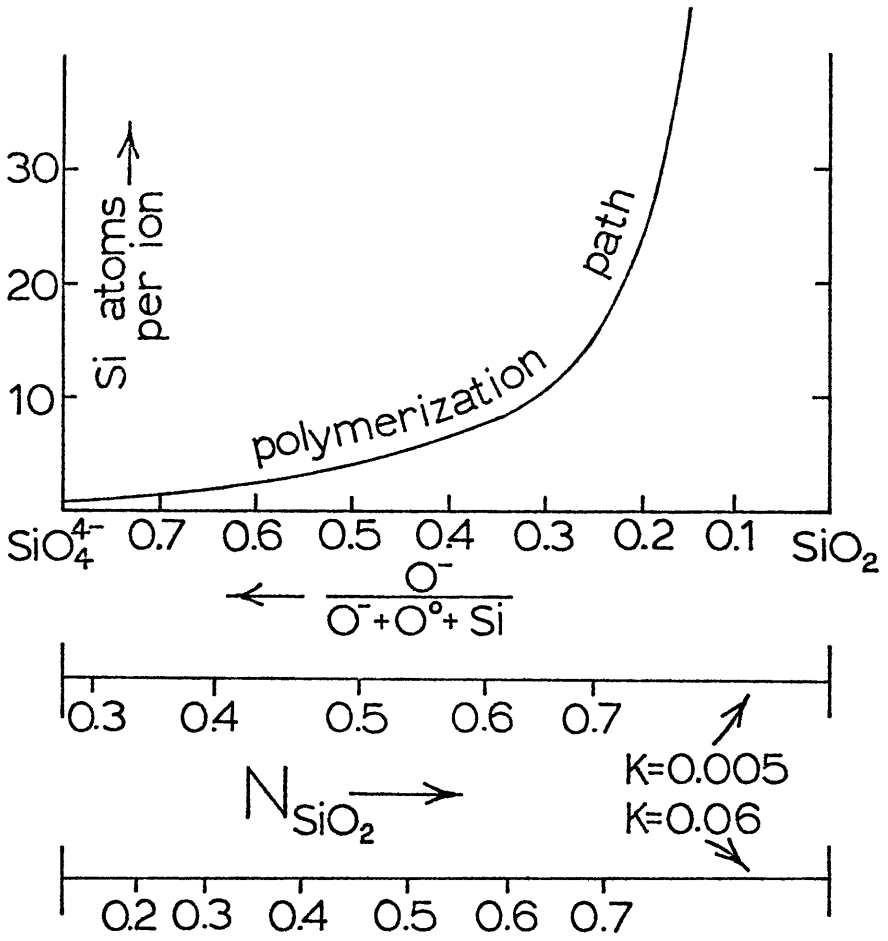


Figure 26. Plot of the proportion of singly bonded oxygen atoms (O^-) in any silicate anion vs. the number of silicon atoms per ion. The mole fraction of SiO_2 (N_{SiO_2}) in a binary silicate melt is indicated on the lower scales for K = 0.005 and 0.06 (from Toop and Samis, 1962a; see text). Note that polymerization curve is similar in overall shape to curves of Fig. 23

values less than about 0.28 are depolymerized to the extent that isolated silicate tetrahedra (SiO_4^{4-}) are the predominant anionic species. This conclusion is strongly suggested by the lack of dependence of D_{Mn}^{Fo-liq} on melt composition for melts with Si/O $\leq$ 0.28, and is predicted by the simple melt structure model of Huggins, et al. (1943). The generality of the Si/O ratio as a melt structure parameter is supported by the fact that numerous melt compositions are represented by the curves in Fig. 23 (see Table 4), and also by the compatibility of two-liquid partitioning data for Mn (K_2O-Al_2O_3-FeO-SiO_2 system) with those obtained on forsterite-liquid pairs (Fig. 27).

The experimental results reported in this thesis add little to the almost non-existent knowledge on temperature dependence of melt structure. However, because all four isothermal curves in Fig. 23 appear to flatten out at an Si/O value of $\sim$0.28, it seems likely that the critical composition for complete breakdown of silicate polymers is relatively insensitive to temperature (at least in the temperature range 1250-1450°C).

The overall picture of silicate melt structure, as deduced from the experiments reported in this thesis, is quite contradictory to the Bernal liquid model (see p. 23), which indirectly predicts an identical distribution of site types in all silicate liquids. My results clearly show that, except in very basic melts, the compatibility of a trace or minor

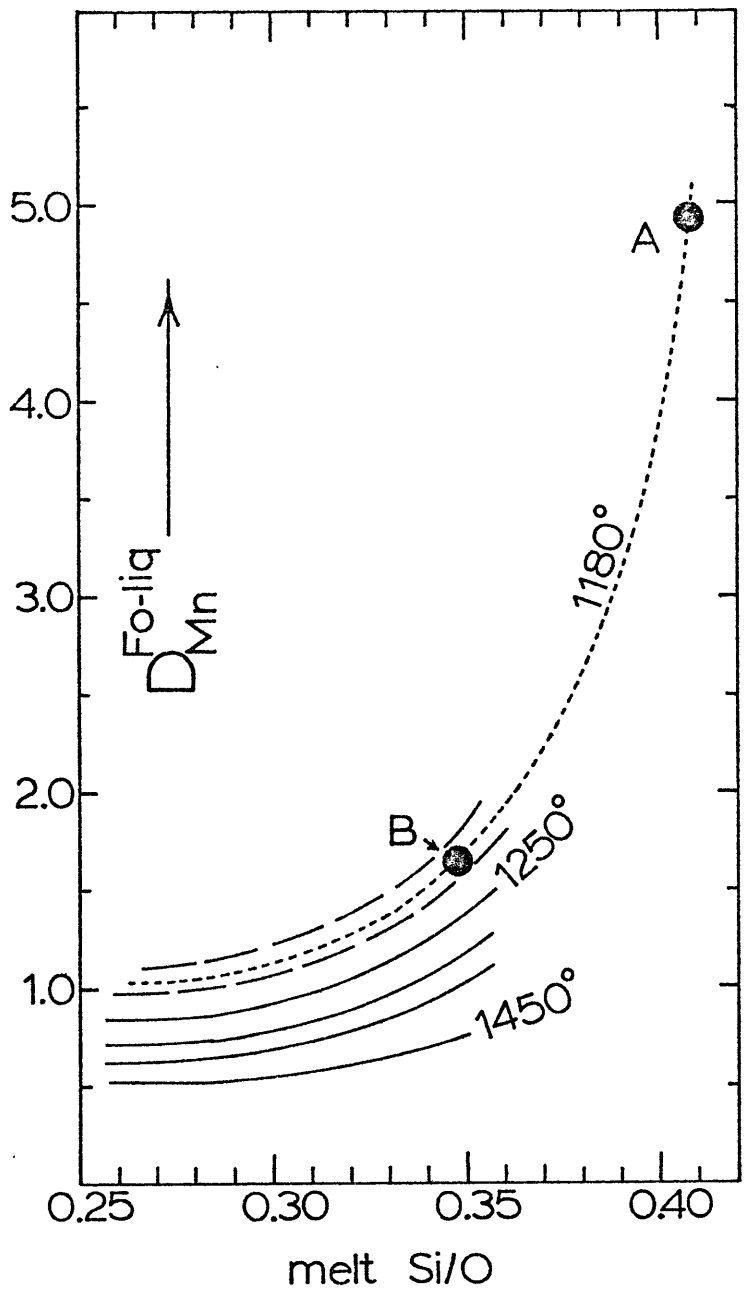


Figure 27. Speculative diagram showing consistency of two-liquid partitioning data for Mn (part I of this thesis) with Fo-liquid partitioning data (part II). Solid curves are taken from Fig. 23(E); dashed curves are extrapolated from the solid curves, and represent 1200° and 1150° isotherms; dotted curve is the speculated 1180° isotherm. Since liquid B has an Si/O value of 0.348, the hypothetical forsterite/liquid B partition coefficient at 1180° is ∿1.7 (point "B"). $D_{B/A}$ for Mn at 1180° is ∿3.0 (see part I of this thesis), so the point labelled "A" can be fixed on this diagram. The fact that the 1180° isotherm can be extended as a smooth curve through "A" suggests that the Si/O parameter is quite general as a relative measure of the compatibility of Mn in a silicate melt.

cation is a function of melt composition (as measured by the Si/O ratio). This dependence of cation compatibility on melt composition means one of two things: either the actual distribution of site types varies with Si/O, or the energy states of cations in the sites depend upon Si/O. Distinguishing between these two alternatives seems neither possible nor necessary at the present time.

2. Geochemistry

The experiments described in this thesis lead to the geochemically important conclusion that crystal-liquid partitioning of trace elements is influenced by bulk melt composition. This dependence is not related in a simple way to the concentration of a major "carrier" element in the melt. The two-liquid experiments suggest in particular that the distribution of small multivalent cations between crystals and melt is very sensitive to changes in melt composition. Phosphorus, for example, is enriched by a factor of $\sim$10 in basic relative to acidic liquid, indicating extreme incompatibility of this element in acidic melts. As a magma fractionates toward more acidic compositions, phosphorus will show a progressively stronger tendency to enter crystalline phases. The high phosphorus content (up to 0.6 wt% P_2O_5) of garnets coexisting with intermediate magmatic liquid (A.J. Irving, personal communication) can be explained by this melt-incompatibility effect.

Crystal-liquid partitioning of rare earth elements, as well as the first series transition elements, will change markedly with bulk melt composition, although the variation should be less pronounced than in the case of phosphorus. It also seems safe to conclude that crystal-liquid partition coefficients for all rare earth elements (except divalent Eu) will shift in parallel fashion as bulk melt composition varies. This conclusion also applies to the first series transition elements if the behavior of Cr, Ti, and Mn can be taken as representative of the entire series.

The results of experiments on manganese partitioning between forsterite and melt confirm the conclusion from the two-liquid experiments that Mn^{2+} is more compatible in basic than in acidic liquid. Furthermore, the rapid (exponential) increase of $D_{Mn}^{Fo\text{-}liq}$ with Si/O shows that the influence of melt composition on trace element partitioning in magmas becomes progressively stronger in fractionating from basic to intermediate and acidic melts. For melts more basic than typical basalt (i.e. $Si/O < 0.29$), the effect of melt composition on trace element partitioning (at least between olivine and melt) is negligible.

From the two-liquid partitioning data discussed in part I of this thesis, it appears that most elements behave as ideal dilute solutes in silicate melts up to levels well above those generally regarded as "trace" concentrations on rocks. This conclusion is in accord with the data of Leeman (1974), who

found that partition coefficients for Mn, Co, and Ni between olivine and basaltic melt are independent of concentration up to levels of several weight per cent. Drake's (1972) data on the concentration dependence of Sm, Ba, and Sr partitioning between plagioclase and melt are also consistent with Henry's law behavior of these elements in the melt to quite high concentration (∿5, 3, and 3 wt%, respectively).

3. Future Work

Two geochemically important questions related to the general topic of this thesis are left unanswered: 1) can the Si/O ratio be used quantitatively to describe melt composition dependence of trace element partitioning between any crystalline phase and silicate liquid, or does it work well only for olivine-liquid equilibria?; and 2) what effect does dissolved water or carbon dioxide in the melt have upon solid-liquid partitioning? These questions can only be answered by further systematic experimentation, but some intelligent speculation is possible at the present time.

1) In part II of this thesis, I proposed a formalism that I feel best represents the actual chemistry of Mn partitioning between olivine and silicate melt:

$$2Mn^{2+}_{melt} + SiO_4^{4-}{}_{melt} \rightleftharpoons Mn_2SiO_4 \text{ olivine}$$

with

$$K_{eq} = \frac{[Mn_2SiO_4]^2_{olivine}}{[Mn^{2+}]^2_{melt}\,[SiO_4^{4-}]_{melt}}$$

If this representation is valid, it is clear that $D_{Mn}^{Fo\text{-}liq}$ depends on the activity of a specific silicate anion (SiO_4^{4-}) in the melt. The Si/O ratio, as a measure of the proportion of nonbridging oxygens, probably takes account of changes in $[SiO_4^{4-}]_{melt}$, and is therefore successful as an empirical "correction factor" for the variation in $D_{Mn}^{Fo\text{-}liq}$ with melt composition. Olivine, however, is a chemically simple mineral -- for other minerals, the ionic reaction describing Mn partitioning will involve more species. The partitioning of Mn between diopside and melt, for example, could be represented by:

$$Ca^{2+}_{melt} + Mn^{2+}_{melt} + (Si_2O_7)^{6-}_{melt} \rightleftarrows CaMnSi_2O_6 \text{ diopside} + O^{2-}_{melt},$$

in which case $D_{Mn}^{Di\text{-}liq}$ depends not only upon the activity of a <u>different</u> silicate anion, but also upon Ca^{2+} and O^{2-} activities in the melt. Thus, from a thermodynamic viewpoint, it does not appear likely that Mn distribution between diopside and melt would vary in a manner parallel to variation in $D_{Mn}^{Fo\text{-}liq}$. In short, the Si/O ratio probably cannot account for simultaneous variation in the activities of several cationic and anionic species. Further experimental work is required to refute or support this suggestion.

2) The effect of dissolved volatiles on crystal-liquid partition coefficients depends upon the specific solution mechanisms that are operative. If, for example, water dissolves

by a depolymerization process that creates nonbridging oxygen ions (reaction [9], p. 42), then the general effect of dissolved water will probably be to lower the activity (i.e. increase the stability) of trace cations in the melt, thus decreasing $D^{x'l-liq}$ relative to the dry system value. As noted in the previous work section of this thesis, Kushiro (1975) observed that additions of H_2O, Na_2O, and K_2O all cause similar liquidus shifts in silicate systems. If this coincidence is taken to mean that the three oxides assume similar structural roles in silicate melts, then I would argue that water content increases melt basicity just as additions of alkali oxides do, and the overall effect on crystal-liqiud partitioning will be the same. Indeed, because of its low molecular weight, the dissolution of even a small weight percentage of water in a melt will cause notable changes in Si/O, and should influence partition coefficients accordingly.

The effect of carbon dioxide is difficult to predict because the solution mechanism for this molecule is not well understood. In acidic melts, where CO_2 dissolves chiefly in molecular form (Mysen, et al., 1976), any influence on crystal-liquid partitioning will be small. In basic melt + crystal assemblages, where CO_2 is probably present in the melt as carbonate anions, trace cations that form stable carbonates may be enriched in the melt relative to CO_2-free systems.

Definitive answers to questions concerning the generality

of the Si/O parameter and the effect of dissolved volatiles on crystal-liqiud partition coefficients are beyond the scope of this thesis. Future work on the subject of melt composition effects on crystal-liquid partitioning should deal with these questions, because the answers are required for accurate modelling of trace element behavior in magmatic systems.

BIBLIOGRAPHY

Albee, A.L. and L. Ray (1970) "Correction Factors for Electron Probe Microanalysis of Silicates, Oxides, Carbonates, Phosphates, and Sulfates", Anal. Chem. 42: 1408-1414.

Banno, S. and Y. Matsui (1973) "On the Formulation of Partition Coefficients for Trace Element Distribution Between Minerals and Magma", Chem. Geol. 11: 1-15.

Bates, T. (1962) in Modern Aspects of the Vitreous State, Vol. 2, pp. 195-243, J.D. Mackenzie, Ed., Butterworth, Inc., Washington, D.C..

Bernal, J.D. (1964) "The Structure of Liquids", Proc. Roy. Soc. (London) A280: 299-322.

Biggar, G.M. (1970) "Molybdenum as a Container for Melts Containing Iron Oxide", Ceram. Bull. 49: 286-288.

Bingham, K. and S. Parke (1965) "Absorption and Fluorescence Spectra of Divalent Manganese in Glasses", Phys. Chem. Glasses 6: 224-232.

Bishay, A. (1959) "Colors and Magnetic Properties of Iron in Glasses of Various Types and Their Implications Concerning Structure: I, High Alkali Silicate Glasses", J. Am. Ceram. Soc. 42: 403-407.

Bockris, J.O'M., J.A. Kitchener, S. Ignatowicz, and J.W. Tomlinson (1948) "The Electrical Conductivity of Silicate Melts: Systems Containing Ca, Mn, Al", Discuss. Faraday Soc. Disc. 4: 281-286.

Bockris, J.O'M. and D.C. Lowe (1954) "Viscosity and Structure of Molten Silicates", Proc. Roy. Soc. (London) A266: 423-435.

Bockris, J.O'M., J.D. Mackenzie, and J.A. Kitchener (1955) "Viscous Flow in Silica and Binary Liquid Silicates", Trans. Faraday Soc. 51: 1734-1748.

Bockris, J.O'M., J.W. Tomlinson, and J.L. White (1956) "Structure of Liquid Silicates - Partial Molar Volumes and Expansivities", Trans. Faraday Soc. 52: 299-310.

Boon, J.A. (1971) "Mössbauer Investigations in the System Na_2O-FeO-SiO_2", Chem. Geol. 7: 153-169.

Boon, J.A. and W.S. Fyfe (1972) "The Coordination Number of Ferrous Ions in Silicate Glasses", Chem. Geol. 10: 287-298.

Bottinga, Y. and D.F. Weill (1972) "The Viscosity of Magmatic Silicate Liquids: A Model for Calculation", Am. J. Sci. 272: 438-475.

Bowen, N.L. (1928) The Evolution of the Igneous Rocks, Princeton University Press, 334 pp.

Bowen, N.L. and J.F. Schairer (1932) "The System, FeO-SiO_2", Am. J. Sci. (fifth series) 24: 177-213.

Burns, R.G. and W.S. Fyfe (1964) "Site of Preference Energy and the Selective Uptake of Transition Metal Ions from a Magma", Science 144: 1001-1003.

Burns, R.G. and W.S. Fyfe (1967) "Trace Element Distribution Rules and Their Significance", Chem. Geol. 2: 89-104.

Cann, J.R. (1971) "Major Element Variations in Ocean-floor Basalts", Phil. Trans. Roy. Soc. London Ser. A, 268: 495-505.

Chayes, F. (1963) "Relative Abundance of Intermediate Members of the Oceanic Basalt-Trachyte Association", J. Geophys. Res. 68: 1519-1534.

Colby, J.W. (1968) "Quantitative Microprobe Analysis of Thin Insulating Films", Advan. X-ray Anal. 11: 287-305.

Crozier, D. and R.W. Douglas (1965) "Study of Sodium Silicate Glasses in the Infra-red by Means of Thin Films", Phys. Chem. Glasses 6: 240-245.

Cukierman, M. and D.R. Uhlmann (1973) "Viscosity of Liquid Anorthite", J. Geophys. Res. 78: 4920-4923.

Day, D.E. and G.E. Rindone (1962a) "Properties of Soda Aluminosilicate Glasses: I, Refractive Index, Density, Molar Refractivity, and Infrared Absorption Spectra", J. Am. Ceram. Soc. 45: 489-496.

Day, E.E. and G.E. Rindone (1962b) "Properties of Soda Aluminosilicate Glasses: III, Coordination of Aluminum Ions", J. Am. Ceram. Soc. 45: 579-581.

Doremus, R.H. (1973) Glass Science, John Wiley and Sons, New York, 349 pp.

Drake, M.J. (1972) "The Distribution of Major and Trace Elements Between Plagioclase Feldspar and Magmatic Silicate Liquid", Ph.D. Thesis, University of Oregon.

Drake, M.J. and D.F. Weill (1972) "New Rare Earth Element Standards for Electron Microprobe Analysis", Chem. Geol. 10: 179-181.

Drake, M.J. and D.F. Weill (1975) "Partition of Sr, Ba, Ca, Y, Eu^{+2}, and Eu^{+3} and other REE Between Plagioclase Feldspar and Magmatic Liquid: An Experimental Study", Geochim. Cosmochim. Acta 38: 689-712.

Duke, J.M. (1976) "Distribution of the Period Four Transition Elements Among Olivine, Calcic Clinopyroxene and Mafic Silicate Liquid: Experimental Results", J. Petrol. (in press).

Eisenman, G. (1962) "Cation Selective Glass Electrodes and Their Mode of Operation", Biophys. Jour. 2: 259-323.

Ewart, A., S.R. Taylor, and A.C. Capp (1968) "Geochemistry of the Pantellerites of Mayor Island, New Zealand", Contrib. Mineral. Petrol. 17: 116-140.

Ferguson, J. and K.L. Currie (1971) "Evidence of Liquid Immiscibility in Alkaline Ultrabasic Dikes at Callander Bay, Ontario", J. Petrol. 12: 561-585.

Finger, L.W. and C.G. Hadidiacos (1972) "Electron Microprobe Automation", Yb. Carnegie Inst. Wash. 71: 598-599.

Flood, H. and W.J. Knapp (1968) "Structural Characteristics of Liquid Mixtures of Feldspar and Silica", J. Am. Ceram. Soc. 51: 259-263.

Glasser, F.P., I. Warshaw, and R. Roy (1960) "Liquid Immiscibility in Silicate Systems", Phys. Chem. Glasses 1: 39-45.

Haller, W., D.H. Blackburn, and J.H. Simmons (1974) "Miscibility Gaps in the Alkali Silicate Binaries - Data and Thermodynamic Interpretation", J. Am. Ceram. Soc. 57: 120-126.

Hanna, R. and G.J. Su (1964) "Infrared Absorption Spectra of Sodium Silicate Glasses from 4 to 30μ", J. Am. Ceram. Soc. 47: 597-601.

Haskin, L.A., M.A. Haskin, F.A. Frey, and T.R. Wildeman (1968) "Relative and Absolute Terrestrial Abundances of the Rare Earths", in Origin and Distribution of the Elements, L.H. Ahrens, Ed., pp. 889-912, Pergamon Press, Oxford.

Hess, P.C. (1970) "Polymer Model of Silicate Melts", Geochim. Cosmochim. Acta 35: 289-306.

Hess, P.C. (1975) "PbO-SiO_2 Melts: Structure and Thermodynamics of Mixing", Geochim. Cosmochim. Acta 39: 671-687.

Hess, P.C. and M.J. Rutherford (1974) "Element Fractionation Between Immiscible Melts", in Lunar Science V, pp. 328-329. Houston, Lunar Science Institute.

Hicks, J.F.G. (1969) "The Configurational Entropy of Vitreous Silica", Phys. Chem. Glasses 10: 164.

Huggins, M.L., K.H. Sun, and A.J. Silverman (1943) "The Vitreous State", J. Am. Ceram. Soc. 26: 393-398.

Irvine, T.N. (1974) "Chromitite Layers in Stratiform Intrusions", Yb. Carnegie Inst. Wash. 73: 300-316.

Irving, A.J. and F.A. Frey (1976) "Effect of Composition on the Partitioning of Rare Earth Elements, Hf, Sc, and Co Between Garnet and Liquid: Experimental and Natural Evidence", Trans. Am. Geophys. Union 57: 339.

Kumar, S. (1959) "Optical Absorption of Glasses Containing Ions with Partially Filled 3d-Orbitals: I", Cent. Glass Ceram. Res. Inst., Bull. 6: 99-126.

Kumar, S. and P. Nath (1966) Trans. Indian Ceram. Soc. 25: 12 (quoted in Doremus, 1973, p. 328).

Kurkjian, C.R. (1970) "Mössbauer Spectroscopy in Inorganic Glasses", J. Noncryst. Solids 3: 157-194.

Kurkjian, C.R. and E.A. Sigety (1968) "Co-ordination of Fe^{3+} in Glass", Phys. Chem. Glasses 9: 73-83.

Kushiro, I. (1975) "On the Nature of Silicate Melt and Its Significance in Magma Genesis: Regularities in the Shift of the Liquidus Boundaries Involving Olivine, Pyroxene, and Silica Minerals", Am. J. Sci. 275: 411-431.

Kushiro, I., H.S. Yoder, Jr., and B.O. Mysen (1976) "Viscosity of Basalt and Andesite Magmas at High Pressures", Trans. Am. Geophys. Union 57: 354.

Leeman, W.P. (1974) "Experimental Determination of Partitioning of Divalent Cations Between Olivine and Basaltic Liquid", Ph.D. Thesis (Part II), University of Oregon.

Lentz, C.W. (1964) "Silicate Minerals as Sources of Trimethylsilyl Silicates and Silicate Structure Analysis of Sodium Silicate Solutions", Inorg. Chem. 3: 574-579.

Levin, E.M. and S. Block (1956) "Structural Interpretation of Immiscibility in Oxide Systems: I, Analysis and Calculation of Immiscibility", J. Am. Ceram. Soc. 40: 95-106.

Lewis, G.N. and M. Randall (1961) Thermodynamics, McGraw-Hill Book Company, Inc., New York, 723 pp.

Longhi, J., D. Walker, and J.F. Hays (1976) "Fe and Mg in Plagioclase", submitted to the Proceedings of the 7th Lunar Science Conference.

Mackenzie, J.D. (1960) "Structure of Some Inorganic Glasses from High Temperature Studies", in Modern Aspects of the Vitreous State, Vol. 1, J.D. Mackenzie, Ed., pp. 188-218, Butterworths, London.

Milberg, M.E. and C.R. Peters (1969) "Cation Distribution in Thallium Silicate Glasses", Phys. Chem. Glasses 10: 46-49.

Morris, R.V. and L.A. Haskin (1974) "EPR Measurement of the Effect of Glass Composition on the Oxidation States of Eu", Geochim. Cosmochim. Acta 38: 1435-1445.

Mozzi, R.L. and B.E. Warren (1969) "The Structure of Vitreous Silica", J. Appl. Cryst. 2: 164-172.

Murase, T. and A.R. McBirney (1973) "Properties of Some Common Igneous Rocks and Their Melts at High Temperature", Geol. Soc. Amer. Bull. 84: 3563-3592.

Mysen, B.O. (1975) "Partitioning of Ni and Sm Between Liquid, Olivine, and Orthopyroxene in the Upper Mantle: Experimental Determination of Limits of Henry's Law Behavior", Trans. Am. Geophys. Union 56: 1075.

Mysen, B.P., D.H. Eggler, M.G. Seitz, and J.R. Holloway (1976) "Carbon Dioxide in Silicate Melts and Crystals. I. Solubility Measurements", Am. Mineralogist (in press).

Nagasawa, H. and C.C. Schnetzler (1971) "Partitioning of Rare Earth Alkali, and Alkaline Earth Elements Between Phenocrysts and Acidic Igneous Magma", Geochim. Cosmochim. Acta 35: 935-968.

Nockolds, S.R. (1954) "Average Chemical Compositions of Some Igneous Rocks", Geol. Soc. Am. Bull. 65: 1007-1032.

Ohlberg, S.M. and J.M. Parsons (1964) "The Distribution of Sodium Ions in Soda-Lime-Silica Glasses", in Physics of Noncrystalline Solids, North Holland, Amsterdam, pp. 31-39.

Pearce, M.L. (1964) "Solubility of Carbon Dioxide and Variation of Oxygen Ion Activity in Soda-Silica Melts", J. Am. Ceram. Soc. 47: 342-347.

Philpotts, A.R. (1971) "Immiscibility Between Feldspathic and Gabbroic Magmas", Nature Phys. Sci. 299: 107-109.

Riebling, E.F. (1966) "Structure of Sodium Aluminosilicate Melts Containing at Least 50 mole % SiO_2 at 1500°C", J. Chem. Phys. 44: 2857-2865.

Riebling, E.F. (1968) "Structural Similarities Between a Glass and Its Melt", J. Am. Ceram. Soc. 51: 143-149.

Roedder, E. (1951) "Low-temperature Liquid Immiscibility in the System K_2O-FeO-Al_2O_3-SiO_2", Am. Mineralogist 36: 282-286.

Roedder, E. and P.W. Weiblen (1971) "Petrology of Silicate Melt Inclusions, Apollo 11 and Apollo 12 and Terrestrial Equivalents", in Proc. Second Lunar Sci. Conf., Geochim. Cosmochim. Acta, Suppl. 2, Vol. 1, pp. 507-528. Cambridge, The M.I.T. Press.

Schairer, J.F. and N.L. Bowen (1955) "The System K_2O-Al_2O_3-SiO_2", Am. J. Sci. 253: 681-746.

Schairer, J.F. and N.L. Bowen (1956) "The System Na_2O-Al_2O_3-SiO_2", Am. J. Sci. 254: 129-195.

Schairer, J.F. and H.S. Yoder, Jr. (1966) "The System Albite-Anorthite-Forsterite at 1 Atmosphere", Yb. Carnegie Inst. Wash. 65: 204-209.

Sigel, G.H. (1971) "Vacuum Ultraviolet Absorption in Alkali Doped Fused Silica and Silicate Glasses", J. Phys. Chem. Solids 32: 2373-2383.

Simon, J. (1960) "Infrared Studies of Glass", in Modern Aspects of the Vitreous State, Vol. 1, pp. 120-151, J.D. Mackenzie, Ed., Butterworths, London.

Temkin, M. (1945) "Mixtures of Fused Salts as Ionic Solutions", Acta Physicochemica, U.S.S.R. 20: 411-420.

Toop, G.W. and C.S. Samis (1962a) "Some New Ionic Concepts of Silicate Slags", Can. Met. Quart. 1: 129-152.

Toop, G.W. and C.S. Samis (1962b) "Activities of Ions in Silicate Melts", Trans. Met. Soc. AIME 224: 878-887.

Turner, W.H. and J.A. Turner (1972) "Ligand-field Spectra and the Structure of Ni in Silicate Glasses", J. Am. Ceram. Soc. 55: 201-207.

Turner, F.J. and J. Verhoogen (1960) Igneous and Metamorphic Petrology, McGraw-Hill, New York, 694 pp.

Urnes, S. (1969) "Studies of the Sodium Distribution in Sodium Silicate Glasses by the Chemical Difference Method", Phys. Chem. Glasses 10: 69-71.

Uys, J.M. and T.B. King (1963) "The Effect of Basicity on the Solubility of Water in Silicate Melts", Trans. Met. Soc. AIME 227: 492-500.

Verhoogen, J. (1962) "Distribution of Titanium Between Silicates and Oxides in Igneous Rocks", Am. J. Sci. 260: 211-220.

Warren, B.E. and J. Biscoe (1938) "The Structure of Silica Glass by X-ray Diffraction Studies", J. Am. Ceram. Soc. 21: 49-54.

Weyl, W.A. (1959) "Colored Glasses", Society of Glass Technology Monograph, Sheffield, England, 541 pp.

Whittaker, E.J.W. (1967) "Factors Affecting Element Ratios in the Crystallization of Minerals", Geochim. Cosmochim. Acta 31: 2275-2288.

Whittaker, E.J.W. and R. Muntus (1970) "Ionic Radii for Use in Geochemistry", Geochim. Cosmochim. Acta 34: 945-956.

Williams, R.J.P. (1959) "Deposition of Trace Elements in Basic Magma", Nature 184: 44.

Wong, J. and C.A. Angell (1970) Appl. Spectrosc. Rev. 4: 97.

Yoder, H.S., Jr. (1973) "Contemporaneous Basaltic and Rhyolitic Magmas", Am. Mineralogist 58: 153-171.

Zachariasen, W.H. (1932) "The Atomic Arrangement in Glass", J. Am. Chem. Soc. 54: 3841-3851.

Zielinski, R.A. and F.A. Frey (1970) "Gough Island: Evaluation of a Fractional Crystallization Model", Contrib. Mineral. Petrol. 29: 242-254.

Appendix I.

Part A. Major element analyses (wt %) of glasses in two-liquid partitioning experiments. Typical standard deviations are: SiO_2, 0.4; Al_2O_3, 0.1; FeO, 0.4; K_2O, 0.1

charges doped with Cs

run no.	CsI	CsII	CsIII
		(acidic glass)	
SiO_2	68.9	69.6	67.8
Al_2O_3	5.7	5.8	5.6
FeO	19.9	20.2	21.4
K_2O	5.9	5.8	5.8
Cs_2O	0.13	0.24	0.39
total	100.5	101.6	101.0
		(basic glass)	
SiO_2	49.6	50.1	51.0
Al_2O_3	3.4	3.5	3.5
FeO	43.9	43.1	42.0
K_2O	2.4	2.4	2.5
Cs_2O	0.04	0.07	0.12
total	99.3	99.2	99.1

charges doped with Ba

run no.	BaI	BaII	BaIII	BaIV	BaV
			(acidic glass)		
SiO_2	67.9	67.3	66.9	66.0	65.6
Al_2O_3	5.8	5.8	5.7	5.5	5.5
FeO	20.2	20.8	20.9	21.3	21.6
K_2O	5.5	5.6	5.5	5.3	5.4
BaO	0.07	0.10	0.20	0.41	0.67
total	99.5	99.6	99.2	98.5	98.8

Appendix I (continued)

charges doped with Ba (continued)

run no.	BaI	BaII	BaIII	BaIV	BaV
			(basic glass)		
SiO_2	49.8	49.9	50.6	50.5	51.0
Al_2O_3	3.5	3.5	3.5	3.5	3.7
FeO	43.8	43.1	42.1	41.0	40.3
K_2O	2.4	2.5	2.6	2.5	2.7
BaO	0.11	0.16	0.29	0.59	0.91
total	99.6	99.2	99.1	98.1	98.6

charges doped with Sr

run no.	SrI	SrII	SrIII
		(acidic glass)	
SiO_2	68.0	67.8	67.9
Al_2O_3	5.6	5.5	5.6
FeO	19.9	20.2	21.6
K_2O	5.7	5.7	5.6
SrO	0.18	0.54	0.60
total	99.4	99.7	101.3
		(basic glass)	
SiO_2	50.6	50.8	51.7
Al_2O_3	3.5	3.6	3.6
FeO	43.5	42.1	41.7
K_2O	2.6	2.6	2.7
SrO	0.24	0.78	1.11
total	100.4	99.9	100.8

Appendix I (continued)

charges doped with Ca

run no.	CaI	CaII	CaIII	CaIV	CaV	CaVI
			(acidic glass)			
SiO_2	68.0	67.1	66.9	66.7	66.1	65.7
Al_2O_3	5.7	5.7	5.6	5.5	5.6	5.5
FeO	20.3	21.9	22.1	22.1	22.8	23.7
K_2O	5.7	5.6	5.6	5.5	5.5	5.5
CaO	0.08	0.13	0.21	0.26	0.37	0.52
total	99.8	100.4	100.4	100.1	100.4	100.9
			(basic glass)			
SiO_2	49.2	50.0	50.2	50.6	51.0	51.6
Al_2O_3	3.6	3.6	3.5	3.7	3.7	3.7
FeO	43.3	43.1	42.6	40.2	39.6	38.9
K_2O	2.3	2.4	2.4	2.6	2.7	2.8
CaO	0.25	0.34	0.49	0.60	0.72	0.93
total	98.7	99.4	99.2	97.7	97.7	97.9

charges doped with Mg

run no.	MgI	MgII	MgIII	MgIV	MgV
			(acidic glass)		
SiO_2	68.4	68.1	67.2	66.6	65.5
Al_2O_3	5.6	5.6	5.7	5.5	5.5
FeO	20.0	21.4	22.7	23.2	23.3
K_2O	5.7	5.8	5.7	5.6	5.5
MgO	0.11	0.22	0.32	0.52	0.55
total	99.8	101.1	101.6	101.4	100.4

Appendix I (continued)

charges doped with Mg (continued)

run no.	MgI	MgII	MgIII	MgIV	MgV
	(basic glass)				
SiO_2	50.1	51.3	51.8	52.0	52.7
Al_2O_3	3.4	3.4	3.5	3.4	3.6
FeO	43.2	42.3	41.3	40.4	40.2
K_2O	2.5	2.6	2.6	2.7	2.7
MgO	0.23	0.49	0.71	1.06	1.18
total	99.4	100.1	99.9	99.6	100.4

charges doped with La

run no.	LaI	LaII	LaIII
	(acidic glass)		
SiO_2	68.1	68.5	69.3
Al_2O_3	5.6	5.5	5.5
FeO	20.1	20.0	19.6
K_2O	5.8	5.9	6.0
La_2O_3	0.07	0.13	0.21
total	99.7	100.0	100.6
	(basic glass)		
SiO_2	49.8	48.1	47.9
Al_2O_3	3.4	3.5	3.6
FeO	43.8	44.2	44.0
K_2O	2.6	2.4	2.4
La_2O_3	0.29	0.49	0.77
total	99.9	98.7	98.7

Appendix I (continued)

charges doped with Sm

run no.	SmI	SmII	SmIII	SmIV	SmV
			(acidic glass)		
SiO_2	68.7	69.1	69.0	69.2	68.9
Al_2O_3	5.5	5.5	5.4	5.7	5.6
FeO	20.2	20.2	19.7	19.7	20.3
K_2O	5.7	5.8	5.6	5.7	5.7
Sm_2O_3	0.04	0.11	0.20	0.27	0.32
total	100.1	100.7	99.9	100.6	100.8
			(basic glass)		
SiO_2	50.5	50.4	50.6	50.0	49.3
Al_2O_3	3.5	3.4	3.3	3.4	3.4
FeO	43.8	44.1	44.4	44.5	43.5
K_2O	2.7	2.6	2.5	2.5	2.6
Sm_2O_3	0.20	0.50	0.86	1.14	1.33
total	100.7	101.0	101.7	101.5	100.1

charges doped with Lu

run no.	LuI	LuII	LuI	LuII
	(acidic glass)		(basic glass)	
SiO_2	68.7	69.2	49.3	48.9
Al_2O_3	5.7	5.6	3.4	3.4
FeO	19.7	19.7	43.9	44.3
K_2O	5.6	5.6	2.5	2.6
Lu_2O_3	0.05	0.15	0.37	0.64
total	99.8	100.3	99.5	99.8

Appendix I (continued)

charges doped with Mn

run no.	MnI	MnII	MnIII	MnIV
		(acidic glass)		
SiO_2	68.0	67.7	67.8	68.3
Al_2O_3	5.4	5.6	5.5	5.4
FeO	20.2	19.9	20.1	19.8
K_2O	5.9	5.8	5.6	6.0
MnO	0.07	0.17	0.26	0.33
total	99.6	99.2	99.3	99.8
		(basic glass)		
SiO_2	50.1	49.4	49.8	50.2
Al_2O_3	3.4	3.3	3.5	3.4
FeO	43.2	43.0	43.6	43.0
K_2O	2.4	2.6	2.5	2.5
MnO	0.22	0.48	0.74	0.96
total	99.3	98.8	100.1	100.1

charges doped with Ti

run no.	TiI	TiII*	TiIII	TiIV*	TiV	TiVI	TiVII
			(acidic glass)				
SiO_2	68.8	68.7	69.1	69.0	70.1	71.0	70.7
Al_2O_3	5.6	5.6	5.7	5.6	5.8	5.9	5.8
FeO	20.2	20.1	20.0	19.5	19.3	18.9	18.8
K_2O	5.7	5.6	5.6	5.7	5.5	5.8	5.7
TiO_2	0.10	0.11	0.13	0.18	0.27	0.32	0.39
total	100.2	100.1	100.4	100.0	101.0	101.9	101.4

* reversal experiments (see text)

Appendix I (continued)

charges doped with Ti (continued)

run no.	TiI	TiII	TiIII	TiIV	TiV	TiVI	TiVII
				(acidic glass)			
SiO_2	50.2	50.0	49.3	49.1	48.2	48.4	48.1
Al_2O_3	3.6	3.6	3.5	3.4	3.3	3.4	3.3
FeO	43.8	43.7	44.1	44.1	44.5	44.9	45.2
K_2O	2.5	2.4	2.4	2.3	2.4	2.3	2.3
TiO_2	0.28	0.32	0.43	0.51	0.81	1.03	1.28
total	100.4	100.0	99.7	99.4	99.2	100.0	100.2

charges doped with Cr

run no.	CrI	CrII	CrI	CrII
	(acidic glass)		(basic glass)	
SiO_2	68.6	68.9	50.0	49.6
Al_2O_3	5.7	5.6	3.4	3.7
FeO	20.3	20.1	43.9	43.8
K_2O	5.8	5.7	2.7	2.6
Cr_2O_3	0.06	0.11	0.19	0.48
total	100.5	100.4	100.2	100.2

charges doped with Ta

run no.	TaI	TaII	TaIII	TaI	TaII	TaIII
	(acidic glass)			(basic glass)		
SiO_2	67.3	68.1	67.9	48.7	48.9	47.6
Al_2O_3	5.5	5.5	5.6	3.4	3.5	3.5
FeO	20.2	19.7	19.8	43.7	43.7	44.2
K_2O	5.7	5.8	5.7	2.5	2.6	2.4
Ta_2O_5	0.09	0.19	0.29	0.39	0.81	1.23
total	98.8	99.3	99.3	98.7	99.5	98.9

Appendix I (continued)

charges doped with Zr

run no.	ZrI	ZrII	ZrIII	ZrIV
		(acidic glass)		
SiO_2	67.6	68.5	68.1	67.9
Al_2O_3	5.3	5.5	5.6	5.4
FeO	20.1	20.4	20.5	20.0
K_2O	6.0	5.7	5.8	5.7
ZrO_2	0.13	0.31	0.38	0.58
total	99.1	100.4	100.4	99.6
		(basic glass)		
SiO_2	49.6	49.5	50.1	50.0
Al_2O_3	3.3	3.4	3.3	3.5
FeO	43.0	43.1	43.9	43.1
K_2O	2.4	2.4	2.5	2.4
ZrO_2	0.33	0.71	0.89	1.32
total	98.6	99.1	100.7	100.3

charges doped with P

run no.	PI	PII	PI	PII
	(acidic glass)		(basic glass)	
SiO_2	68.7	69.2	49.2	48.9
Al_2O_3	5.7	5.8	3.6	3.5
FeO	18.9	19.1	44.2	45.5
K_2O	5.7	5.8	2.5	2.5
P_2O_5	0.04	0.09	0.55	0.73
total	99.0	100.0	100.1	101.1

Appendix I.

Part B. Standards used for major element analyses in two-liquid partitioning experiments

standard name	element standardized	weight per cent oxides								
		SiO_2	TiO_2	Al_2O_3	FeO	MgO	CaO	Na_2O	K_2O	BaO
ORTHOCLASE GLASS	K	64.39		18.58				1.14	14.92	0.82
DIOPSIDE65-JADEITE35	Al	56.88		8.82		12.10	16.83	5.36		
DIOPSIDE	Si	55.47				18.62	25.90			
COSSYRITE	Fe	40.93	8.71		40.99			6.93		

Appendix II.

Part A. counting times, peak/background ratios, and counting errors for trace and minor element analyses in two-liquid partitioning experiments

	Basic Glass			Acidic Glass		
run no.	count time per spot (s)	peak/BG ratio	error (1σ,%)	count time per spot (s)	peak/BG ratio	error (1σ,%)
CsI	300	1.12	8.2	100	1.36	4.2
CsII	200	1.20	5.8	100	1.64	3.0
CsIII	100	1.31	5.1	100	2.01	2.1
BaI	200	1.14	12.3	200	1.10	18.5
BaII	200	1.18	9.6	200	1.13	14.3
BaIII	100	1.42	6.3	100	1.37	7.8
BaIV	100	1.69	3.9	100	1.55	5.2
BaV	50	2.07	3.8	50	1.93	4.7
SrI	300	1.15	8.0	500	1.10	8.3
SrII	100	1.38	4.7	100	1.25	7.1
SrIII	100	1.56	3.3	100	1.28	6.4
CaI	50	2.78	3.5	100	1.63	6.0
CaII	50	3.24	2.6	50	2.03	5.6
CaIII	50	4.27	2.2	50	2.45	4.1
CaIV	50	5.13	1.9	50	2.71	3.5
CaV	50	6.32	1.7	50	3.33	2.8
CaVI	50	7.07	1.5	50	4.48	2.2
MgI	100	1.92	7.6	200	1.63	8.2
MgII	100	3.11	3.9	200	2.26	4.6
MgIII	100	3.98	3.1	100	3.14	4.3
MgIV	100	5.08	2.5	100	4.08	3.3
MgV	50	5.42	3.3	50	4.32	4.4

Appendix II, Part A (continued)

	Basic Glass			Acidic Glass		
run no.	count time per spot (s)	peak/BG ratio	error (1σ,%)	count time per spot (s)	peak/BG ratio	error (1σ,%)
LaI	100	1.45	5.5	300	1.12	12.0
LaII	100	1.76	3.4	200	1.23	7.9
LaIII	50	2.17	1.6	200	1.36	5.2
LuI	200	1.28	8.1	500	1.07	26.0
LuII	100	1.51	7.0	400	1.17	10.8
SmI	200	1.17	7.8	500	1.04	22.4
SmII	100	1.42	4.7	20,000 cts	1.12	9.1
SmIII	10,000 cts	1.72	3.0	100	1.21	9.9
SmIV	60	1.95	3.0	60	1.29	9.6
SmV	60	2.10	2.6	60	1.34	8.2
MnI	200	1.53	7.9	400	1.26	12.1
MnII	100	2.13	5.8	200	1.54	9.0
MnIII	100	2.75	4.1	100	1.84	8.6
MnIV	100	3.28	3.4	100	2.09	7.0
CrI	100	1.33	6.2	300	1.13	9.6
CrII	100	1.82	2.7	100	1.25	8.9
TiI	100	2.01	2.9	100	1.42	6.7
TiII*	100	2.15	2.6	100	1.47	6.1
TiIII	100	2.55	2.0	100	1.64	4.6
TiIV*	50	2.82	2.5	50	1.79	5.4
TiV	10,000 cts	3.88	1.5	100	2.20	2.7
TiVI	50	4.67	1.5	50	2.41	3.4
TiVII	10,000 cts	5.57	1.3	50	2.72	2.9

* reversal experiments (see text)

Appendix II, Part A (continued)

	Basic Glass			Acidic Glass		
run no.	count time per spot (s)	peak/BG ratio	error (1σ,%)	count time per spot (s)	peak/BG ratio	error (1σ,%)
ZrI	100	1.44	6.7	200	1.22	10.0
ZrII	100	2.20	3.0	100	1.51	6.5
ZrIII	100	2.78	2.3	100	1.62	5.4
ZrIV	100	3.40	1.8	100	1.95	3.8
TaI	100	1.24	11.4	300	1.07	23.9
TaII	100	1.51	5.8	300	1.14	12.1
TaIII	100	1.76	4.0	200	1.22	9.7
PI	100	1.88	3.8	300	1.09	18.4
PII	100	2.16	3.0	300	1.18	10.3

Appendix II, Part B.

Summary of standards used for trace and minor element analyses in two-liquid partitioning study (analyses in weight per cent oxides)

Glass standards synthesized specifically for this study

Std for:	Cs	Ba	P	Ta	Zr	Sr
SiO_2	49.20	47.23	46.89	47.78	47.83	45.89
Al_2O_3	19.69	18.90	18.77	19.12	19.14	18.37
FeO	20.78	19.95	19.80	20.18	20.20	19.38
K_2O	6.53	6.27	6.22	6.34	6.35	6.09
	2.97%Cs_2O	6.06%BaO	6.73%P_2O_5	4.97%Ta_2O_5	4.87%ZrO_2	8.71%SrO

Rare earth standards of Drake and Weill (1972)

Std for:	Sm&Lu		La
SiO_2	27.07		27.15
Al_2O_3	30.63		30.72
CaO	25.26		25.33
Nd_2O_3	4.26	Y_2O_3	4.08
Sm_2O_3	4.26	La_2O_3	4.28
Yb_2O_3	4.26	Ce_2O_3	4.00
Lu_2O_3	4.26	Pr_2O_3	4.44

Appendix II, Part B (continued)

Geophysical Laboratory standards

Std for:	Ti	Mg & Ca	Cr	Mn
Std name:	COSSYRITE	Di65-Jd35	Di96CrCATS4	Mn Ilmenite
SiO_2	40.93	56.88	54.24	---
TiO_2	8.71	---	---	51.61
Al_2O_3	---	8.82	0.82	---
FeO	40.99	---	---	45.41
MgO	---	12.10	17.86	0.25
CaO	---	16.83	25.78	---
Na_2O	6.93	5.36	---	---
K_2O	---	---	---	---
MnO	---	---	---	1.43
Cr_2O_3	---	---	1.26	---